THE
PHYSICAL REVIEW
A journal of experimental and theoretical physics established by E. L. Nichols in 1893

SECOND SERIES, VOL. 63, NOS. 5 AND 6 MARCH 1 AND 15, 1943

Strong Coupling Mesotron Theory of Nuclear Forces

R. SERBER AND S. M. DANCOFF
University of Illinois, Urbana, Illinois
(Received December 23, 1942)

A theory of nuclear forces is developed, based on the hypothesis that the interaction between a nuclear particle and the mesotron field is strong. Two types of mesotron fields are considered, the charged scalar and the neutral pseudoscalar. The latter, for large enough separation, gives forces between two nuclear particles of the same type as those obtained from perturbation theory and, hence, with the spin dependence and exchange properties required to fit experiment. However, at closer approach the forces become ordinary (non-spin-dependent). It is found impossible to obtain spin dependent forces which, at the same time, extend to small separations and are of sufficient strength to account for the properties of the deuteron.

I. INTRODUCTION

IT is well known that the interaction between mesotrons and nuclear particles cannot be treated as small; such perturbation treatments are not only inconsistent—they lead to inacceptable nuclear forces and to a much too large scattering cross section for the mesotron.* Oppenheimer and Schwinger[1] have shown that the strong coupling theory affords an explanation of the smallness of the scattering cross section; the question of nuclear forces was left open by these authors.

It is not difficult to see that in the limit of very strong coupling, the nuclear forces will not be right. For this there are two related reasons:

(1) For strong enough coupling, the mesotron field due to the interaction of two nuclear particles becomes large compared to the field of a single mesotron; field fluctuations become unimportant, and the equations of the field may be treated classically. The classical solutions of the field equations of course exhibit the same singularities as arise in the lowest order perturbation theory. (2) At the same time, the interaction energy becomes large compared to the excitation energy of proton and neutron isobars, so that it is energetically favorable to excite many isobaric states; the total spin of each particle (intrinsic spin or isotopic spin, plus spin or isotopic spin of the associated mesotron field) becomes effectively very large, and behaves also in an essentially classical manner. The spins are thus free to orient themselves in such a way as to reduce the potential energy to a minimum. It follows that the interaction energy is an ordinary potential, non-exchange and spin independent, with singularities as bad as those of the perturbation theory. In the following sections it will be shown that these expectations are fully borne out by the detailed quantum-mechanical calculations.

It is, of course, true that with fixed magnitude

* See W. Pauli, Abstract No. 25, Bull. Am. Phys. Soc. **18**, No. 1 (1943). Professor Pauli considers the possibility of removing divergent terms associated with a point source by a subtraction formalism, while reducing the scattering cross section by means of radiation reaction.

[1] J. R. Oppenheimer and J. Schwinger, Phys. Rev. **60**, 150 (1941).

of the coupling constant, the interaction energy between two nuclear particles becomes small as the distance between them increases; for sufficiently large separation, the interaction energy becomes smaller than the energy of excitation of isobars, and beyond this point the forces change over to the type predicted by perturbation theory. The question that now arises, and which is the subject of our investigation, is whether a theory with an intermediate coupling strength can give a satisfactory account of the forces and whether the coupling constant can be so chosen that the region of spin dependent exchange forces is sufficiently extensive and the forces in this region sufficiently strong.

As we have just seen, for a theory with spin dependent coupling the nuclear forces remain spin dependent only for separations large enough to make

$$g^2e^{-\kappa r}/\kappa r<(\kappa a)/g^2,$$

where g is the coupling constant, a the radius of a nuclear particle, and $(\kappa)^{-1}$ the range of the forces. The observed scattering cross section demands $\kappa a<0.1$. It should be remarked that the condition for the validity of a perturbation treatment is that the self-energy of a nucleon due to its interaction with the field be small compared to the mesotron rest energy, $g^2/(\kappa a)^3<1$. Weak coupling would thus require $g^2<(\kappa a)^3 \sim 0.001$. Forces derived from these constants are 100 times weaker than actual nuclear forces. Thus we have only to consider $g^2\gg(\kappa a)^3$, or strong coupling.

The second decisive point in our investigation is this: Although for $g^2e^{-\kappa r}/\kappa r<(\kappa a)/g^2$, the forces given by the strong coupling theory are of the same type and radial dependence as those of perturbation theory, they are reduced by a numerical factor f : $\frac{1}{4}$ for the charged scalar, $\frac{1}{9}$ for neutral pseudoscalar, charged and symmetrical pseudoscalar.[2] These factors arise because the spin and charge of a nucleon oscillate with high frequency in their own fields even in the absence of a second nucleon; their components responsible for the nuclear interaction have smaller expectation values.

[2] We are indebted to Professor Pauli for the results in the charged and symmetrical pseudoscalar cases.

If now $g^2<1$, the spin dependent forces are too small; if $g^2>1$, the forces are spin dependent only for $\kappa r>\sim 2$, and their maximum depth will be less than $\sim 10^{-2}\mu c^2$ or 1 Mev. Thus we see that with $\kappa a\leqslant 0.1$, no value of g^2 gives spin dependent forces large enough to agree with experience.[3]

It may be remarked that values of a of the order $(\kappa)^{-1}$ not only conflict with the data on mesotron scattering, but essentially render nugatory a field theory of forces, since for $r\sim a$ these forces are entirely determined by the nature of the source, and not by that of the field.

II. CLASSICAL THEORY

As has been pointed out in the introduction, the main features of the strong coupling theory of nuclear forces can already be seen in a classical theory. We shall, therefore, begin with an investigation of the symmetrical scalar theory in the classical limit.

The heavy particle will be supposedly spread over a finite region of radius a with a density $U(\mathbf{r})$, $\int d\mathbf{r}\,U(\mathbf{r})=1$. In accordance with our above remarks concerning the size of the source we suppose $\kappa a\ll 1$ where $\kappa=\mu c/\hbar$ and μ is the mesotron's rest mass. The Hamiltonian of the symmetrical scalar theory when two heavy particles are present is

$$H=\tfrac{1}{2}\int d\mathbf{r}[\{\boldsymbol{\pi}(\mathbf{r})\}^2+\boldsymbol{\phi}(\mathbf{r})\cdot\omega^2\boldsymbol{\phi}(\mathbf{r})]$$

$$-g(4\pi)^{\frac{1}{2}}\int d\mathbf{r}[U_a(\mathbf{r})\boldsymbol{\tau}_a\cdot\boldsymbol{\phi}(\mathbf{r})+U_b(\mathbf{r})\boldsymbol{\tau}_b\cdot\boldsymbol{\phi}(\mathbf{r})]. \quad (1)$$

Here U_a and U_b are the source functions of the two heavy particles, $\boldsymbol{\tau}_a$ and $\boldsymbol{\tau}_b$ their isotopic spins. The wave function $\boldsymbol{\phi}$ is a vector in $\boldsymbol{\tau}$ space; its x and y components are the real and imaginary parts of the charged field, its z component is the neutral field. The operator $\omega^2=(\kappa^2-\Delta)$, whereas the coupling constant g is related to the dimensionless parameter g' through $g=g'(\hbar c)^{\frac{1}{2}}$.[4] The

[3] According to investigations of Nelson and Oppenheimer (unpublished) strong coupling pair theories give a mesotron scattering cross section equal to the square of the range of the forces, and forces which are therefore inacceptable. In addition, in these theories it is impossible to combine spin dependence with saturation.

[4] We adopt rational units throughout: $\hbar=c=1$.

equations of motion are:

$$\ddot{\phi}+\omega^2\phi=g(4\pi)^{\frac{1}{2}}(\tau_a U_a+\tau_b U_b), \tag{2}$$

$$\hbar\dot{\tau}_a=-g(4\pi)^{\frac{1}{2}}\tau_a\times\int d\mathbf{r}\phi(\mathbf{r})U_a(\mathbf{r}), \tag{3}$$

$$\hbar\dot{\tau}_b=-g(4\pi)^{\frac{1}{2}}\tau_b\times\int d\mathbf{r}\phi(\mathbf{r})U_b(\mathbf{r}).$$

These equations will be treated classically; that is, we shall ignore all commutators of the quantities which appear.

For strong coupling, $g\gg1$, we can find a class of solutions which are non-radiating (i.e., involve only frequencies smaller than κ, and thus no wave zone field). We take

$$\tau_a=\tau_b=\tau_0+\tau_1 e^{i\nu t},\quad \tau_a{}^2=\tau_b{}^2=\tau_0{}^2+\tau_1{}^2=1.$$

The real and imaginary parts of the complex vector $\tau_1 e^{i\nu t}$ are the components of τ_a and τ_b along two axes which form, with τ_0, an orthogonal axis system. The solution of (2) is then

$$\phi(\mathbf{r})=g(4\pi)^{\frac{1}{2}}\tau_0\int Y(\mathbf{r},\mathbf{r}')[U_a(\mathbf{r}')+U_b(\mathbf{r}')]d\mathbf{r}'$$

$$+g(4\pi)^{\frac{1}{2}}\tau_1 e^{i\nu t}\int Y_\nu(\mathbf{r},\mathbf{r}')[U_a(\mathbf{r}')+U_b(\mathbf{r}')]d\mathbf{r}'. \tag{4}$$

Where Y is the Yukawa potential:

$$Y(\mathbf{r},\mathbf{r}')=1/4\pi\frac{\exp(-\kappa|\mathbf{r}-\mathbf{r}'|)}{|\mathbf{r}-\mathbf{r}'|}$$

and

$$Y_\nu(\mathbf{r},\mathbf{r}')=1/4\pi\frac{\exp[-(\kappa^2-\nu^2)^{\frac{1}{2}}|\mathbf{r}-\mathbf{r}'|]}{|\mathbf{r}-\mathbf{r}'|}.$$

This expression for ϕ substituted in (3) gives

$$i\nu\tau_1=4\pi g^2(\tau_0\times\tau_1)\int\int d\mathbf{r}d\mathbf{r}'[Y(\mathbf{r},\mathbf{r}')$$

$$-Y_\nu(\mathbf{r},\mathbf{r}')][U_a(\mathbf{r}')+U_b(\mathbf{r}')]U_a(\mathbf{r}) \tag{5}$$

or, expanding Y_ν in powers of ν to order ν^2:

$$i\nu\tau_1=g^2(\tau_0\times\tau_1)(\nu^2/2\kappa)(R+S)$$

with

$$R=\int\int d\mathbf{r}d\mathbf{r}'U_a(\mathbf{r})U_a(\mathbf{r}')\exp(-\kappa|\mathbf{r}-\mathbf{r}'|)\sim1,\quad(\kappa a\ll1)$$

$$S=\int\int d\mathbf{r}d\mathbf{r}'U_a(\mathbf{r})U_b(\mathbf{r}')\exp(-\kappa|\mathbf{r}-\mathbf{r}'|)\sim e^{-\kappa d},$$

d being the separation of the two sources. Hence we obtain a solution if

$$\nu=2\kappa/g^2(R+S)\tau_0. \tag{6}$$

Solutions with τ_a not parallel to τ_b give high frequencies of order $4\pi g^2\int\int d\mathbf{r}d\mathbf{r}'U_a(\mathbf{r})U_b(\mathbf{r}')Y(\mathbf{r},\mathbf{r}')$ in contrast to the quasi-static solution just found.

The energy associated with our quasi-static fields can be calculated from (1) which gives, to order $1/g^2$:

$$H=\frac{2\kappa}{g^2(R+S)}\frac{\tau_1{}^2}{\tau_0{}^2}-g^2(I+J), \tag{7}$$

$$I=4\pi\int\int d\mathbf{r}d\mathbf{r}'U_a(\mathbf{r})U_a(\mathbf{r}')Y(\mathbf{r},\mathbf{r}')\sim1/a,\quad(\kappa a\ll1),$$

$$J=4\pi\int\int d\mathbf{r}d\mathbf{r}'U_a(\mathbf{r})U_b(\mathbf{r}')Y(\mathbf{r},\mathbf{r}')\sim e^{-\kappa d}/d,\quad(d\gg a).$$

The dominant g^2 term contains the self-energy of the two heavy particles, $-g^2I$, and the interaction energy between them, $-g^2J$. The small term in $1/g^2$ may be rewritten in terms of the charge vector $\mathbf{Q}=\int(\phi\times\pi)d\mathbf{r}$, whose z component gives the mesotron charge in units e. Using (4) we find $\mathbf{Q}=-2\tau_1 e^{i\nu t}$, in agreement with the constancy of the total charge vector $\mathbf{Q}+\tau_a+\tau_b$. The first term in (7) is thus

$$\frac{\kappa}{2g^2(R+S)}\frac{Q^2}{1-Q^2}$$

and represents the classical analogue of the heavy particle isobar energy discussed by Wentzel.[5] This non-radiating solution can be obtained only for values of the charge $Q<1$.

The most striking feature of the classical calculation is that, for the solution of minimum energy, there is a strong coupling between the

[5] G. Wentzel, Helv. Phys. Acta **13**, 269 (1940).

directions of the isotopic spins of the heavy particles causing them to line up parallel to each other. This has as a consequence that the interaction energy $-g^2J$ is an "ordinary" potential, completely independent of isotopic spin. It will be observed also that for $a\to 0$ the singularity in the potential is of the same type as yielded by perturbation theoretic treatment.

This treatment of the classical theory is due to Professor J. R. Oppenheimer. We are very grateful to him for permission to quote his results.

III. CHARGED SCALAR THEORY

We shall begin our consideration of quantum field theory with a discussion of the charged scalar field, the mesotron theory originally proposed by Yukawa. Although this simple theory cannot be expected to yield the observed nuclear forces, all the cogent results can already be obtained—no essentially new factors appear in the more complex fields which have been invoked to explain nuclear forces.

A. One Nuclear Particle

A treatment of a single heavy particle coupled to the charged scalar field has been given by Schwinger.[6] However, we wish to introduce a somewhat different mathematical treatment than was used by Schwinger, or by the present authors in their original work.[7] The change consists in expanding the fields in terms of the Yukawa function $\omega^{-2}U(\mathbf{r})$, instead of in terms of the source function $U(\mathbf{r})$ itself. This more convenient treatment was suggested by Professor W. Pauli and it is with deep appreciation that we acknowledge his permission to use it in this paper.

The Hamiltonian of the heavy particle plus mesotron field is

$$H=\int d\mathbf{r}[\bar{\pi}(\mathbf{r})\pi(\mathbf{r})+\bar{\phi}(\mathbf{r})\omega^2\phi(\mathbf{r})] +g(4\pi)^{\frac{1}{2}}\int d\mathbf{r}\,U(\mathbf{r})[\tau_-\bar{\phi}(\mathbf{r})+\tau_+\phi(\mathbf{r})]. \quad (8)$$

The notation is the same as that used in Section II except that $\phi(\mathbf{r})$ is a complex mesotron field amplitude and $\pi(\mathbf{r})$ its canonical conjugate.

$$[\pi(\mathbf{r}),\,\phi(\mathbf{r}')]=-i\delta(\mathbf{r}-\mathbf{r}'). \quad (9)$$

The operators τ_- and τ_+ change the projection of the heavy particle's isotopic spin from proton to neutron and from neutron to proton, respectively. We introduce also

$$N=4\pi\int d\mathbf{r}[U(\mathbf{r})]^2,$$

$$\mathrm{X}(\mathbf{r})=4\pi\omega^{-2}U(\mathbf{r}),$$

that is

$$(\kappa^2-\Delta)\mathrm{X}(\mathbf{r})=4\pi U(\mathbf{r}),$$

$$I=\int d\mathbf{r}\mathrm{X}(\mathbf{r})U(\mathbf{r}), \quad (10)$$

$$\xi(\mathbf{r})=\mathrm{X}(\mathbf{r})/I,$$

so that

$$\int d\mathbf{r}\xi(\mathbf{r})U(\mathbf{r})=1.$$

It is convenient to split ϕ and π into "coupled" and "uncoupled" components as follows:

$$\phi(\mathbf{r})=(4\pi)^{-\frac{1}{2}}\phi_0\xi(\mathbf{r})+\phi_1(\mathbf{r}),$$
$$\pi(\mathbf{r})=(4\pi)^{\frac{1}{2}}\pi_0U(\mathbf{r})+\pi_1(\mathbf{r}), \quad (11)$$

where we require of the functions $\phi_1(\mathbf{r})$ and $\pi_1(\mathbf{r})$ that

$$\int d\mathbf{r}\phi_1(\mathbf{r})U(\mathbf{r})=\int d\mathbf{r}\pi_1(\mathbf{r})\xi(\mathbf{r})=0. \quad (12)$$

ϕ_0 and π_0 are canonically conjugate expansion amplitudes. They can be determined by

$$\phi_0=(4\pi)^{\frac{1}{2}}\int d\mathbf{r}\phi(\mathbf{r})U(\mathbf{r}),$$
$$\pi_0=(4\pi)^{-\frac{1}{2}}\int d\mathbf{r}\pi(\mathbf{r})\xi(\mathbf{r}). \quad (13)$$

$\pi_1(\mathbf{r})$ and $\phi_1(\mathbf{r})$, however, are not exact canonical conjugates, but satisfy the commutation relation

$$[\pi_1(\mathbf{r}),\,\phi_1(\mathbf{r}')]=-i[\delta(\mathbf{r}-\mathbf{r}')-U(\mathbf{r})\xi(\mathbf{r}')]. \quad (14)$$

[6] J. Schwinger, unpublished.
[7] S. M. Dancoff and R. Serber, Phys. Rev. **61**, 394 (1942).

In terms of these variables

$$H=N\bar{\pi}_0\pi_0+\bar{\phi}_0\phi_0/I+g(\tau_-\bar{\phi}_0+\tau_+\phi_0)+\int d\mathbf{r}[\bar{\phi}_1(\mathbf{r})\omega^2\phi_1(\mathbf{r})+\bar{\pi}_1(\mathbf{r})\pi_1(\mathbf{r})]+(4\pi)^{\frac{1}{2}}\bar{\pi}_0\int d\mathbf{r}\pi_1(\mathbf{r})U(\mathbf{r})+(4\pi)^{\frac{1}{2}}\pi_0\int d\mathbf{r}\bar{\pi}_1(\mathbf{r})U(\mathbf{r}). \quad (15)$$

Introduce polar coordinates:

$$\begin{aligned}&\phi_0=q_0e^{-i\theta},\\&\pi_0=\tfrac{1}{2}e^{i\theta}[p_0+(i/q_0)(p_\theta+\tfrac{1}{2}-\Sigma)],\\&\bar{\phi}_0=q_0e^{i\theta},\\&\pi_0=\tfrac{1}{2}e^{-i\theta}[p_0-(i/q_0)(p_\theta-\tfrac{1}{2}-\Sigma)],\end{aligned} \quad (16)$$

$$\phi_1(\mathbf{r})=q_1(\mathbf{r})e^{-i\theta},\quad \pi_1(\mathbf{r})=p_1(\mathbf{r})e^{i\theta},\qquad \bar{\phi}_1(\mathbf{r})=\bar{q}_1(\mathbf{r})e^{i\theta},\quad \bar{\pi}_1(\mathbf{r})=\bar{p}_1(\mathbf{r})e^{-i\theta}, \quad (17)$$

where

$$\Sigma=-i\int d\mathbf{r}[\pi_1(\mathbf{r})\phi_1(\mathbf{r})-\bar{\pi}_1(\mathbf{r})\bar{\phi}_1(\mathbf{r})].$$

Here (p_0, q_0) and (p_θ, θ) are real canonically conjugate variables. The total mesotronic charge is given by

$$-i\int d\mathbf{r}[\pi(\mathbf{r})\phi(\mathbf{r})-\bar{\pi}(\mathbf{r})\bar{\phi}(\mathbf{r})]=p_\theta. \quad (18)$$

The complex variables $p_1(\mathbf{r})$, $q_1(\mathbf{r})$ satisfy the same commutation relation as do $\pi_1(\mathbf{r})$, $\phi_1(\mathbf{r})$, namely, (14). The Hamiltonian becomes

$$H=(N/4)[p_0^2+(1/q_0^2)(p_\theta^2-1/4)]+q_0^2/I+gq_0(\tau_-e^{i\theta}+\tau_+e^{-i\theta})+\int d\mathbf{r}[\bar{q}_1(\mathbf{r})\omega^2q_1(\mathbf{r})+\bar{p}_1(\mathbf{r})p_1(\mathbf{r})]+(4\pi)^{\frac{1}{2}}(p_0/2)\int d\mathbf{r}\,U(\mathbf{r})[p_1(\mathbf{r})+\bar{p}_1(\mathbf{r})]+(4\pi)^{\frac{1}{2}}(i/2q_0)p_\theta\int d\mathbf{r}\,U(\mathbf{r})\times[\bar{p}_1(\mathbf{r})-p_1(\mathbf{r})].^{8} \quad (19)$$

[8] p_0^3 is a symbolic expression for $(1/q_0)p_\theta q_0 p_0$. We have neglected terms of the type Σ/q_0 because, as the later work shows, Σ vanishes in the absence of free (unbound) mesotrons. Such terms are of higher order in $1/g$ and are negligible if $g/p_\theta\gg 1$.

We transform to a representation in which the interaction energy is diagonal. The eigenstates of the heavy particle for this term are not proton and neutron, respectively, but are derived from the latter by a unitary transformation $F'=SF$ where S is the unitary operator $\exp(i\tau_z\theta/2)$. When the states of the heavy particle are represented as proton and neutron τ_-, τ_+, and τ_z are given by the matrices

$$\begin{pmatrix}0&0\\1&0\end{pmatrix},\quad \begin{pmatrix}0&1\\0&0\end{pmatrix},\quad \begin{pmatrix}1&0\\0&-1\end{pmatrix}.$$

After the S transformation[9] the Hamiltonian becomes $H'=SHS^{-1}$. In particular the expression $(\tau_-e^{i\theta}+\tau_+e^{-i\theta})$ is transformed into $(\tau_-+\tau_+)=\tau_x$. If we choose for the states of the heavy particle a representation in which τ_z is diagonal, the interaction energy is found to be diagonalized with eigenvalues $\pm gq_0$. On the other hand, off diagonal terms are introduced elsewhere in H, since $p_\theta\rightarrow p_\theta+\tau_z/2$ and in this representation τ_x is off diagonal. In the strong coupling limit, we may choose the lowest value of the interaction energy and neglect terms linear in τ_x, as coupling widely separated states. The condition implied is

$$g/p_\theta\gg 1. \quad (20)$$

The Hamiltonian becomes

$$H'=(N/4)(p_0^2+p_\theta^2/q_0^2)+q_0^2/I-gq_0+\cdots. \quad (21)$$

The term linear in q_0 is eliminated by a shift in origin:

$$Q_0=q_0-gI/2. \quad (22)$$

Since $gI/2$ is a constant, p_0 is conjugate to Q_0. We get

$$H'=(N/4)(p_0^2+p_\theta^2/q_0^2)-g^2I/4+Q_0^2/I+\cdots. \quad (23)$$

The leading term, $-g^2I/4$, gives the energy, to order g^2, of the static field bound to the heavy particle.

It is convenient to resolve the complex components of the field into real and imaginary parts:

$$\begin{aligned}p_1(\mathbf{r})&=(1/\sqrt{2})[p_x(\mathbf{r})+ip_y(\mathbf{r})],\\q_1(\mathbf{r})&=(1/\sqrt{2})[q_x(\mathbf{r})-iq_y(\mathbf{r})].\end{aligned} \quad (24)$$

[9] For previous use of the S transformation, see W. Pauli, Helv. Phys. Acta **12**, 147 (1930); also reference 12.

Here again (p_x, q_x) and (p_y, q_y) are real pseudo-conjugate pairs satisfying the commutation relations (14). The Hamiltonian separates into two commuting parts:

$$H'=-g^2I/4+H_x+H_y,$$

$$H_x=\tfrac{1}{4}Np_0^2+q_0^2/I+\tfrac{1}{2}\int d\mathbf{r}q_x(\mathbf{r})\omega^2q_x(\mathbf{r})$$
$$+(4\pi)^{\frac{1}{2}}p_0/\sqrt{2}\int d\mathbf{r}p_x(\mathbf{r})U(\mathbf{r})$$
$$+\tfrac{1}{2}\int d\mathbf{r}[p_x(\mathbf{r})]^2, \quad (25)$$

$$H_y=Np_\theta^2/4q_0^2+\tfrac{1}{2}\int d\mathbf{r}$$
$$\times[q_y(\mathbf{r})\omega^2q_y(\mathbf{r})+p_y(\mathbf{r})p_y(\mathbf{r})]$$
$$+(p_\theta/\sqrt{2}q_0)(4\pi)^{\frac{1}{2}}\int d\mathbf{r}p_y(\mathbf{r})U(\mathbf{r}).$$

H_x gives the energy of free oscillations about the equilibrium position $q_0=gI/2$. For, if we construct the functions,

$$\phi_x(\mathbf{r})=(4\pi)^{-\frac{1}{2}}Q_0\xi(\mathbf{r})+(1/\sqrt{2})q_x(\mathbf{r}),$$
$$\pi_x(\mathbf{r})=\sqrt{\pi}p_0U(\mathbf{r})+(1/\sqrt{2})p_x(\mathbf{r}).$$

Then ϕ_x and π_x are canonically conjugate and

$$H_x=\int d\mathbf{r}\{[\pi_x(\mathbf{r})]^2+\phi_x(\mathbf{r})\omega^2\phi_x(\mathbf{r})\}. \quad (26)$$

H_x is diagonalized in plane waves and represents a field of unscattered mesotrons.

Meanwhile H_y can be transformed into a similar form if we first eliminate the term linear in $p_y(r)$ by applying a unitary transformation.

$$F=e^{iU}F'e^{-iU}=F'+i[U, F]$$
$$+\frac{i^2}{2!}[U, [U, F]]+\cdots, \quad (27)$$

where

$$U=\frac{(4\pi)^{\frac{1}{2}}\sqrt{2}p_\theta}{g\int d\mathbf{r}[\mathrm{X}(\mathbf{r})]^2}\int d\mathbf{r}\mathrm{X}(\mathbf{r}')q_y'(\mathbf{r}'). \quad (28)$$

This produces a canonical transformation from the variables (p_y, q_y) to (p_y', q_y'), each pair satisfying (14). To first order in $1/g$:

$$p_y(\mathbf{r})=p_y'(\mathbf{r})-(4\pi)^{\frac{1}{2}}\sqrt{2}(p_\theta/g)\Big[U(\mathbf{r})/I$$
$$-\mathrm{X}(\mathbf{r})\Big/\int d\mathbf{r}[\mathrm{X}(\mathbf{r})]^2\Big]+\cdots, \quad (29)$$
$$q_y(\mathbf{r})=q_y'(\mathbf{r})+\cdots.$$

It can be shown that the criterion for neglect of succeeding terms in (29) is, once again, $g/p_\theta\gg1$. If (29) is substituted into (25), the linear term is eliminated, and

$$H_y=4\pi p_\theta^2\Big/g^2\int d\mathbf{r}\{\mathrm{X}(\mathbf{r})\}^2$$
$$+\tfrac{1}{2}\int d\mathbf{r}[\{p_y'(\mathbf{r})\}^2+q_y'(\mathbf{r})\omega^2q_y'(\mathbf{r})]. \quad (30)$$

Here we have substituted for q_0 the equilibrium value $gI/2$ in accordance with the strong coupling approximation, a procedure which can be proved valid for $g\gg1$. The latter two terms in (30) would, in analogy to H_x, respesent the energy of a set of free mesotrons except that p_y' and q_y' are not exact canonical conjugates. We will not here calculate the eigenstates of H_y; we will only remark that they can be represented at large distances as plane+scattered wave, leading to a scattering of free mesotrons by the heavy particle.[10] Since we are interested only in the heavy particle in the absence of unbound mesotrons, we may assume that none of the unscattered "x" waves nor any of the scattered "y" waves are present. The total energy then reduces to

$$H=-g^2I/4+4\pi p_\theta^2\Big/g^2\int d\mathbf{r}\{\mathrm{X}(\mathbf{r})\}^2. \quad (31)$$

The latter term thus appears as a correction to the static self-energy of order $1/g^2$. Since for the states under consideration the expectation value of $\tau_z=0$, it follows that the expectation value of the charge of the heavy particle core $=\frac{1}{2}$. Hence, if Q is the total charge of the system $p_\theta=Q-\frac{1}{2}$. For small sources, $(\kappa a\gg1)$,

$$(1/4\pi)\int d\mathbf{r}\{\mathrm{X}(\mathbf{r})\}^2=1/2\kappa.$$

[10] J. Schwinger, unpublished.

Hence the isobar energy takes the form

$$2\mu c^2(Q-\tfrac{1}{2})^2/g^2. \tag{32}$$

We are restricted by our approximation to isobars for which $(Q-\frac{1}{2})/g \ll 1$.

B. Two Nuclear Particles

The Hamiltonian is

$$H=\int d\tau[\bar{\pi}(\mathbf{r})\pi(\mathbf{r})+\bar{\phi}(\mathbf{r})\omega^2\phi(\mathbf{r})]$$
$$+g(4\pi)^{\frac{1}{2}}\int d\tau\{U^A(\mathbf{r})[\tau_-{}^A\bar{\phi}(\mathbf{r})+\tau_+{}^A\phi(\mathbf{r})]$$
$$+U^B(\mathbf{r})[\tau_-{}^B\bar{\phi}(\mathbf{r})+\tau_+{}^B\phi(\mathbf{r})]\}. \tag{33}$$

The procedure parallels closely that for a single heavy particle. We introduce

$$\mathrm{X}^A(\mathbf{r})=4\pi\omega^{-2}U^A(\mathbf{r});$$
$$\mathrm{X}^B(\mathbf{r})=4\pi\omega^{-2}U^B(\mathbf{r});$$
$$N=4\pi\int d\tau[U^A(\mathbf{r})]^2=4\pi\int d\tau[U^B(\mathbf{r})]^2,$$
$$M=4\pi\int d\tau[U^A(\mathbf{r})U^B(\mathbf{r})],$$

and define

$$I=\int d\tau \mathrm{X}^A(\mathbf{r})U^A(\mathbf{r})=\int d\tau \mathrm{X}^B(\mathbf{r})U^B(\mathbf{r}),$$
$$J=\int d\tau \mathrm{X}^A(\mathbf{r})U^B(\mathbf{r})=\int d\tau \mathrm{X}^B(\mathbf{r})U^A(\mathbf{r}).$$

We now introduce functions orthogonal to the U's:

$$\int d\tau\xi^A(\mathbf{r})U^B(\mathbf{r})=\int d\tau\xi^B(\mathbf{r})U^A(\mathbf{r})=0,$$
$$\int d\tau\xi^A(\mathbf{r})U^A(\mathbf{r})=\int d\tau\xi^B(\mathbf{r})U^B(\mathbf{r})=1.$$

Such functions are

$$\xi^A=\frac{I\mathrm{X}^A-J\mathrm{X}^B}{I^2-J^2};\quad \xi^B=\frac{I\mathrm{X}^B-J\mathrm{X}^A}{I^2-J^2}. \tag{34}$$

We expand ϕ, π into coupled and uncoupled components:

$$\phi(\mathbf{r})=(4\pi)^{-\frac{1}{2}}\{\phi_0{}^A\xi^A(\mathbf{r})+\phi_0{}^B\xi^B(\mathbf{r})\}+\phi_1(\mathbf{r}),$$
$$\pi(\mathbf{r})=(4\pi)^{\frac{1}{2}}\{\pi_0{}^AU^A(\mathbf{r})+\pi_0{}^BU^B(\mathbf{r})\}+\pi_1(\mathbf{r}), \tag{35}$$

where we require

$$\int d\tau\phi_1(\mathbf{r})U^A(\mathbf{r})=\int d\tau\phi_1(\mathbf{r})U^B(\mathbf{r})=0,$$
$$\int d\tau\pi_1(\mathbf{r})\xi^A(\mathbf{r})=\int d\tau\pi_1(\mathbf{r})\xi^B(\mathbf{r})=0. \tag{36}$$

The amplitudes ϕ_0 and π_0 are determined by

$$\phi_0{}^A=(4\pi)^{\frac{1}{2}}\int d\tau\phi(\mathbf{r})U^A(\mathbf{r});$$
$$\phi_0{}^B=(4\pi)^{\frac{1}{2}}\int d\tau\phi(\mathbf{r})U^B(\mathbf{r}),$$
$$\pi_0{}^A=(4\pi)^{-\frac{1}{2}}\int d\tau\pi(\mathbf{r})\xi^A(\mathbf{r}); \tag{37}$$
$$\pi_0{}^B=(4\pi)^{-\frac{1}{2}}\int d\tau\pi(\mathbf{r})\xi^B(\mathbf{r}).$$

$(\phi_0{}^A,\ \pi_0{}^A)$ and $(\phi_0{}^B,\ \pi_0{}^B)$ are conjugate pairs. However,

$$[\pi_1(\mathbf{r}),\phi_1(\mathbf{r}')]=-i[\delta(\mathbf{r}-\mathbf{r}')$$
$$-U^A(\mathbf{r})\xi^A(\mathbf{r}')-U^B(\mathbf{r})\xi^B(\mathbf{r}')]. \tag{38}$$

In terms of these variables

$$H=N(\bar{\pi}_0{}^A\pi_0{}^A+\bar{\pi}_0{}^B\pi_0{}^B)+M(\bar{\pi}_0{}^A\pi_0{}^B+\bar{\pi}_0{}^B\pi_0{}^A)$$
$$+[1/(I^2-J^2)][I(\bar{\phi}_0{}^A\phi_0{}^A+\bar{\phi}_0{}^B\phi_0{}^B)$$
$$-J(\bar{\phi}_0{}^A\phi_0{}^B+\bar{\phi}_0{}^B\phi_0{}^A)]$$
$$+g[\tau_-{}^A\bar{\phi}_0{}^A+\tau_+{}^A\phi_0{}^A+\tau_-{}^B\bar{\phi}_0{}^B+\tau_+{}^B\phi_0{}^B]$$
$$+(4\pi)^{\frac{1}{2}}\pi_0{}^A\int d\tau U^A(\mathbf{r})\bar{\pi}_1(\mathbf{r})$$
$$+(4\pi)^{\frac{1}{2}}\bar{\pi}_0{}^A\int d\tau U^A(\mathbf{r})\pi_1(\mathbf{r})$$
$$+(4\pi)^{\frac{1}{2}}\pi_0{}^B\int d\tau U^B(\mathbf{r})\bar{\pi}_1(\mathbf{r})$$
$$+(4\pi)^{\frac{1}{2}}\bar{\pi}_0{}^B\int d\tau U^B(\mathbf{r})\pi_1(\mathbf{r})$$
$$+\int d\tau[\bar{\pi}_1(\mathbf{r})\pi_1(\mathbf{r})+\bar{\phi}_1(\mathbf{r})\omega^2\phi_1(\mathbf{r})]. \tag{39}$$

We introduce polar coordinates for ϕ_0^A, ϕ_0^B:

$$\phi_0^A = q_0^A \exp(-i\theta_A); \quad \phi_0^B = q_0^B \exp(-i\theta_B).$$

It is more convenient, however, to use instead of θ_A, θ_B the quantities

$$\theta = (\theta_A+\theta_B)/2; \quad \psi = (\theta_A-\theta_B)/2,$$
$$p_\theta = p_\theta^A + p_\theta^B; \quad p_\psi = p_\theta^A - p_\theta^B.$$

The canonical transformation takes the form:

$$\begin{aligned}
&\phi_0^A = q_0^A e^{-i(\theta+\psi)};\\
&\pi_0^A = [e^{i(\theta+\psi)}/2][p_0^A + (i/q_0^A)\\
&\qquad \times\{(p_\theta+p_\psi)/2+\tfrac{1}{2}-\tfrac{1}{2}\Sigma\}],\\
&\bar\phi_0^A = q_0^A e^{i(\theta+\psi)};\\
&\bar\pi_0^A = [e^{-i(\theta+\psi)}/2][p_0^A - (i/q_0^A)\\
&\qquad \times\{(p_\theta+p_\psi)/2-\tfrac{1}{2}-\tfrac{1}{2}\Sigma\}],\\
&\phi_0^B = q_0^B e^{-i(\theta-\psi)};\\
&\pi_0^B = [e^{i(\theta-\psi)}/2][p_0^B + (i/q_0^B)\\
&\qquad \times\{(p_\theta-p_\psi)/2+\tfrac{1}{2}-\tfrac{1}{2}\Sigma\}],\\
&\bar\phi_0^B = q_0^B e^{i(\theta-\psi)};\\
&\bar\pi_0^B = [e^{-i(\theta-\psi)}/2][p_0^B - (i/q_0^B)\\
&\qquad \times\{(p_\theta-p_\psi)/2-\tfrac{1}{2}-\tfrac{1}{2}\Sigma\}],\\
&\phi_1(\mathbf{r}) = q_1(\mathbf{r})e^{-i\theta}; \quad \pi_1(\mathbf{r}) = p_1(\mathbf{r})e^{+i\theta},\\
&\bar\phi_1(\mathbf{r}) = \bar q_1(\mathbf{r})e^{i\theta}; \quad \bar\pi_1(\mathbf{r}) = \bar p_1(\mathbf{r})e^{-i\theta},\\
&\Sigma = -i\int d\mathbf{r}[\pi_1(\mathbf{r})\phi_1(\mathbf{r}) - \bar\pi_1(\mathbf{r})\bar\phi_1(\mathbf{r})].
\end{aligned} \tag{40}$$

The independent conjugate pairs are (p_0^A, q_0^A), (p_0^B, q_0^B), (p_θ, θ), and (p_ψ, ψ). $p_1(\mathbf{r})$ and $q_1(\mathbf{r})$ commute with the other quantities, but

$$[p_1(\mathbf{r}), q_1(\mathbf{r}')] = -i[\delta(\mathbf{r}-\mathbf{r}') - U^A(\mathbf{r})\xi^A(\mathbf{r}') - U^B(\mathbf{r})\xi^B(\mathbf{r}')].$$

The total charge is

$$\begin{aligned}
&-i\int d\mathbf{r}[\pi(\mathbf{r})\phi(\mathbf{r}) - \bar\pi(\mathbf{r})\bar\phi(\mathbf{r})]\\
&= -i[\pi_0^A\phi_0^A - \bar\pi_0^A\bar\phi_0^A] - i[\pi_0^B\phi_0^B - \bar\pi_0^B\bar\phi_0^B] + \Sigma\\
&= \tfrac{1}{2}(p_\theta+p_\psi-\Sigma) + \tfrac{1}{2}(p_\theta-p_\psi-\Sigma) + \Sigma = p_\theta.
\end{aligned}$$

Before writing down H, we shall consider just the leading, or interaction term. This becomes

$$g[q_0^A(\tau_-^A e^{i(\theta+\psi)} + \tau_+^A e^{-i(\theta+\psi)}) + q_0^B(\tau_-^B e^{i(\theta-\psi)} + \tau_+^B e^{-i(\theta-\psi)})].$$

Again apply an S transformation, where

$$S = \exp[i\tau_z^A(\theta+\psi)/2]\exp[i\tau_z^B(\theta-\psi)/2].$$

The interaction energy becomes

$$g[q_0^A\tau_x^A + q_0^B\tau_x^B].$$

This is diagonal in a representation in which τ_z^A and τ_x^B are diagonal. The lowest eigenvalue is $-g[q_0^A+q_0^B]$. Off diagonal terms coupling widely separated states are introduced elsewhere in H, since under the S transformation

$$p_\theta \to p_\theta + \tfrac{1}{2}(\tau_z^A+\tau_z^B) \quad \text{and} \quad p_\psi \to p_\psi + \tfrac{1}{2}(\tau_z^A-\tau_z^B).$$

As before, we neglect terms linear in τ_z^A and τ_z^B since these quantities have no diagonal matrix elements for the lowest eigenstate of the interaction energy. The Hamiltonian becomes (neglecting Σ as before):

$$\begin{aligned}
H^{11} &= (N/4)[(p_0^A)^2 + (p_\theta+p_\psi)^2/4(q_0^A)^2]\\
&\quad + (N/4)[(p_0^B)^2 + (p_\theta-p_\psi)^2/4(q_0^B)^2]\\
&\quad + \tfrac{1}{2}M\cos 2\psi[p_0^A p_0^B + (p_\theta^2 - p_\psi^2)/4q_0^A q_0^B]\\
&\quad + (M/4)\sin 2\psi[p_0^A(p_\theta-p_\psi)/q_0^B\\
&\quad - p_0^B(p_\theta+p_\psi)/q_0^A] + [1/(I^2-J^2)]\\
&\quad \times[I\{(q_0^A)^2 + (q_0^B)^2\} - 2Jq_0^A q_0^B\cos 2\psi]\\
&\quad - g(q_0^A+q_0^B) + (4\pi)^{\frac{1}{2}}(p_0^A/2)\int d\mathbf{r}\, U^A(\mathbf{r})\\
&\quad \times[p_1(\mathbf{r})e^{-i\psi} + \bar p_1(\mathbf{r})e^{i\psi}] + (4\pi)^{\frac{1}{2}}(p_0^B/2)\\
&\quad \times\int d\mathbf{r}\, U^B(\mathbf{r})[p_1(\mathbf{r})e^{i\psi} + \bar p_1(\mathbf{r})e^{-i\psi}]\\
&\quad + i(4\pi)^{\frac{1}{2}}\{(p_\theta+p_\psi)/4q_0^A\}\\
&\quad \times\int d\mathbf{r}\, U^A(\mathbf{r})[\bar p_1(\mathbf{r})e^{i\psi} - p_1(\mathbf{r})e^{-i\psi}]\\
&\quad + (4\pi)^{\frac{1}{2}}i\{(p_\theta-p_\psi)/4q_0^B\}\\
&\quad \times\int d\mathbf{r}\, U^B(\mathbf{r})[\bar p_1(\mathbf{r})e^{-i\psi} - p_1(\mathbf{r})e^{i\psi}]\\
&\quad + \int d\mathbf{r}[\bar p_1(\mathbf{r})p_1(\mathbf{r}) + \bar q_1(\mathbf{r})\omega^2 q_1(\mathbf{r})].
\end{aligned} \tag{41}$$

[11] The argument for the neglect of terms involving Σ is the same as in note (6). Where products of the form $p_\psi f(\psi)$ appear, they will always be considered symmetrized.

1. *Freezing of the Isotopic Spin*

We first concern ourselves with the elimination of the linear term. This requires shifts in the origins of q_0^A and q_0^B:

$$\begin{aligned} q_0^A &= Q_0^A + (g/2)(I^2-J^2)/(I-J\cos 2\psi), \\ q_0^B &= Q_0^B + (g/2)(I^2-J^2)/(I-J\cos 2\psi). \end{aligned} \tag{42}$$

The part of H quadratic in q_0^A and q_0^B becomes

$$\begin{aligned} &-(g^2/2)(I^2-J^2)/(I-J\cos 2\psi) \\ &\quad +[1/(I^2-J^2)][I\{(Q_0^A)^2+(Q_0^B)^2\} \\ &\quad\quad -2JQ_0^AQ_0^B\cos 2\psi]. \end{aligned} \tag{43}$$

The first term is the static self-energy of the two-particle system and the dominant part of H in the limit of strong coupling. It is a function of the separation of the two sources through its dependence on J. ψ is the angle variable whose canonical conjugate is $p_\psi = p_{\theta A} - p_{\theta B}$, the difference of charges. In the limit of large g, ψ will adjust itself so as to make the energy a minimum, i.e., $\cos 2\psi = 1$, $\psi = 0$ or π. In this limit, the leading term becomes simply

$$-(g^2/2)(I+J), \tag{44}$$

a result analogous to that obtained in II for the classical symmetrical scalar theory. For $\kappa a \ll 1$, the part of (44) depending on the separation, $-g^2J/2$, reduces to $-g^2(\mu c^2)e^{-\kappa d}/2\kappa d$, where d is the separation. Because of its non-exchange character, this is an inadmissable potential for nuclear problems.

The condition $\psi = 0$ or $\psi = \pi$ describes a "freezing" of the two isotopic spins with respect to each other. It does not follow that this freezing will occur for all values of d because the leading potential term—that of order g^2—falls off rapidly with increasing d and may eventually be dominated by other terms in the Hamiltonian whose minimizing does not require the freezing of the isotopic spin. That this is indeed the case may be seen by considering the approach of two heavy particles. At infinite separation they may be thought of simply as two independent systems such as described in Section IIIA. They have, together, an energy given by (31):

$$H = -g^2I/2 + 4\pi(p_{\theta_1}^2 + p_{\theta_2}^2) \Big/ g^2 \int d\mathbf{r}\{\mathrm{X}(\mathbf{r})\}^2,$$

which can also be written

$$H = -g^2I/2 + \mu c^2(p_\theta^2 + p_\psi^2)/g^2. \tag{45}$$

At this stage the value of ψ is completely arbitrary. As the particles approach each other, corrections appear to both terms in (45). By comparison with (43) one sees that the g^2 term gets a correction $-g^2J\cos 2\psi/2$. The isobar energy levels are also perturbed, but the correction is small down to separations of the order of κ^{-1}. For the purposes of this argument we will not be concerned with smaller separations and hence will use the second term in (45) unchanged. We can predict that freezing will set in when the separation becomes less than a certain critical value determined by

$$\kappa/g^2 = -g^2J/2,$$

or

$$2/g^4 = e^{-\kappa d}/\kappa d. \tag{46}$$

When the particles have approached to a separation equal to the range, $\kappa d = 1$, the isotopic spins will still be "liquid" if g is not larger than 1.2. For larger values of g, freezing will take place at larger separations, according to (46). An essentially identical, but somewhat more trustworthy estimate of the freezing radius will be given later by (55).

2. *Exchange Forces at Large Separation*

For separations larger than the critical one defined above, this theory does indeed lead to exchange forces. For here we may treat the expression $-g^2J\cos 2\psi/2$ as a perturbation to the zero-order energy, $\mu c^2 p_\psi^2/g^2$. The unperturbed stationary states are $\begin{cases}\sin n\psi \\ \cos n\psi\end{cases}$, where n gives the number of charge units by which the two systems differ. If the charge difference is zero, the perturbation vanishes in first order (proton-proton or neutron-neutron). For one unit charge difference, there are two independent states, symmetric and anti-symmetric in the isotopic spin coordinate, namely $\cos\psi$ and $\sin\psi$. The corresponding perturbation energies are

$$\begin{aligned} V_{\text{anti-s}} &= +g^2J/4, \\ V_{\text{sym}} &= -g^2J/4. \end{aligned} \tag{47}$$

This differs only by the factor $\frac{1}{4}$ from the result obtained in perturbation theory. The occurrence

of this factor is connected with the fact, which will be demonstrated presently, that half of the field [see, for comparison, H_y of (25)] consists of unbound mesotrons which contribute nothing in order g^2 to the self-field of the systems. The interaction (47) has numerous defects. If the antisymmetry of the total wave function of the deuteron is invoked, then the state $\sin\psi$ can be identified with the "triplet" state of the deuteron, and $\cos\psi$ with the "singlet." Equation (47) would then predict the singlet to lie lower, in contradiction to experience. Furthermore, it could not explain the quadrupole moment of the deuteron. The strong coupling theory has the additional weakness that the exchange character of the force may disappear inside a critical freezing radius. It will be useful, for comparison with the pseudoscalar theory which will be treated later, to investigate the freezing condition more thoroughly and without using the approximation introduced above.

3. *The "Almost Frozen" System*

We consider values of g and of the separation which are of such a magnitude that the minimum of H is determined, to first order, by minimizing the g^2 term in (43). In other words, we will consider ψ to be in the neighborhood of 0 or π, so that $\cos 2\psi \sim 1-2\psi^2$. In the remainder of the Hamiltonian, we keep only the leading terms in the expansion of $\cos 2\psi$, $\sin 2\psi$, etc. We obtain

$$\begin{aligned}H=&(N/4)[(p_0{}^A)^2+(p_\theta+p_\psi)^2/4(q_0{}^A)^2]\\&+(N/4)[(p_0{}^B)^2+(p_\theta-p_\psi)^2/4(q_0{}^B)^2]\\&+(M/2)[p_0{}^Ap_0{}^B+(p_\theta{}^2-p_\psi{}^2)/4q_0{}^Aq_0{}^B]\\&-g^2(I+J)/2+g^2J\psi^2(I+J)/(I-J)\\&+[1/(I^2-J^2)][I\{(Q_0{}^A)^2+(Q_0{}^B)^2\}\\&-2JQ_0{}^AQ_0{}^B]+(4\pi)^{\frac{1}{2}}(p_0{}^A/2)\int d\mathbf{r}\,U^A(\mathbf{r})\\&\times[p_1(\mathbf{r})+\bar{p}_1(\mathbf{r})]+(4\pi)^{\frac{1}{2}}(p_0{}^B/2)\\&\times\int d\mathbf{r}\,U^B(\mathbf{r})[p_1(\mathbf{r})+\bar{p}_1(\mathbf{r})]\\&+(4\pi)^{\frac{1}{2}}i[(p_\theta+p_\psi)/4q_0{}^A]\int d\mathbf{r}\,U^A(\mathbf{r})\\&\times[\bar{p}_1(\mathbf{r})-p_1(\mathbf{r})]+(4\pi)^{\frac{1}{2}}i[(p_\theta-p_\psi)/4q_0{}^B]\\&\times\int d\mathbf{r}\,U^B(\mathbf{r})[\bar{p}_1(\mathbf{r})-p_1(\mathbf{r})]\\&+\int d\mathbf{r}[\bar{p}_1(\mathbf{r})p_1(\mathbf{r})+\bar{q}_1(\mathbf{r})\omega^2q_1(\mathbf{r})]. \quad (48)\end{aligned}$$

Eigenstates for oscillations of the system about the position of minimum energy may once again be obtained by resolving p_1 and q_1 into real and imaginary parts:

$$\begin{aligned}p_1(\mathbf{r})&=(1/\sqrt{2})[p_x(\mathbf{r})+ip_y(\mathbf{r})],\\q_1(\mathbf{r})&=(1/\sqrt{2})[q_x(\mathbf{r})-iq_y(\mathbf{r})],\\H&=-g^2(I+J)/2+H_x+H_y,\end{aligned}$$

where

$$\begin{aligned}H_x=&(N/4)[(p_0{}^A)^2+(p_0{}^B)^2]+(M/2)p_0{}^Ap_0{}^B\\&+[I\{(Q_0{}^A)^2+(Q_0{}^B)^2\}-2JQ_0{}^AQ_0{}^B]/(I^2-J^2)\\&+(4\pi)^{\frac{1}{2}}(p_0{}^A/\sqrt{2})\int d\mathbf{r}\,U^A(\mathbf{r})p_x(\mathbf{r})\\&+(4\pi)^{\frac{1}{2}}(p_0{}^B/\sqrt{2})\int d\mathbf{r}\,U^B(\mathbf{r})p_x(\mathbf{r})\\&+\tfrac{1}{2}\int d\mathbf{r}[\{p_x(\mathbf{r})\}^2+q_x(\mathbf{r})\omega^2q_x(\mathbf{r})]. \quad (49)\end{aligned}$$

Introduce the canonically conjugate variables

$$\begin{aligned}\phi_x(\mathbf{r})&=(4\pi)^{-\frac{1}{2}}\{Q_0{}^A\xi^A(\mathbf{r})+Q_0{}^B\xi^B(\mathbf{r})\}+(1/\sqrt{2})q_x(\mathbf{r}),\\\pi_x(\mathbf{r})&=(4\pi)^{\frac{1}{2}}\{\tfrac{1}{2}p_0{}^AU^A(\mathbf{r})\\&\qquad+\tfrac{1}{2}p_0{}^BU^B(\mathbf{r})\}+(1/\sqrt{2})p_x(\mathbf{r}),\\H_x&=\int d\mathbf{r}[\{\pi_x(\mathbf{r})\}^2+\phi_x(\mathbf{r})\omega^2\phi_x(\mathbf{r})],\end{aligned}$$

representing a system of unscattered mesotrons. Meanwhile

$$\begin{aligned}H_y=&(N/16)[(p_\theta+p_\psi)^2/(q_0{}^A)^2+(p_\theta-p_\psi)^2/(q_0{}^B)^2]\\&+(M/8)(p_\theta{}^2-p_\psi{}^2)/q_0{}^Aq_0{}^B+g^2J\psi^2(I+J)/(I-J)\\&+(4\pi)^{\frac{1}{2}}\{\sqrt{2}(p_\theta+p_\psi)/4q_0{}^A\}\int d\mathbf{r}p_y(\mathbf{r})\,U^A(\mathbf{r})\\&+(4\pi)^{\frac{1}{2}}\{\sqrt{2}(p_\theta-p_\psi)/4q_0{}^B\}\int d\mathbf{r}p_y(\mathbf{r})\,U^B(\mathbf{r})\\&+\tfrac{1}{2}\int d\mathbf{r}[\{p_y(\mathbf{r})\}^2+q_y(\mathbf{r})\omega^2q_y(\mathbf{r})]. \quad (50)\end{aligned}$$

The terms linear in p_y are to be eliminated by a unitary transformation of the type (27), (29).

To first order, q_ν is unchanged and

$$p_\nu(\mathbf{r})=p_\nu'(\mathbf{r})-((4\pi)^{\frac{1}{2}}/\sqrt{8}q_0)\times[(p_\theta+p_\psi)(U^A(\mathbf{r})-cX^A(\mathbf{r})-dX^B(\mathbf{r}))+(p_\theta-p_\psi)(U^B(\mathbf{r})-dX^A(\mathbf{r})-cX^B(\mathbf{r}))]. \quad (51)$$

We have replaced $q_0{}^A$ and $q_0{}^B$ by their equilibrium values

$$q_0{}^A=q_0{}^B=q_0=\frac{g}{2}(I+J).$$

The constants c and d [which may be determined, e.g., by the condition that $p_\nu'(\mathbf{r})$ be orthogonal to $\xi^A(\mathbf{r})$ and $\xi^B(\mathbf{r})$, a condition that is already fulfilled by $p_\nu(\mathbf{r})$] are given by

$$c=\frac{IR-SJ}{R^2-S^2};\quad d=\frac{JR-SI}{R^2-S^2},$$

where

$$R=\int d\mathbf{r}[X^A(\mathbf{r})]^2=\int d\mathbf{r}[X^B(\mathbf{r})]^2,$$

$$S=\int d\mathbf{r}X^A(\mathbf{r})X^B(\mathbf{r}).$$

The condition for the convergence of the expansion (51) is $p_\theta/g\ll 1$ and $p_\psi/g\ll 1$. H_ν becomes

$$H_\nu=\tfrac{1}{2}\int d\mathbf{r}[\{p_\nu'(\mathbf{r})\}^2+q_\nu'(\mathbf{r})\omega^2q_\nu'(\mathbf{r})]+\frac{4\pi p_\theta{}^2}{8q_0{}^2}\frac{(I+J)^2}{R+S}+\frac{4\pi p_\psi{}^2}{8q_0{}^2}\frac{(I-J)^2}{R-S}+g^2J\psi^2\frac{I+J}{I-J}. \quad (52)$$

The first two terms give the energy of a set of scattered waves, p_ν' and q_ν' being quasi-conjugate quantities satisfying (38). The isobar energy is

$$H_I=\frac{4\pi p_\theta{}^2}{2g^2(R+S)}+\frac{4\pi p_\psi{}^2}{2g^2(R-S)}\left(\frac{I-J}{I+J}\right)^2+g^2J\psi^2\frac{I+J}{I-J}. \quad (53)$$

Since $\tau_z{}^A$ and $\tau_z{}^B$ are diagonal, the average heavy particle charge is the expectation value of $(1+\tau_z{}^A)/2+(1+\tau_z{}^B)/2=1$. Consequently, if M is the total charge, the first term can be written

$$\frac{4\pi(M-1)^2}{2(R+S)g^2},$$

giving a parabolic dependence on the total charge of the two particle system, the minimum lying at $M=1$.

The rest of H_I describes harmonic oscillations of ψ about the "frozen" position. The zero-point amplitude of these oscillations is

$$\bar{\psi}=\frac{1}{g}\left[\left(\frac{I-J}{I+J}\right)^3\frac{4\pi}{8J(R-S)}\right]^{\frac{1}{2}}. \quad (54)$$

For sources separated by d and of radius $a\ll d$ with a defined by

$$a^{-1}=4\pi\int d\mathbf{r}U^A(\mathbf{r})\frac{1}{\omega^2}U^A(\mathbf{r})=\int\int d\mathbf{r}d\mathbf{r}'U^A(\mathbf{r})\frac{U^B(\mathbf{r}')\exp[-\kappa|\mathbf{r}-\mathbf{r}'|]}{|\mathbf{r}-\mathbf{r}'|};$$

the various constants are given (approximately) by:

$$I=1/a,$$

$$J=e^{-\kappa d}/d,$$

$$R/4\pi=1/2\kappa,$$

$$S/4\pi=e^{-\kappa d}/2\kappa.$$

Since $J/I\ll 1$, (54) simplifies to

$$\bar{\psi}=\frac{1}{g}\left[\frac{4\pi}{8J(R-S)}\right]^{\frac{1}{2}}. \quad (55)$$

We may take $\bar{\psi}=1$ as the maximum amplitude for which the isotopic spins can be regarded as even approximately frozen. This determines a value for g corresponding to any given value for d. For $\kappa d=1$, this gives $g=1.0$ as a minimum value below which the system will start to thaw and exchange forces will make an appearance. But since $g>1$ is a condition for the validity of the above calculations, it is clear that with the strong coupling hypothesis, it is not possible to obtain exchange forces in the charged scalar theory for separations as small as $(\kappa)^{-1}$.

IV. THE NEUTRAL PSEUDOSCALAR THEORY

This theory, in the perturbation approximation, gives charge independent, but spin dependent forces through a coupling of the heavy particle spin with the gradient of the mesotron wave function. We shall treat first the one-source, then the two-source problem.

A. One Nuclear Particle

The Hamiltonian is:

$$H=\tfrac{1}{2}\int d\mathbf{r}[\{\pi(\mathbf{r})\}^2+\phi(\mathbf{r})\omega^2\phi(\mathbf{r})]$$
$$-\{g(4\pi)^{\frac{1}{2}}/\kappa\}\int d\mathbf{r}U(\mathbf{r})\boldsymbol{\sigma}\cdot\mathbf{grad}\,\phi(\mathbf{r}). \quad (56)$$

$\boldsymbol{\sigma}$ is the heavy particle's spin vector. All quantities are defined as before with the exception of the following:

$$N=4\pi\int d\mathbf{r}\left[\frac{\partial}{\partial x_i}U(\mathbf{r})\right]^2, \qquad i=1,\,2,\,3$$

$$\mathrm{X}(\mathbf{r})=4\pi\omega^{-2}U(\mathbf{r}),$$

$$I=\int d\mathbf{r}\frac{\partial \mathrm{X}(\mathbf{r})}{\partial x_i}\frac{\partial U(\mathbf{r})}{\partial x_i}, \qquad i=1,\,2,\,3$$

$$\xi=\mathrm{X}/I \text{ so that } \int d\mathbf{r}\frac{\partial\xi(\mathbf{r})}{\partial x_i}\frac{\partial U(\mathbf{r})}{\partial x_j}=\delta_{ij}.$$

We split ϕ, π as follows:

$$\phi(\mathbf{r})=(4\pi)^{-\frac{1}{2}}\boldsymbol{\phi}_0\cdot\mathbf{grad}\,\xi(\mathbf{r})+\phi_1(\mathbf{r}),$$
$$\pi(\mathbf{r})=(4\pi)^{\frac{1}{2}}\boldsymbol{\pi}_0\cdot\mathbf{grad}\,U(\mathbf{r})+\pi_1(\mathbf{r}) \quad (57)$$

with auxiliary conditions

$$\int d\mathbf{r}\phi_1(\mathbf{r})\,\mathbf{grad}\,U(\mathbf{r})=0,$$

$$\int d\mathbf{r}\pi_1(\mathbf{r})\,\mathbf{grad}\,\xi(\mathbf{r})=0.$$

It follows that

$$\boldsymbol{\phi}_0=(4\pi)^{\frac{1}{2}}\int d\mathbf{r}\phi(\mathbf{r})\,\mathbf{grad}\,U(\mathbf{r});$$

$$\boldsymbol{\pi}_0=(4\pi)^{-\frac{1}{2}}\int d\mathbf{r}\pi(\mathbf{r})\,\mathbf{grad}\,\xi(\mathbf{r}). \quad (58)$$

$(\boldsymbol{\pi}_{0i}, \boldsymbol{\phi}_{0i})$ are canonical pairs, whereas

$$[\pi_1(\mathbf{r}), \phi_1(\mathbf{r}')]=-i[\delta(\mathbf{r}-\mathbf{r}')$$
$$-\mathbf{grad}\,U(\mathbf{r})\cdot\mathbf{grad}\,\xi(\mathbf{r}')].$$

We obtain

$$H=\tfrac{1}{2}N(\boldsymbol{\pi}_0)^2+(\boldsymbol{\phi}_0)^2/2I+\frac{g}{\kappa}\boldsymbol{\sigma}\cdot\boldsymbol{\phi}_0$$
$$+(4\pi)^{\frac{1}{2}}\boldsymbol{\pi}_0\cdot\int d\mathbf{r}\pi_1(\mathbf{r})\,\mathbf{grad}\,U(\mathbf{r})$$
$$+\tfrac{1}{2}\int d\mathbf{r}[\{\pi_1(\mathbf{r})\}^2+\phi_1(\mathbf{r})\omega^2\phi_1(\mathbf{r})]. \quad (59)$$

The cross term in $\boldsymbol{\pi}_0\pi_1(\mathbf{r})$ may be eliminated by a unitary transformation of the type (27), with

$$U=+(4\pi)^{\frac{1}{2}}\boldsymbol{\pi}_0\cdot\int d\mathbf{r}\phi_1(\mathbf{r})\,\mathbf{grad}\,\xi(\mathbf{r})/R, \quad (60)$$

with

$$R=\int d\mathbf{r}[\partial\xi(\mathbf{r})/\partial x_i]^2, \qquad i=1,\,2,\,3$$

$$\pi_1(\mathbf{r})=\pi_1'(\mathbf{r})-(4\pi)^{\frac{1}{2}}\boldsymbol{\pi}_0\cdot[\mathbf{grad}\,U(\mathbf{r})-\mathbf{grad}\,\xi(\mathbf{r})/R]$$
$$\phi_1(\mathbf{r})=\phi_1'(\mathbf{r}).$$

Substitution gives

$$H=\frac{4\pi}{2R}(\boldsymbol{\pi}_0)^2+\frac{1}{2I}(\boldsymbol{\phi}_0)^2+\frac{g}{\kappa}\boldsymbol{\sigma}\cdot\boldsymbol{\phi}_0$$
$$+\tfrac{1}{2}\int d\mathbf{r}[\{\pi_1'(\mathbf{r})\}^2+\phi_1'(\mathbf{r})\omega^2\phi_1'(\mathbf{r})]. \quad (61)$$

It is to be observed that (60) also generates a change in $\boldsymbol{\phi}_0$ which is not taken account of here. A more detailed analysis, parallel to that carried out for the scalar field, shows that this correction is negligible in the limit of strong coupling. The effect of the additional terms which would appear in H would be to spoil the exact separation of (61) into a set (π_1', ϕ_1') of unbound waves and a set $(\boldsymbol{\pi}_0, \boldsymbol{\phi}_0)$ of bound states. The condition governing the validity of this approximation is $(\kappa a/g)L\ll 1$, where L is the total angular momentum of the bound mesotron field defined below.[12]

[12] A more complete discussion of the strong coupling condition in this case is to be found in W. Pauli and S. M. Dancoff, Phys. Rev. **62**, 85 (1942).

We assume that none of the (π_1', ϕ_1') states are excited, and proceed to treat the system defined by

$$H=\frac{4\pi}{2R}(\pi_0)^2+\frac{1}{2I}(\phi_0)^2+\frac{g}{\kappa}\boldsymbol{\sigma}\cdot\boldsymbol{\phi}_0. \tag{62}$$

It is convenient to introduce an orthogonal system of unit vectors, $\mathbf{n}_1$, $\mathbf{n}_2$, $\mathbf{n}_3$, defined as follows: $\mathbf{n}_3$ is parallel to $\boldsymbol{\phi}_0$ and $\mathbf{n}_1$ has the direction of the intersection with the xy plane of the plane perpendicular to $\mathbf{n}_3$. The co-latitude and azimuth of $\mathbf{n}_3$ are α and β, respectively. The components of the unit vectors are

$\mathbf{n}_1$: $(-\sin\beta; \cos\beta; 0)$,

$\mathbf{n}_2$: $(-\cos\alpha\cos\beta; -\cos\alpha\sin\beta; \sin\alpha)$,

$\mathbf{n}_3$: $(\sin\alpha\cos\beta; \sin\alpha\sin\beta; \cos\alpha)$.

It follows that

$$\begin{aligned}\boldsymbol{\phi}_0&=q_0\mathbf{n}_3,\\ \boldsymbol{\pi}_0&=p_0\mathbf{n}_3-\mathbf{n}_2p_\alpha/q_0+\mathbf{n}_1p_\beta\Big/q_0\sin\alpha.\end{aligned} \tag{63}$$

Canonical pairs are (p_0, q_0), (p_α, α), and (p_β, β). The angular momentum of the mesotron field is

$$\mathbf{L}=\int d\mathbf{r}\boldsymbol{\pi}(\mathbf{r})\mathfrak{L}\boldsymbol{\phi}(\mathbf{r}),$$

where $\mathfrak{L}$ is the angular momentum operator. For our case, this becomes

$$\begin{aligned}\mathbf{L}&=[\boldsymbol{\phi}_0\times\boldsymbol{\pi}_0]\\ &=p_\alpha\mathbf{n}_1+p_\beta\mathbf{n}_2/\sin\alpha.\end{aligned}$$

We can also write

$$\boldsymbol{\pi}_0=p_0\mathbf{n}_3+(\mathbf{L}\times\mathbf{n}_3)/q_0.$$

The energy becomes

$$H=(4\pi/2R)[p_0^2+(L^2-1)/q_0^2]+q_0^2/2I+(g/\kappa)q_0\boldsymbol{\sigma}\cdot\mathbf{n}_3, \tag{64}$$

where $L^2=p_\alpha^2+p_\beta^2/\sin^2 a$.

We transform to a representation in which the interaction energy is diagonal. The corresponding unitary operator is $S=\exp[i\sigma_y\alpha/2]\exp[i\sigma_z\beta/2]$. The transformation $F'=SF$ is applied to the wave function and $H'=SHS^{-1}$ to the Hamiltonian. In particular, $\boldsymbol{\sigma}\cdot\mathbf{n}_3$ is transformed into σ_z. By choosing for the states of the heavy particle a representation in which σ_z is diagonal, the interaction energy is diagonalized with eigenvalues $\pm(g/\kappa)q_0$. The angular momentum becomes

$$\mathbf{L}\rightarrow\mathbf{L}-\tfrac{1}{2}[\mathbf{n}_1\sigma_y+(\mathbf{n}_2/\sin\alpha)\times(\sigma_z\cos\alpha-\sigma_x\sin\alpha)], \tag{65}$$

and its square is transformed into

$$L^2\rightarrow p_\alpha^2+p_\beta^2/\sin^2\alpha+\tfrac{1}{4}+1/4\sin^2\alpha-p_\beta\sigma_z\cos\alpha/\sin^2\alpha. \tag{66}$$

Terms linear in σ_x and σ_y have been neglected as they couple widely separated states. Aside from the additive constant, $\frac{1}{4}$, (66) is simply the square of the total angular momentum of a completely symmetric rigid rotator, the angular momentum corresponding to the third Euler angle being $\sigma_z/2$. The eigenvalues of (66) are therefore $j(j+1)-\frac{3}{4}$, where j is the quantum number for the total angular momentum of the heavy particle plus mesotron field.

We choose the lowest eigenvalue of the interaction energy, and get

$$H=\frac{4\pi}{2R}\left[p_0^2+\frac{J^2-\frac{3}{4}}{q_0^2}\right]+q_0^2/2I-gq_0/\kappa. \tag{67}$$

The linear term is eliminated by the shift

$$Q_0=q_0-gI/\kappa,$$

with the result:

$$H=-g^2I/2\kappa^2+4\pi p_0^2/2R+Q_0^2/2I+(J^2-\tfrac{3}{4})/2Rq_0^2. \tag{68}$$

The leading term in (68) is the static self-energy. The two succeeding terms may be described as the energy of oscillation of the variable q_0 about its position of equilibrium, gI/κ. We treat the case where this degree of freedom is unexcited, i.e., when there are no positive energy mesotrons in the field. Hence, in the last term of (68) we substitute for q_0 its equilibrium value, and obtain for the isobar energy

$$H_I=(4\pi\kappa^2/2g^2I^2R)[j(j+1)-\tfrac{3}{4}].$$

For $\kappa a \ll 1$,

$$I^2R=\int d\mathbf{r}\left[\frac{\partial X(\mathbf{r})}{\partial x}\right]^2 \sim 4\pi/3a,$$
$$H_I=\frac{3\mu c^2}{2}(\kappa a/g^2)[j(j+1)-\tfrac{3}{4}], \tag{69}$$

in conventional units. The lowest state of this system is identified as the proton-neutron ($j=\frac{1}{2}$).

B. Two Nuclear Particles

The Hamiltonian is the following:

$$H=\tfrac{1}{2}\int d\mathbf{r}[\{\pi(\mathbf{r})\}^2+\phi(\mathbf{r})\omega^2\phi(\mathbf{r})]$$
$$-(g(4\pi)^{\frac{1}{2}}/\kappa)\int d\mathbf{r}[U(\mathbf{r}^A)\boldsymbol{\sigma}^A\cdot\mathbf{grad}\,\phi(\mathbf{r})$$
$$+U(\mathbf{r}^B)\boldsymbol{\sigma}^B\cdot\mathbf{grad}\,\phi(\mathbf{r})]. \tag{70}$$

Introduce

$$X(\mathbf{r}^A)=4\pi\omega^{-2}U(\mathbf{r}^A),$$
$$X(\mathbf{r}^B)=4\pi\omega^{-2}U(\mathbf{r}^B),$$
$$N=4\pi\int d\mathbf{r}\left[\frac{\partial U(\mathbf{r}^A)}{\partial x_i}\right]^2=4\pi\int d\mathbf{r}\left[\frac{\partial U(\mathbf{r}^B)}{\partial x_i}\right]^2,$$
$$M_i=4\pi\int d\mathbf{r}\frac{\partial U(\mathbf{r}^A)}{\partial x_i}\frac{\partial U(\mathbf{r}^B)}{\partial x_i}, \qquad i=1,\,2,\,3$$
$$I=\int d\mathbf{r}\frac{\partial X(\mathbf{r}^A)}{\partial x_i}\frac{\partial U(\mathbf{r}^A)}{\partial x_i}=\int d\mathbf{r}\frac{\partial X(\mathbf{r}^B)}{\partial x_i}\frac{\partial U(\mathbf{r}^B)}{\partial x_i},$$
$$J_i=\int d\mathbf{r}\frac{\partial X(\mathbf{r}^A)}{\partial x_i}\frac{\partial U(\mathbf{r}^B)}{\partial x_i}=\int d\mathbf{r}\frac{\partial X(\mathbf{r}^B)}{\partial x_i}\frac{\partial U(\mathbf{r}^A)}{\partial x_i}.$$

Note that all integrals vanish which involve derivatives with respect to two different x_i's. States orthogonal to the U's are defined as follows:

$$\int d\mathbf{r}\frac{\partial\xi_i(\mathbf{r}^A)}{\partial x_i}\frac{\partial U(\mathbf{r}^B)}{\partial x_i}=\int d\mathbf{r}\frac{\partial\xi_i(\mathbf{r}^B)}{\partial x_i}\frac{\partial U(\mathbf{r}^A)}{\partial x_i}=0,$$
$$\int d\mathbf{r}\frac{\partial\xi_i(\mathbf{r}^A)}{\partial x_i}\frac{\partial U(\mathbf{r}^A)}{\partial x_i}=\int d\mathbf{r}\frac{\partial\xi_i(\mathbf{r}^B)}{\partial x_i}\frac{\partial U(\mathbf{r}^B)}{\partial x_i}=1.$$

We find

$$\xi_i(\mathbf{r}^A)=\frac{IX(\mathbf{r}^A)-J_iX(\mathbf{r}^B)}{I^2-J_i^2};$$
$$\xi_i(\mathbf{r}^B)=\frac{IX(\mathbf{r}^B)-J_iX(\mathbf{r}^A)}{I^2-J_i^2}.$$

The fields are split as follows:

$$\phi(\mathbf{r})=(4\pi)^{-\frac{1}{2}}\Big\{\sum_i\phi_{0i}^A\frac{\partial}{\partial x_i}\xi_i(\mathbf{r}^A)$$
$$+\sum_i\phi_{0i}^B\frac{\partial}{\partial x_i}\xi_i(\mathbf{r}^B)\Big\}+\phi_1(\mathbf{r}) \tag{71}$$
$$\pi(\mathbf{r})=(4\pi)^{\frac{1}{2}}\{\pi_0^A\cdot\mathbf{grad}\,U(\mathbf{r}^A)$$
$$+\pi_0^B\cdot\mathbf{grad}\,U(\mathbf{r}^B)\}+\pi_1(\mathbf{r}),$$

with the auxiliary conditions:

$$\int d\mathbf{r}\phi_1(\mathbf{r})\frac{\partial}{\partial x_i}U(\mathbf{r}^A)=\int d\mathbf{r}\phi_1(\mathbf{r})\frac{\partial}{\partial x_i}U(\mathbf{r}^B)=0, \qquad i=1,\,2,\,3$$
$$\int d\mathbf{r}\pi_1(\mathbf{r})\frac{\partial}{\partial x_i}\xi_i(\mathbf{r}^A)=\int d\mathbf{r}\pi_1(\mathbf{r})\frac{\partial}{\partial x_i}\xi_i(\mathbf{r}^B)=0.$$

The amplitudes $\boldsymbol{\phi}_0$ and $\boldsymbol{\pi}_0$ are determined by

$$\phi_{0i}^A=(4\pi)^{\frac{1}{2}}\int d\mathbf{r}\phi(\mathbf{r})\frac{\partial}{\partial x_i}U(\mathbf{r}^A);$$
$$\phi_{0i}^B=(4\pi)^{\frac{1}{2}}\int d\mathbf{r}\phi(\mathbf{r})\frac{\partial}{\partial x_i}U(\mathbf{r}^B),$$
$$\pi_{0i}^A=(4\pi)^{-\frac{1}{2}}\int d\mathbf{r}\pi(\mathbf{r})\frac{\partial}{\partial x_i}\xi_i(\mathbf{r}^A);$$
$$\pi_{0i}^B=(4\pi)^{-\frac{1}{2}}\int d\mathbf{r}\pi(\mathbf{r})\frac{\partial}{\partial x_i}\xi_i(\mathbf{r}^B),$$
$$[\pi_{0i}^A,\,\phi_{0j}^A]=[\pi_{0i}^B,\,\phi_{0j}^B]=-i\delta_{ij},$$
$$[\pi_1(\mathbf{r}),\,\phi_1(\mathbf{r}')]=-i\Big[\delta(\mathbf{r}-\mathbf{r}')-\sum_i\frac{\partial}{\partial x_i}U(\mathbf{r}^A)$$
$$\times\frac{\partial}{\partial x_i}\xi_i(\mathbf{r}^{A'})-\sum_i\frac{\partial}{\partial x_i}U(\mathbf{r}^B)\frac{\partial}{\partial x_i}\xi_i(\mathbf{r}^{B'})\Big].$$

In terms of these variables

$$H=\frac{N}{2}\{(\pi_0{}^A)^2+(\pi_0{}^B)^2\}+\sum_i M_i\overset{A}{\pi}_{0i}\overset{B}{\pi}_{0i}$$
$$+\sum_i\frac{1}{I^2-J_i^2}\left[\frac{I}{2}\{(\overset{A}{\phi}_{0i})^2+(\overset{B}{\phi}_{0i})^2\}-J_i\overset{A}{\phi}_{0i}\overset{B}{\phi}_{0i}\right]$$
$$+(4\pi)^{\frac{1}{2}}\boldsymbol{\pi}_0{}^A\cdot\int d\mathbf{r}\boldsymbol{\pi}_1(\mathbf{r})\ \mathbf{grad}\ U(\mathbf{r}^A)$$
$$+(4\pi)^{\frac{1}{2}}\boldsymbol{\pi}_0{}^B\cdot\int d\mathbf{r}\boldsymbol{\pi}_1(\mathbf{r})\ \mathbf{grad}\ U(\mathbf{r}^B)$$
$$+\tfrac{1}{2}\int d\mathbf{r}[\{\boldsymbol{\pi}_1(\mathbf{r})\}^2+\phi_1(\mathbf{r})\omega^2\phi_1(\mathbf{r})]$$
$$+(g/\kappa)(\boldsymbol{\sigma}^A\cdot\boldsymbol{\phi}_0{}^A+\boldsymbol{\sigma}^B\cdot\boldsymbol{\phi}_0{}^B). \quad (72)$$

The cross terms involving $\boldsymbol{\pi}_1$ are eliminated by a unitary transformation like (27), (60), but with

$$U=(4\pi)^{\frac{1}{2}}\sum_i\left[\overset{A}{\pi}_{0i}\int d\mathbf{r}\phi_1(\mathbf{r})\frac{\partial}{\partial x_i}\{R_i\xi_i(\mathbf{r}^A)-S_i\xi_i(\mathbf{r}^B)\}+\overset{B}{\pi}_{0i}\int d\mathbf{r}\phi_1(\mathbf{r})\times\frac{\partial}{\partial x_i}\{R_i\xi_i(\mathbf{r}^B)-S_i\xi_i(\mathbf{r}^A)\}\right]\Big/(R_i^2-S_i^2), \quad (73)$$

where

$$R_i=\int d\mathbf{r}\left[\frac{\partial}{\partial x_i}\xi_i(\mathbf{r}^A)\right]^2=\int d\mathbf{r}\left[\frac{\partial}{\partial x_i}\xi_i(\mathbf{r}^B)\right]^2,$$
$$S_i=\int d\mathbf{r}\frac{\partial}{\partial x_i}\xi_i(\mathbf{r}^A)\frac{\partial}{\partial x_i}\xi_i(\mathbf{r}^B).$$

It follows that

$$\boldsymbol{\pi}_1(\mathbf{r})=\boldsymbol{\pi}_1'(\mathbf{r})-(4\pi)^{\frac{1}{2}}\sum_i\left[\overset{A}{\pi}_{0i}\times\frac{\partial}{\partial x_i}\left\{U(\mathbf{r}^A)-\frac{R_i\xi_i(\mathbf{r}^A)-S_i\xi_i(\mathbf{r}^B)}{R_i^2-S_i^2}\right\}+\overset{B}{\pi}_{0i}\frac{\partial}{\partial x_i}\left\{U(\mathbf{r}^B)-\frac{R_i\xi_i(\mathbf{r}^B)-S_i\xi_i(\mathbf{r}^A)}{R_i^2-S_i^2}\right\}\right],$$
$$\phi_1(\mathbf{r})=\phi_1'(\mathbf{r}).$$

We have, as a result

$$H=4\pi\sum_i\left[\{(\overset{A}{\pi}_{0i})^2+(\overset{B}{\pi}_{0i})^2\}\frac{R_i}{2}-\overset{A}{\pi}_{0i}\overset{B}{\pi}_{0i}S_i\right]\Big/(R_i^2-S_i^2)+\sum_i\left[\{(\overset{A}{\phi}_{0i})^2+(\overset{B}{\phi}_{0i})^2\}\frac{I}{2}-\overset{A}{\phi}_{0i}\overset{B}{\phi}_{0i}J_i\right]\Big/(I^2-J_i^2)$$
$$+(g/\kappa)(\boldsymbol{\sigma}^A\cdot\boldsymbol{\phi}_0{}^A+\boldsymbol{\sigma}^B\cdot\boldsymbol{\phi}_0{}^B)$$
$$+\tfrac{1}{2}\int d\mathbf{r}[\{\boldsymbol{\pi}_1'(\mathbf{r})\}^2+\phi_1'(\mathbf{r})\omega^2\phi_1'(\mathbf{r})]. \quad (74)$$

As in the one source case, changes generated by (73) in $\boldsymbol{\phi}_0{}^A$ and $\boldsymbol{\phi}_0{}^B$ are neglected here. Again, the $(\boldsymbol{\pi}_1', \phi_1')$ system of states is taken empty so that its contribution to (74) vanishes. We introduce two systems of unit vectors $\mathbf{n}_1{}^A$, $\mathbf{n}_2{}^A$, $\mathbf{n}_3{}^A$ and $\mathbf{n}_1{}^B$, $\mathbf{n}_2{}^B$, $\mathbf{n}_3{}^B$ defined as above through two sets of angles α^A, β^A and α^B, β^B

$$\boldsymbol{\phi}_0{}^A=q_0{}^A\mathbf{n}_3{}^A,{}^{13}$$
$$\boldsymbol{\pi}_0{}^A=p_0{}^A\mathbf{n}_3{}^A-\mathbf{n}_2{}^Ap_\alpha{}^A/q_0{}^A+\mathbf{n}_1{}^Ap_\beta{}^A\Big/q_0{}^A\sin\alpha^A,$$
$$\boldsymbol{\phi}_0{}^B=q_0{}^B\mathbf{n}_3{}^B,$$
$$\boldsymbol{\pi}_0{}^B=p_0{}^B\mathbf{n}_3{}^B-\mathbf{n}_2{}^Bp_\alpha{}^B/q_0{}^B+\mathbf{n}_1{}^Bp_\beta{}^B\Big/q_0{}^B\sin\alpha^B.$$

Using

$$\mathbf{L}^A=\mathbf{n}_1{}^Ap_\alpha{}^A+\mathbf{n}_2{}^Ap_\beta{}^A/\sin\alpha^A,$$
$$\mathbf{L}^B=\mathbf{n}_1{}^Bp_\alpha{}^B+\mathbf{n}_2{}^Bp_\beta{}^B/\sin\alpha^B,$$

we find for the total angular momentum of the mesotron field:

$$\mathbf{L}=\mathbf{L}^A+\mathbf{L}^B.$$

We now obtain the minimum eigenvalue of the interaction energy by applying an S transformation, with

$$S=\exp[i\sigma_y{}^A\alpha^A/2]\exp[i\sigma_z{}^A\beta^A/2]\times\exp[i\sigma_y{}^B\alpha^B/2]\exp[i\sigma_z{}^B\beta^B/2].$$

The interaction energy becomes

$$(g/\kappa)(q_0{}^A\sigma_z{}^A+q_0{}^B\sigma_z{}^B). \quad (75)$$

[13] Symmetrization with respect to p_α and functions of α is to be understood throughout.

We choose a representation in which both σ_z^A and σ_z^B are diagonal, and consider the state in which each has the eigenvalue -1. The effect of the S transformation on $\mathbf{L}^A$, $\mathbf{L}^B$ and their squares is indicated by (65), (66). For example, $(L^A)^2$ becomes $(J^A)^2+\frac{1}{4}$ where $\mathbf{J}^A$ is the total angular momentum of source A plus its associated field.

So far the orientation of the space axes is quite arbitrary and we may assume the z axis to lie in the direction of the line separating the two sources. Then we may write $R_y=R_x=R_\perp$, $S_x=S_y=S_\perp$, $J_x=J_y=J_\perp$; in general $J_\perp\neq J_z$, etc.

The separation of the static self-energy is accomplished by the elimination of the terms linear in the q's. The part of the Hamiltonian involved is

$$\sum_i\Big[\{(\phi_{0i}^A)^2+(\phi_{0i}^B)^2\}\frac{I}{2}-\phi_{0i}^A\phi_{0i}^B J_i\Big]\Big/(I^2-J_i^2)-(g/\kappa)(q_0^A+q_0^B). \quad (76)$$

It is not hard to show that the absolute minimum of (76) is attained when the vectors $\boldsymbol{\phi}_0^A$ and $\boldsymbol{\phi}_0^B$ coincide in magnitude and in the magnitude of their components. If $J_i>0$, then $\phi_{0i}^A=\phi_{0i}^B$, while if $J_i<0$, then $\phi_{0i}^A=-\phi_{0i}^B$. In any case, $q_0^A=q_0^B=q_0$. Equation (76) may be written

$$\sum_i\frac{(\phi_{0i}^A)^2}{I+|J_i|}-2gq_0/\kappa. \quad (77)$$

The direction of $\boldsymbol{\phi}_0^A$ which minimizes (77) is determined by the relative magnitudes of J_z and $J_\perp$. In our case ($\kappa a\ll 1$), J_z is negative and has a greater magnitude than $J_\perp$. Consequently, both $\boldsymbol{\phi}_0^A$ and $-\boldsymbol{\phi}_0^B$ (i.e., $\mathbf{n}_3^A$ and $-\mathbf{n}_3^B$) point in the positive z direction for a minimum of (77). The minimizing value of q_0 is

$$q_0=-(g/\kappa)(I+|J_z|),$$

and (77) becomes

$$-(g^2/\kappa^2)(I+|J_z|). \quad (78)$$

1. *Forces at Small Separation*

If the sources are sufficiently close together, the minimum of the Hamiltonian is essentially given by the minimum of (76), namely (78). Both $\boldsymbol{\phi}_0^A$ and $\boldsymbol{\phi}_0^B$ are "frozen" and are equal to

$$\boldsymbol{\phi}_0^B=-(g/\kappa)(I+|J_z|)\mathbf{n}_z;$$
$$\boldsymbol{\phi}_0^A=(g/\kappa)(I+|J_z|)\mathbf{n}_z.$$

Equation (78) contains, in addition to the sum of the self-energies of two separated sources, the space dependent part $-g^2|J_z|/\kappa^2$ which in this theory is quite singular, varying as $1/d^3$ for small separations. Equation (78) is moreover an "ordinary" force, showing neither spin dependence nor exchange properties. We must, therefore, investigate the possibility of thawing of the spins due to the first term of (74). We expand the Hamiltonian about the frozen position; (74) becomes

$$\begin{aligned}&4\pi[\{(p_0^A)^2+(p_0^B)^2\}R_z/2-p_0^Ap_0^BS_z]/(R_z^2-S_z^2)+4\pi[\{(J^A)^2\\&+(J^B)^2\}R_\perp/2-\mathbf{J}^A\cdot\mathbf{J}^BS_\perp]\Big/(R_\perp^2-S_\perp^2)q_0^2\\&+[\{(Q_0^A)^2+(Q_0^B)^2\}I/2-Q_0^AQ_0^B|J_z|]/(I^2-J_z^2)\\&+\Big[\{(\alpha^A)^2+(\alpha^B)^2\}\frac{I|J_z|+J_\perp^2}{2(I+|J_z|)}\\&-\alpha^A\alpha^B\cos(\beta^A-\beta^B)J_\perp\Big]q_0^2/(I^2-J_\perp^2)\\&-(g^2/\kappa^2)(I+|J_z|). \quad (79)\end{aligned}$$

Here we have used

$$\mathbf{J}^A=\mathbf{n}_1^Ap_\alpha^A+\mathbf{n}_2^A(p_\beta^A+\tfrac{1}{2})/\sin\alpha^A,$$
$$(J^A)^2=(p_\alpha^A)^2+(p_\beta^A+\tfrac{1}{2})^2/\sin^2\alpha^A,$$
$$\sin\alpha^A\sim\alpha^A;\qquad \sin\alpha^B\sim\alpha^B,$$
$$\cos\alpha^A\sim 1-(\alpha^A)^2/2;\quad \cos\alpha^B\sim -1+(\alpha^B)^2/2,$$
$$q_0^A=q_0+Q_0^A$$

with analogous definitions for source B. Q_0^A, the displacement from the equilibrium amplitude, is canonically conjugate to p_0^A. We may separate off the first and third lines of (79) which we call

H_s and bring to principal axes by means of the canonical transformation:

$$\begin{aligned} p^+&=(1/\sqrt{2})(p_0{}^A+p_0{}^B),\\ q^+&=(1/\sqrt{2})(Q_0{}^A+Q_0{}^B),\\ p^-&=(1/\sqrt{2})(p_0{}^A-p_0{}^B),\\ q^-&=(1/\sqrt{2})(Q_0{}^A-Q_0{}^B), \end{aligned} \tag{80}$$

$$H_s=\frac{4\pi p_+{}^2}{2(R_s+S_s)}+\frac{q_+{}^2}{2(I+|J_s|)} +\frac{4\pi p_-{}^2}{2(R_s-S_s)}+\frac{q_-{}^2}{2(I-|J_s|)}. \tag{81}$$

As in the one-source case, all the states of these two oscillator systems are taken empty.

Lines 2 and 4 of (79) give the energy of excitation of the bound system above its minimum position, which we shall call $H_\perp$. First we substitute.

$$p_\beta+\tfrac{1}{2}=p_\beta', \quad \beta=\beta'$$

for both sources. Then introduce Cartesian coordinates

$$x=\sin\alpha\cos\beta\sim\alpha\cos\beta,$$

$$y=\sin\alpha\sin\beta\sim\alpha\sin\beta,$$

$$\begin{aligned} H_\perp=4\pi\Big[&\{(p_x{}^A)^2+(p_y{}^A)^2 +(p_x{}^B)^2+(p_y{}^B)^2\}R_\perp/2\\ &-\{p_x{}^Ap_x{}^B+p_y{}^Ap_y{}^B\}S_\perp\Big]\Big/(R_\perp{}^2-S_\perp{}^2)q_0{}^2\\ &+\Big[\{(x^A)^2+(y^A)^2 +(x^B)^2+(y^B)^2\}\frac{I|J_s|+J_\perp{}^2}{2(I+|J_s|)}\\ &-\{x^Ax^B+y^Ay^B\}J_\perp\Big]q_0{}^2/(I^2-J_\perp{}^2) \end{aligned} \tag{82}$$

aside from a constant. This consists of two identical systems of which it will suffice to consider either: we shall treat that involving x^A, x^B. Normal coordinates are

$$\begin{aligned} v_I&=(x^A+x^B)/\sqrt{2}, \quad p_I=(p^A+p^B)/\sqrt{2},\\ v_{II}&=(x^A-x^B)/\sqrt{2}, \quad p_{II}=(p^A-p^B)/\sqrt{2}, \end{aligned} \tag{83}$$

$$H_{\perp s}=\frac{4\pi p_I{}^2}{2q_0{}^2(R_\perp+S_\perp)}+\frac{4\pi p_{II}{}^2}{2q_0{}^2(R_\perp-S_\perp)} +\frac{v_I{}^2q_0{}^2(|J_s|-J_\perp)}{2(I+|J_s|)(I+J_\perp)}+\frac{v_{II}{}^2q_0{}^2(|J_s|+J_\perp)}{2(I+|J_s|)(I-J_\perp)}. \tag{84}$$

The integrals of interest are tabulated below for the limit $\kappa a\ll 1$ and also $a\ll d$ where d is the separation

$$I\sim 1/a^3,$$

$$J_\perp\sim\frac{e^{-\kappa d}}{d}(1/d^2+\kappa/d),$$

$$J_s\sim-\frac{e^{-\kappa d}}{d}(2/d^2+2\kappa/d+\kappa^2),$$

$$R_\perp=R_s=4\pi a^5/3.$$

$S_\perp$ and S_s are of order κa^6. In this limit J/I and S/R may be neglected. Consider the (p_{II}, v_{II}) oscillator. The amplitude of zero-point oscillations is

$$\bar{\psi}=(\kappa/g)\left[8\frac{RI^2}{4\pi}(|J_s|+J_\perp)\right]^{-\frac{1}{4}}.$$

Thawing takes place only when $\bar{\psi}>1$,

$$\kappa d e^{+\kappa d}\Big/\left(1+\frac{3}{\kappa d}+\frac{3}{\kappa^2d^2}\right)<\frac{8}{3}\frac{g^4}{\kappa a},$$

or, with $g\sim 1$, $\kappa a\sim 0.1$, when $\kappa r>3$.

2. *Forces at Large Separation*

This problem is handled by a perturbation method. In zero order, one takes the sum of the energies of two infinitely separated sources [see (68)].

$$H_0=-g^2I/\kappa^2 +4\pi[(J^A)^2+(J^B)^2-\tfrac{3}{2}]/2Rq_0{}^2, \tag{85}$$

where

$$(J^A)^2=(p_\alpha{}^A)^2+(p_\beta{}^A)^2/\sin^2\alpha^A +1/4\sin^2\alpha^A+p_\beta\cos\alpha^A/\sin^2\alpha^A.$$

In this order, the angles α^A, β^A, α^B, β^B are completely unrestricted. As the sources approach, the leading modification of H_0 is the addition of the space dependent part of the interaction energy, which is obtainable from (74), and is

$$H_1=\{-J_z\cos\alpha^A\cos\alpha^B - J_\perp\sin\alpha^A\sin\alpha^B\cos(\beta^A-\beta^B)\}g^2/\kappa^2. \quad (86)$$

Other modifications of (85) contained in (74) are less important as long as the separation is appreciably greater than a.

We require first the eigenfunctions of (85) or, more simply, the eigenfunctions of $(J^A)^2$ and $(J^B)^2$. $(J)^2$ may be rewritten:

$$(J)^2=p_\alpha{}^2+p_\beta{}^2+(1/\sin^2\alpha)(p_\beta\cos\alpha+\tfrac{1}{2})^2. \quad (87)$$

We assume a solution of the form $A(\alpha)e^{in\beta}$. Single-valuedness of the wave function in β requires that n be a half integer, since the original wave function is related to the eigenfunction here obtained through the S transformation: $F=S^{-1}F'$, with

$$S=\exp[i\sigma_y\alpha/2]\exp[i\sigma_z\beta/2].$$

Since σ_z has the eigenvalue -1, the above requirement on n follows. The equation for A[14] is

$$\frac{d^2A}{d\alpha^2}+\frac{\cos\alpha}{\sin\alpha}\frac{dA}{d\alpha}-\frac{1}{\sin^2\alpha}\times(n\cos\alpha+\tfrac{1}{2})^2A+(E-n^2)A=0, \quad (88)$$

where E is the eigenvalue of (87). This can be transformed into the hypergeometric equation by the introduction of a new variable

$$z=(1+\cos\alpha)/2,$$

and a new dependent variable

$$A=Zz^{|n-\frac{1}{2}|/2}(z-1)^{|n+\frac{1}{2}|/2}$$

$$z(1-z)\frac{d^2Z}{dz^2}+[\gamma-(\alpha_0+\beta_0+1)z]\frac{dZ}{dz}-\alpha_0\beta_0Z=0, \quad (89)$$

where

$$\alpha_0=|n|+\tfrac{1}{2}+(E+\tfrac{1}{4})^{\frac{1}{2}},$$

$$\beta_0=|n|+\tfrac{1}{2}-(E+\tfrac{1}{4})^{\frac{1}{2}},$$

$$\gamma=|n-\tfrac{1}{2}|+1.$$

Z is the hypergeometric function, $F(\alpha_0,\beta_0,\gamma,z)$, and the solution for the eigenfunction of (87) is

$$e^{in\beta}\{z^{|n-\frac{1}{2}|}(z-1)^{|n+\frac{1}{2}|}\}^{\frac{1}{2}}F(\alpha_0,\beta_0,\gamma,z). \quad (90)$$

For this function to be regular at $\alpha=0$, π, the hypergeometric series must terminate, i.e., β_0 must be a negative integer or zero. This means that E is restricted to the values $(|n|+k)\times(|n|+k+1)$, where k is a positive integer or zero. Each value of $j=|n|+k$ corresponds to an isobaric level of the system, each level being multiply degenerate, according to the number of combinations of n and k which satisfy the above relation, namely $2j+1$.

We are concerned with the attraction between two systems which approach each other in their lowest isobaric levels, i.e., with $k=0$, $j=\frac{1}{2}$, $n=\pm\frac{1}{2}$. This level is a doublet whose wave functions may be written

$$(\sin\alpha/2)e^{i\beta/2},\qquad(\cos\alpha/2)e^{-i\beta/2}. \quad (91)$$

These two states, corresponding to $n=\pm\frac{1}{2}$, are to be thought of as representing the two projections of the "empirical" spin of the heavy particle (to be distinguished from $\boldsymbol{\sigma}$, the spin vector introduced above for the heavy particle core).

We now calculate the expectation value of (86). The term involving J_z has a finite matrix element only if the projections n^A and n^B both remain unchanged. Its expectation value is $\pm(-g^2J_z/9\kappa^2)$, corresponding to $n^A=\pm n^B$. It can be written $(-g^2J_z/9\kappa^2)s_z{}^As_z{}^B$ where $\mathbf{s}(s_x,s_y,s_z)$ is the spin projection operator for the doublet under consideration. On the other hand, the term in $J_\perp$ contributes only if the projection is increased by one unit for system and decreased by one unit for the other. The expectation value is $(-g^2J_\perp/9\kappa^2)(s_x{}^As_x{}^B+s_y{}^As_y{}^B)$. The energy of

[14] R. deL. Kronig and I. I. Rabi, Phys. Rev. **29**, 262 (1927).

interaction is consequently

$$V_1=-\frac{g^2}{9\kappa^2}[J_z s_z^A s_z^B+J_\perp(s_x^A s_x^B+s_y^A s_y^B)].$$

Introduce the unit vector $\hat{\mathbf{r}}$ along the line joining the two systems (in the z direction). Then

$$V_1=\frac{-g^2}{9\kappa^2}[J_\perp \mathbf{s}^A\cdot\mathbf{s}^B+(J_z-J_\perp)(\mathbf{s}^A\cdot\hat{\mathbf{r}})(\mathbf{s}^B\cdot\hat{\mathbf{r}})].$$

The integrals J_z and $J_\perp$ are given by (84). Letting $\kappa d=x$, we have

$$V_1=\frac{g^2\kappa e^{-x}}{9(4\pi x)}\Big[(1/3)\mathbf{s}^A\cdot\mathbf{s}^B+\{(\mathbf{s}^A\cdot\hat{\mathbf{r}})(\mathbf{s}^B\cdot\hat{\mathbf{r}})-(1/3)\mathbf{s}^A\cdot\mathbf{s}^B\}\Big\{\frac{3}{x^2}+\frac{3}{x}+1\Big\}\Big]. \quad (92)$$

Aside from the factor $\frac{1}{9}$, this is precisely the interaction between two heavy particles derived from the same Hamiltonian by perturbation methods.

Acknowledgments are due Professor W. Pauli and Professor J. R. Oppenheimer for illuminating discussions on all parts of this work.

PHYSICAL REVIEW VOLUME 63, NUMBERS 5 AND 6 MARCH 1 AND 15, 1943

Cloud-Chamber and Counter Studies of Cosmic Rays Underground

VOLNEY C. WILSON AND DONALD J. HUGHES
Ryerson Laboratory, The University of Chicago, Chicago, Illinois

(Received January 20, 1943)

A counter controlled cloud chamber and two counter coincidence sets were used to study the nature of the cosmic rays observable underground. The experiments were performed in a copper mine at depths of 71, 141, 582, and 657 meters water equivalent. The data are easily interpreted, if one assumes that underground the primary rays are mesotrons and that the soft rays and showers are electronic secondaries produced by the penetrating mesotrons.

INTRODUCTION

AT the time of the cosmic-ray symposium[1] held at Chicago in June, 1939, it was evident that there was as yet much unknown about the nature of cosmic rays underground as well as considerable disagreement concerning the known material. The shape of the total intensity *vs.* depth curve seemed to be quite well established. When plotted on a log log scale, the data fall on a line composed of two straight portions, the change in slope occurring at about 250 to 400 meters water equivalent. However, concerning the nature of the rays responsible for the two parts of the curve, there was a diversity of opinion. Several observers had found evidence for the non-ionizing character of the rays which carry the energy down to great depths; Wataghin and Santos[2] at 250 and 400 m,[3] Barnothy and Forro[4] at 1000 m. However, Wilson's[5] experiments at 30 m and 300 m indicated that the penetrating rays responsible for the observed intensity at both these depths are ionizing. Clay's[6] interpretation was that protons are predominant below the break in the intensity curve.

Neither data nor interpretation were clear-cut on the matter of shower production and the abundance of soft particles. The ratio of soft to hard components, as measured by counter absorption experiments, varied greatly, and it was quite evident that much of this disagreement

[1] V. C. Wilson, Rev. Mod. Phys. **11**, 230 (1939).

[2] G. Wataghin and M. Damy de Souza Santos, Ann. Acad. Brasil. Sci. **11** (March 11, 1939).

[3] m means meters water equivalent of rock calculated on a density basis.

[4] J. Barnothy and M. Forro, Phys. Rev. **55**, 870 (1939).

[5] V. C. Wilson, Phys. Rev. **55**, 6 (1939).

[6] J. Clay, Rev. Mod. Phys. **11**, 128 (1939).

was caused by differences in geometry of counters, absorbers, and surrounding material. Thus, Wilson had found a 7 percent soft component, Nielsen and Morgan 24 percent, and Auger 9 percent, all at 30 m depth. Both Wilson and

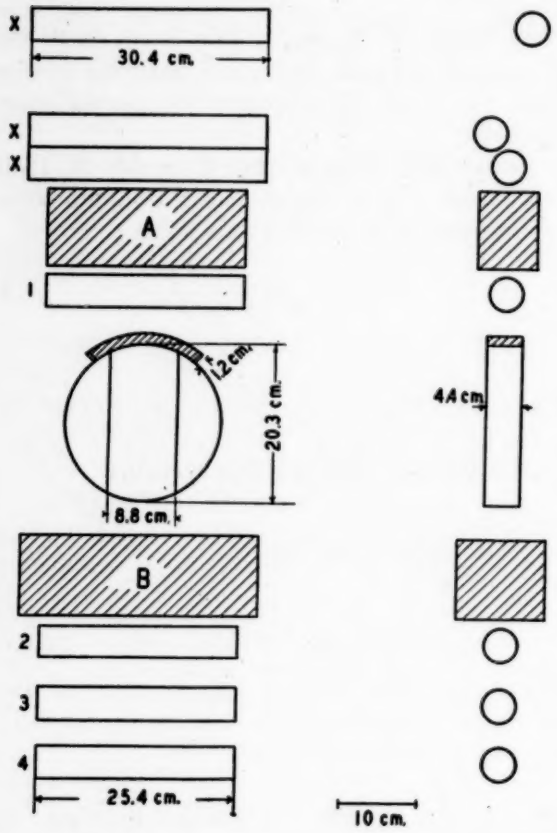

FIG. 1. Cloud chamber and Geiger-Mueller tube arrangement to study the nature of cosmic rays at 71 m.

Clay found that the ratio of soft to hard rays increases with depth at moderate depths, and Clay observed a marked decrease below 400 m. Auger's data showed a constant decrease with depth. According to these observers, shower intensities vary with depth in about the same way as the soft component although it is difficult to distinguish between variation in shower intensity and possible variation in the nature of the showers themselves, such as size, angular spread, etc.

The question of the nature and production of the showers is intimately related to the study of the nature of the penetrating rays at different depths. The experiments of Auger, Wilson, Janossy, Nielsen, and Morgan indicated that the showers at moderate depth are ordinary electronic multiplicative ones, accompanying the ionizing primaries which produce them. Barnothy and Forro felt that the great bulk of the ionization at depths below the break in the intensity curve is made up of soft particles, secondaries of a penetrating non-ionizing radiation. Wataghin also found a production by non-ionizing primaries at both moderate and great depths, it being the only method of production at the great depths. The interpretation of Clay, however, was that at great depths, the secondary showers, few in number, are progeny of the protons which are the particles penetrating to such depths.

Thus, it was realized that much more experimental work was needed to help clear up this diversity of fact and interpretation. Clear-cut data were needed to show the kinds of rays present at a particular location and the processes taking place there, and to show the way in which these things vary as the cosmic-ray energy is carried downward to greater depths. It was decided, therefore, to perform a series of experiments which might aid in the resolution of some of the difficulties mentioned. The work was carried on in the fall and winter of 1940–41, at the Isle Royale copper mine near Houghton, Michigan. Although it was necessary to terminate the experiments at the end of December, enough data were obtained in the time available to give results of definite value.

CLOUD-CHAMBER EXPERIMENTS

Since the interpretation of counter tube experiments underground is often difficult and uncertain, it seemed desirable to supplement them by the use of a cloud chamber. The immediate phenomena recorded in the chamber are more obvious than interpretation of counter readings, but quantitative results are, of course, much more uncertain. It was felt, however, that cloud-chamber results combined with counter data would give a good picture of the complex of rays present underground. The chamber would show directly what was being measured quantitatively with the counters; the latter would give some idea of the frequency of occurrence of the processes seen in the former.

The chamber was of the conventional diaphragm type, 20 cm in diameter, automatic in operation, and counter-controlled. It was mounted between the poles of a 600-lb. Alnico permanent magnet, which produced a field of 1250 gauss in the plane of the chamber. Illumination was provided by two 36-volt coil-coil line filament bi-post lamps, which, when flashed in parallel on 110 volts and focused with cylindrical lenses, produced a brilliant sheet of light of chamber depth. It was found possible to let the apparatus run continuously in the mine. It was visited daily to check adjustments, remove film, etc.[7]

The cosmic-ray intensity in the mine, and hence, rate of expansion of the chamber, was so low that in the time available it was felt best to get as many pictures as possible at one depth, the "1st level," 71 m, and use the counter data alone to infer the variation of phenomena with depth. The counter control and lead absorbers used to obtain a general picture of the rays and processes present at this depth are shown in Fig. 1. Three general arrangements were used:

I. Coincidences of tubes 1, 2, 3, and 4 controlling the expansions, no Pb absorber present.

II. Same counter control as I but with 10 cm Pb at B.

III. Coincidences of tubes 1, 2, 3, and 4 controlling expansions; 3 to 10 cm Pb at $A+1.2$ cm on chamber; tubes X, in parallel, light a neon lamp when they discharge coincidently with 1, 2, 3, and 4.

The purpose of I is to give a cross section of the rays in equilibrium with the rock at this depth undistorted by Pb absorbers. Arrangement II shows the effect of the usual method of removing the soft component in a counter absorption experiment—the lead under the chamber allowed only penetrating rays to be observed without the addition of rays produced in the absorber itself. In III the more complicated picture of penetrating rays plus secondaries produced in the lead above the chamber is observed, the neon lamp indicating whether secondary production was by ionizing or non-ionizing primaries. For these three groups, with an expansion rate of about two per hour, a total of 1248 pictures was obtained. A shower arrangement of tubes was also tried, but the counting rate was prohibitively low, power line failures causing more expansions than showers.

For the single tracks, visible in both of the stereoscopic views, passing through the control counters, and long enough for curvature measurement, the pc value (300 $H\rho$) was determined by use of the micrometer device described by Jones and Hughes.[7] There were 364 such tracks, divided among the three groups as shown in Table I with momentum spectra as in Fig. 2. The momentum range shown does not extend above 10^9 ev. The tracks with higher measured values are classified with the "straight" tracks.

The table and momentum spectra show that for group I (no Pb absorber), there is an excess of negative particles of low energy. These are, of course, secondaries and are undoubtedly knock-on electrons separated sufficiently from their primaries to appear singly. Aside from this explicable excess, there seems to be a positive-negative equality. A proton with an energy low enough to be measured in this apparatus would be quickly absorbed by its great ionization loss. Therefore, this is not evidence against the presence of positive protons in the penetrating group. Incidentally, except for a few contamination alphas, no particles with heavier ionization than electronic were observed in any of these pictures.

TABLE I. Rays photographed with the three counter arrangements at 71 m depth.

Group	+	−	Straight (>10^9 ev)	Total	$\frac{10^8-10^9}{\text{total}}$
I. No Pb	22	35	117	174	33%
II. 10 cm Pb below chamber	5	3	23	31	26%
III. 3–10 cm Pb above chamber	18	23	118	159	26%
				364	

The expansion rate of the chamber was 2.10 per hour in I and 1.98 in II, a 5 percent decrease in counting rate with 10 cm Pb. The last column

[7] The chamber resembled closely that described by H. Jones and D. Hughes, Rev. Sci. Inst. **11**, 79 (1940). The magnet was an enlarged version of the one described by Herzog, Phys. Rev. **59**, 117 (1941). We wish to thank Dr. Herzog also for the use of an electronic timing circuit.

of Table I, which is a rough measure of the "shape" of the spectrum, indicates that the rays absorbed are of low energy. Comparison of the momentum spectra of I and II (Fig. 2) shows this even more clearly, for the low energy group of I does not appear in II. There are now no rays of momentum less than 2.1×10^8 ev, which checks well with the fact that the momentum value for mesotrons of range 10 cm Pb is 2.3×10^8 ev. The eight rays still present in II with measurable momentum are almost certainly mesotrons; electrons of such momentum could never penetrate the absorber because of radiation loss; nor could protons because of the increased ionization loss at these momentum values (a proton of momentum 8.2×10^8 ev has a 10 cm range). The uncertainty in curvature measurement for the higher momentum particles in this group would perhaps permit their interpretation as protons of actually higher momentum; however, of the three over 5×10^8 ev, two are negative. Of the five most certain mesotrons, of momentum under 5×10^8, four are positive. Protons of such momentum value also would show increased ionization, which is not the case.

Those secondary rays which travel close to

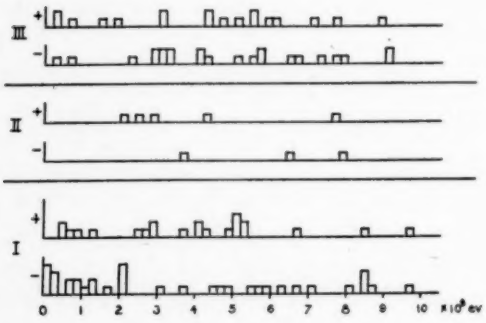

FIG. 2. Momentum spectra taken from cloud-chamber photographs at 71 m.

their penetrating primaries are not revealed by a decreased counting rate when Pb is interposed in a counter experiment. It follows that for this particular geometrical arrangement (roof 80 cm above upper counter) 5 percent of the total are soft rays separated enough from their primaries to set off a counter train missed by the primary rays. The actual soft component is of course greater than 5 percent by an amount which will be larger the greater the coherence of the secondaries to the primaries. A rough estimate can be made by an actual count of the secondary rays observable in the chamber accompanying the penetrating rays of group II—the resulting figure is 13 percent, which should be increased somewhat to allow for those secondaries which pass out of the illuminated area. Thus, in a rough way, we see that an actual 13 percent soft component would be measured as 5 percent—or even less if the counter train were nearer the overlying rock. This point is, of course, closely related to the counter absorption experiments described below.

Group III concerns the more complicated case in which the Pb block absorbs some particles but also creates others, which are observed in the chamber. In this sense, the phenomena observed are a combination of those in I and II, and it is seen in the momentum spectra and Table I that the results lie between those of the first two groups. Under the Pb block there is an approximate positive-negative equality—as would be expected from multiplication of those soft rays in the absorber which are not absorbed. Of more interest in this group than the momentum spectra are the nature and mode of production of the showers observed.

The secondaries and showers observed with the three arrangements are shown in Table II. Again, the relative number of coincidences caused by showers to those due to single rays is not the ratio of occurrence of these phenomena, but depends on the geometry and the surrounding material. Still another reason is seen here for the fact that the decrease in counting rate with insertion of 10 cm Pb gives a low value for the soft component, for an appreciable number of showers present in I are removed by the Pb, each of which would be counted as only one soft ray by the counter absorption method. The difference in size distribution of showers for the three arrangements is quite marked. The Pb-produced showers in III seem to contain a greater number of larger size than the rock-produced ones in I; this would be expected from the difference in material but, of course, can be due simply to the proximity of the producer in III. The large production of showers in a few cm of Pb as shown in III and their complete absorption by the Pb in II indicate their nature as

ordinary multiplicative showers—at least, no evidence is present of an unusual shower type. The additional, admittedly subjective, but important fact can be added that the showers look just like all those photographed at sea level with the same apparatus.

The neon lamp data in group III give definite information on the mode of production of the ionizing rays created in the Pb, which set off the counters below the Pb and are seen in the chamber. A lamp flash on the film signifies that coincident with the expansion an ionizing ray has passed through the counters X above the chamber. On 11 of 251 coincidences, there were no neon flashes. Without the cloud chamber evidence, we might conclude from this that under the Pb $4\frac{1}{2}$ percent of the ionizing rays were produced by non-ionizing primaries; furthermore, the primaries were unaccompanied by ionizing rays, hence were not photons—an important finding. But there would always be the question in such a result as to whether there might be an error in interpretation. Perhaps side showers, scattering, or insufficient coverage by counters X could explain the apparent production by non-ionizing penetrating rays. Here, however, we have the additional evidence of the chamber, and, seeing the actual ionizing rays in the chamber, we can project them upwards to see if their ionizing primaries would have fired the counters X. When this is done, it is found that in none of the 11 pictures showing no neon flashes is there a ray visible whose projection passes through X. In 7 of these pictures no rays are visible (a ray can miss the chamber and fire the counters); inclined showers are present in 2 of them; and the final 2 show single rays inclined so as to hit the ends of the control counters but not counters X. So, of the 162 rays photographed with arrangement III, there is no evidence of production by a non-ionizing agent which is unaccompanied by ionizing rays. Photons are not ruled out by this evidence, but production by any penetrating non-ionizing ray (which would not be accompanied by numerous secondary ionizing rays), as suggested by several experimenters, must be extremely rare.

TABLE II. Secondaries and showers accompanying the counter control rays.

Group	Rays	Single secondaries	Shower size 2–5 rays	6–10	11–20	21–30	31–40	>40	Total
I	174	29%	15	4	2	1	0	1	23
II	31	13%	11	0	0	0	0	0	11
III	159	11%	11	2	1	2	2	2	20

A number of knock-on electrons created in the gas of the chamber were observed. The great majority of these have ranges lying entirely in the chamber; hence, their energies can be estimated even when scattering prevents curvature measurement. The probability of ejection of a knock-on of energy E electron volts is given by[8]

$$p(E)dE=0.3\frac{z}{A}\frac{mc^2}{\beta^2}\frac{dE}{E^2}dx,$$

provided E is small as in the cases considered here. The electronic rest energy is mc^2 and dx is measured in g per cm^2. If the momentum of the primary particles is high enough so that $\beta=1$, then this probability is independent of the momentum and mass of the primaries. As all the rays recorded were of electronic ionization density (hence with $\beta=1$), a study of the distribution in energy of the knock-ons in the gas will give no information on the mass of the primary particles. Nevertheless, it is interesting to check the validity of the above formula by counting the observed total number of knock-on electrons. For 390 rays there are 48 knock-on electrons with range greater than 0.5 cm in the chamber, i.e., of energy greater than 18 kev. Integrating the formula with respect to E between the limits 18 kev and infinity, we find 3.89 per g/cm^2 of argon or per 516 cm track length in the chamber. Thus, for 390 tracks of average observable length of 18 cm, or 7030 cm track length, we would expect $7030/516\times3.89$ or 53 knock-on electrons as compared to the 48 observed. The number of cases is too small to allow any significant comparison between the observed and expected distributions in energy.

Contrasted to statistical data on their energy distribution, cases of individual knock-on elec-

[8] B. Rossi and K. Greisen, Rev. Mod. Phys. 13, 240 (1941).

trons, where angles and momenta can be measured, furnish excellent methods of mass determination. In order to estimate the mass of the primary with any accuracy, the collision must be almost head-on and the primary momentum must be relatively low, as can be seen from the formula

$$E=\frac{2mc^2(\mu_0/k)^2\cos^2\theta}{\{[(\mu_0/k)^2+1]^{\frac{1}{2}}+1/k\}^2-(\mu_0/k)^2\cos^2\theta}$$

which gives knock-on energy E (electron volts) in terms of the angle of ejection θ of the knock-on electron by the primary, of mass km, of momentum μ_0 mc. For the knock-on electrons observed, θ, μ_0, and E could be measured at least approximately, but in most of these cases the values were such (θ large, μ_0 large) that k could not be determined with any accuracy. The two knock-on electrons shown in Fig. 3 illustrate this.

All in all, the cloud-chamber data show that at 71 meters depth the kinds of rays and interactions which are observed are just those well-known at sea level. There are penetrating ionizing rays, soft secondaries (with an excess of negatives), and ordinary multiplicative showers. The penetrating rays of high energy may be mesotrons or protons, there being definite evidence only for the presence of mesotrons. A soft component, composed of low energy rays, is present. The fraction of soft rays is greater than would be indicated by counting rate ratios in an absorption experiment. The soft rays apparently are largely produced by well-known knock-on processes; the number of electrons ejected in the chamber gas checking with theoretical knock-on probability, and the greater number of absorbable secondary rays being negative. Under a shower producer of moderate thickness the number and size of the showers increase just as observed at sea level, and the energy of the individual rays is likewise similar. The mode of production of showers at this depth seems to show nothing unusual; in particular, there is no evidence of production by penetrating non-ionizing primaries. The evidence is mainly qualitative, the more quantitative data and the important change of the phenomena with depth can be obtained from the counter data.

ABSORPTION EXPERIMENT

It was mentioned in the introduction that some observers think the penetrating rays are ionizing and others believe that below 250 m the energy is carried down by a non-ionizing ray that produces softer ionizing secondaries. The cloud-chamber work shows that at 71 m, most of the rays are penetrating and ionizing. There might be, however, a small fraction of secondaries created by non-ionizing primaries. If, as the rays pass to greater depths, the ionizing rays are absorbed, the majority of the remaining rays observed might be secondaries from these non-ionizing primaries. If this is the case, the absorption of rays present at great depths would be greater with material between the counters than with material above the counters. Material between the counters would give the absorption curve for the secondaries produced in the rock, and material above would give the absorption for the primaries. Figure 4 shows a Geiger-counter arrangement used under exactly similar conditions at 71 m and at 657 m. Each group of three tubes was connected together to form one large tube. Lead surrounding the second and third tubes shielded these tubes from side showers. The upper four tubes were connected to one coincidence circuit and the lower four to another in order to take two sets of data simultaneously. The coincidences were recorded by two pens on a moving tape. The ceiling was one meter from the top group of tubes, and the same vein of rock was overhead at the two locations. Figures 5 and 6 show the absorption curves obtained. It is immediately apparent that at both depths, the observed rays are very penetrating. The comparatively rapid decrease in the counting rates in the first 10 cm of lead was caused by the absorption of the soft rays. As pointed out when discussing the cloud-chamber data, this initial drop cannot be used to calculate the relative number of soft to hard rays, but if this ratio should increase with depth, then the initial drop would be greater at 657 m. The similarity of the curves indicates that the ratio of soft to hard rays is about the same at the two depths. This also suggests that the rays at 657 m are similar to those at 71 m. Certainly any possibility of a large fraction of non-ionizing

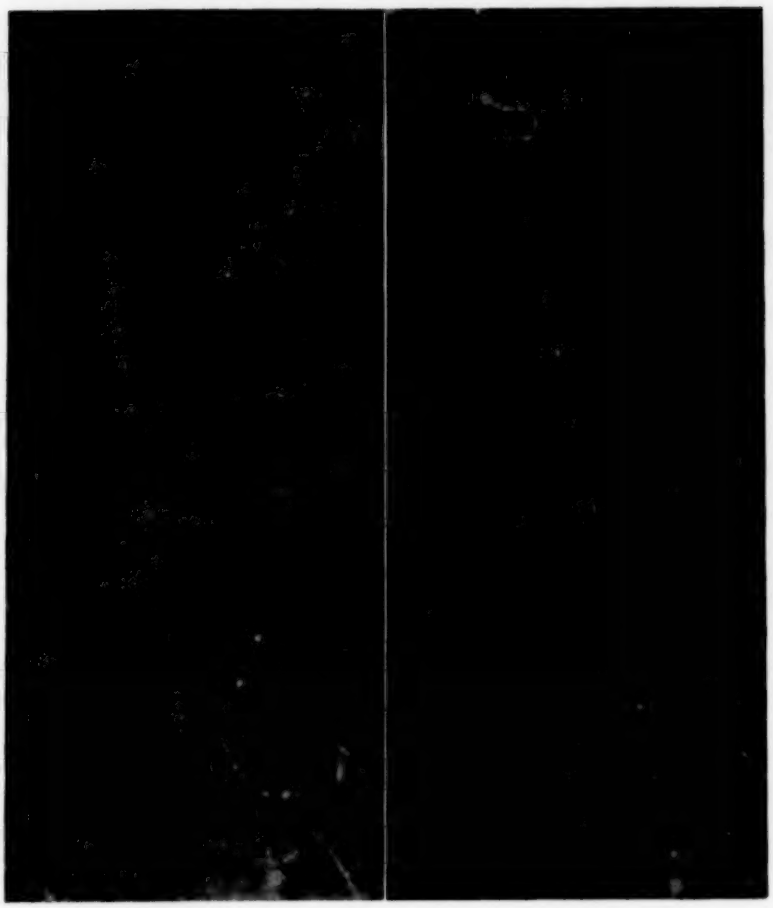

(a) (b)

FIG. 3. Two knock-on electrons observed at 71 m. (a) *Counter arrangement* I. The primary is negative, of momentum 4.7×10^{8} ev ($\mu_0=940$). The energy of the knock-on electron is 215 kev ($\epsilon=0.43$, where energy$=\epsilon mc^2$) and θ is about 60°. For proton mass, the measured values for μ_0 and θ give $\epsilon=0.094$, thus definitely ruling out this possibility. For $k=200$, the resulting ϵ is 0.62, which becomes 0.45 for $\theta=64°$, agreeing very well with the measured value. But assumption of electronic mass results in almost the same values ($\epsilon=0.48$ for $\theta=64°$). Here then elimination of the proton is definite but no distinction is possible between the mesotron and electron as the primary particle. (b) *Arrangement* II. Primary momentum 2.9×10^{8}, $\epsilon=0.08$, $\theta\geqq60°$. For $k=200$ the observed ϵ is obtained for $\theta=78°$ while for protonic mass, θ would have to be 45°. θ is certainly greater than 45° so the primary is not a proton. Also the ionization density is too low for a proton which at this momentum value would ionize five times as heavily as an electron. As for (a), distinction between $k=1$ and 200 is impossible for large θ values ($\theta=79°$ gives the correct ϵ for $k=1$), but here, the fact that the primary penetrates 10 cm of Pb eliminates the electron. Thus, in this case, identification as a mesotron is certain, but quantitative mass determination is impossible.

primaries is ruled out. With Pb only in A, a non-ionizing ray to be detected would need to produce two secondaries—one in the ceiling and one in A. With the same amount of Pb divided and placed in A and B, three secondaries would need to be produced to cause a coincidence. This probability would be much lower. However, the points L_{10-5} (10 cm Pb in A and 5 cm Pb in B) and L_{23-10} do not fall below the curve, thus further ruling out the non-ionizing primaries.

SHOWER EXPERIMENT

Showers detected by counter tubes are produced in the material surrounding the tubes.

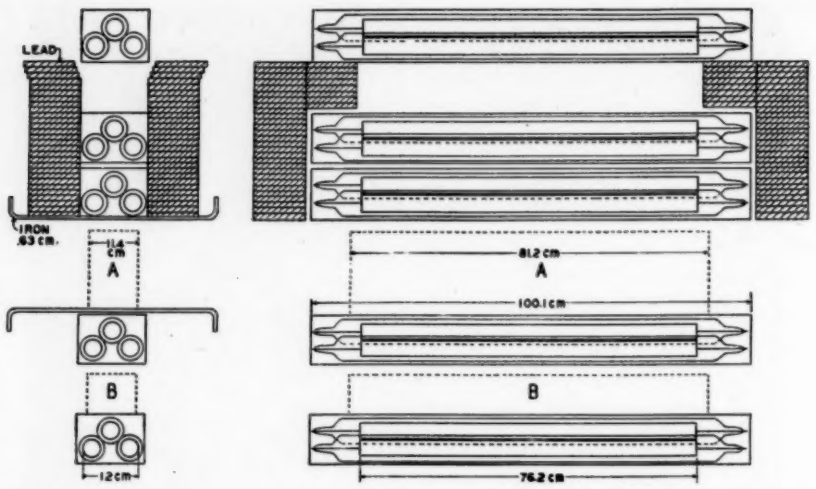

FIG. 4. Experimental arrangement used at 71 m and 657 m to measure absorption and relative numbers of soft and hard cosmic rays.

Therefore, to make a comparison of the shower properties at various depths, the counter tube arrangement used (Fig. 7) was completely surrounded by Pb. The Pb was 15 cm thick on the top, 10 cm on the sides and ends, and 2.5 cm on the bottom. It was thought that these thicknesses would be sufficient to insure that all shower particles observed in the cavity would have originated in the Pb and not in the surrounding rock. By moving this entire arrangement from one depth to another, any change observed in the nature of the showers should be caused by a change in the rays producing the showers and not by the geometry of the surrounding material.

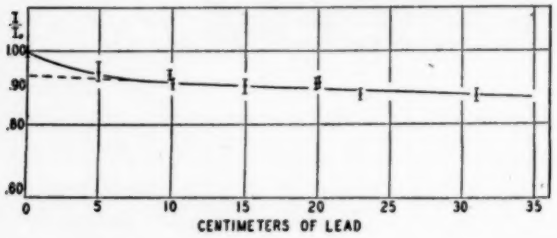

FIG. 5. Absorption of cosmic rays at 71 m.

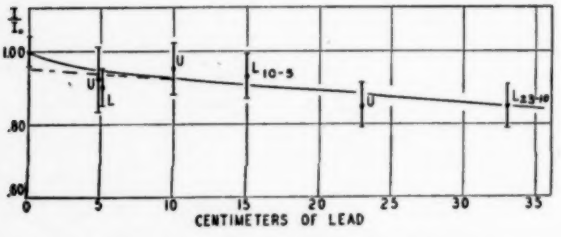

FIG. 6. Absorption of cosmic rays at 657 m.

The five tubes marked X were electrically connected in parallel to operate as one tube. Similarly, the Y tubes were connected together to form one large tube. Figure 8 is a block diagram of the circuits, each block representing a standard coincidence circuit. The counts from each were recorded upon a telephone message counter driven by a multivibrator. The threefold circuits $X12$, $X23$, $X34$, $X45$, $X24$, and $X15$ recorded showers of two or more particles. Small condensers coupled the plates of the threefold output tubes to the twofold coincidence circuits $X123$, $X234$, and $X345$. In this way, showers of three or more particles were recorded. Similarly, the outputs from $X123$ and $X345$ were combined in $X12345$ to count showers of five or more particles. The outputs from the above ten circuits were combined with the pulses from the Y tubes in ten more twofold circuits ($XY12$————$XY12345$). This arrangement made it possible to obtain twenty sets of data simultaneously. Combining the outputs not only reduced the number of vacuum tubes needed, but also reduced the capacity connected to each Geiger-Mueller tube, thus short resolving times could be maintained.

This apparatus was first taken to the 29th level, 2100 m, and operated from the same power line as was used for the experiment. No coinci-

dences were observed in fourteen hours. Apparently surges in the power line would not cause false counts. Tests showed that there was no intercoupling of the circuits which would cause a circuit to count falsely even when the other nineteen circuits were activated. Measurements of individual counting rates and of twofold coincidences were made, and from these values, the time constants of the threefold circuits were found to be 3×10^{-6} min. The calculated threefold chance counts were one in 2000 days. At the surface, where both the Y and the $X12$ etc. counting rates were much greater, the estimated Y–$X12$, etc. chance counts were one in three days. All other chance counts were much lower. Data were taken at the surface, at 71 m, 141 m, and 582 m.

The function of the Y counters was to furnish some information on the mode of production of the observed showers. As mentioned above, it was thought that cascade showers could not penetrate the 15 cm of Pb above the X tubes, and the showers observed would have originated in the lead. Therefore, if a Y tube was discharged simultaneously with an observed shower, one should conclude that the shower was caused by an ionizing ray. Only about 40 percent of the area and solid angle above the X counters was covered by the Y tubes, and no measurements were made of the efficiency or sensitive area of the counter tubes; therefore, this arrangement was used not to determine the actual fraction of showers caused by ionizing rays, but rather to see if there is any change in this fraction with depth.

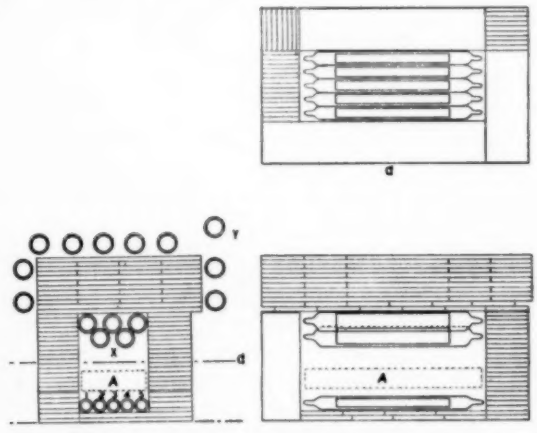

FIG. 7. Shower apparatus used at various depths.

Table III shows that the percentage of showers produced by ionizing rays does not change with depth. Since it is generally assumed that most of the showers at sea level are produced by mesotrons and since the cloud-chamber work at 71 m

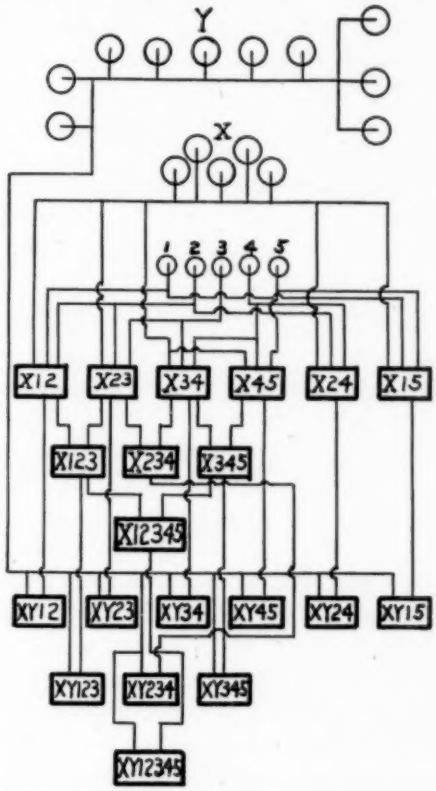

FIG. 8. Circuit diagram for shower apparatus.

depth gave no evidence of a non-ionizing shower producer, one may assume that practically all showers down to 582 m are produced by ionizing primaries.

Concerning now the size of showers, it is seen that the threefold circuits, $X12$, $X23$, etc. counted all sized showers; i.e., two or more particles. The $X123$, $X234$, and $X345$ circuits recorded showers of three or more particles. If a shower discharged $X12$ but not $X123$, one cannot say that that shower consisted of only two particles, but rather that the shower was small and particles penetrated only two of the lower counters. Similarly, a coincidence $X12345$ represented a shower of five or more particles. It is more probable that such a coincidence was caused by a very large shower than by one of only five particles. One can only say that the

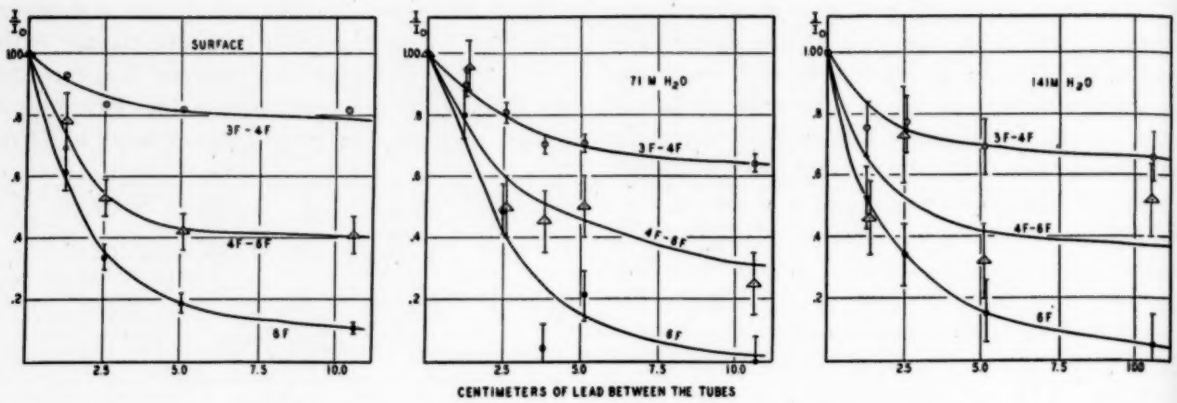

FIG. 9. Absorption of the individual particles in showers at different depths.

TABLE III. Percentage of showers accompanied by a discharge of a Y counter.

Depth	Percentage
Surface	36.6±0.4
71 m	31.1±1.5
141 m	30.8±2.0
582 m	38.6±6.0

density of shower particles was sufficiently high for at least one particle to pass through each tube. We shall call the showers which tripped two of the lower tubes but not three ($3F$–$4F$) small showers; showers which tripped three but not five lower tubes ($4F$–$6F$) medium-sized showers; and showers which tripped all the lower counters ($6F$) large showers.

The percentage of small, medium, and large showers at the different depths is shown in Table IV. The data show quite consistently the steady increase in the relative number of large showers with depth. Furthermore, as the third column shows, the increase in the relative number is greater for the large showers than for the medium-sized showers. At the extreme position, 582 m, it is interesting to note that the number of showers large enough to set off at least three of the lower tubes is actually larger than the number of small showers. Since the Y data show that there is no significant change in the nature of the shower-producing rays, this increase of size is most probably a manifestation of the increase in mean energy of the penetrating rays with depth.

Table V gives the absorption data for various sized showers.

Table IV shows that the large showers are relatively more abundant at greater depths. Table V states the same thing in a different way; namely, that the rays producing the large showers are more penetrating. This is to be expected, since the more energetic a ray, the larger is the shower it can produce, and also the greater is its probable penetration.

These tables explain why shower absorption experiments performed by various observers can give such different results. For example, an experiment designed to measure shower intensity *vs.* depth will also be affected by the change in shower size with depth.

To measure the absorption of the individual particles in the showers, counts were taken with various thicknesses of Pb at A, between the X counters and counters 1, 2, 3, 4, and 5.

TABLE IV. Percentage of small, medium, and large showers at different depths.

Depth	Small	Medium	Large
Surface	75	19	06
71 m	58	22	20
141 m	53	23	24
582 m	45	($M+L=55$)	*

*At 582m the $X12345$ circuit did not record because of a faulty vacuum tube.

TABLE V. Ratio of $\frac{\text{counts/hour}}{\text{counts/hour at surface}}$.

Depth	$3F$	$4F$	$6F$	$3F$–$6F$	$4F$–$6F$
Surface	1.00	1.00	1.00	1.00	1.00
71 m	0.11	0.19	0.37	0.08	0.13
141 m	0.04	0.08	0.18	0.03	0.05
582 m	0.003	0.008	—	0.002	—

Figure 9 shows these absorption curves. It is apparent that at all three depths the individual particles in the large showers are less penetrating than in the medium-sized showers, and these, in turn, are less penetrating than the particles in the small showers. This is probably because in the larger cascade showers the energy of the original particle has been divided many more times, and so the average energy of the individual particles is less than in the small showers. Of course, there is no way to prevent showers from being formed in the Pb absorber *A*. These, moreover, would be confined to a narrow bundle in the Pb; and so would have a greater probability of being detected as small showers than as large showers. These showers formed in *A* will not reduce in number with increasing thicknesses of *A*. This explains why the particles in the small showers appear to be hard. The difference at any one depth in the absorption curves for particles of various sized showers thus can be interpreted simply and probably is not of great significance. But the fact that these groups of curves are very similar at several depths indicates that the showers are also similar in nature at the different depths. At sea level, the showers are known to be cascade showers; apparently, this is also true at the other depths.

Showers are produced by knock-on electrons or radiated photons. If protons are present and are more penetrating than the mesotrons, at the greatest depth the protons alone will remain. Clay has pointed out that at high energies, the protons do not radiate as efficiently as the mesotrons. Thus, if the most penetrating primaries are protons, as one goes to the greatest depths, the relative number of showers will decrease. These data do not show any decrease; however, there may be a maximum between 141 and 582 m, or the ratio may fall off at still greater depths. Plans have been made to continue these experiments to detect the presence of protons underground.

CONCLUSIONS

The results of the various experiments of the present series are all consistent with the interpretation that the cosmic rays underground are mesotrons accompanied by electronic secondaries (knock-ons and their progeny). No evidence could be found for a non-ionizing primary. The data at the greatest depths are not sufficient to rule out the possible existence of high energy protons underground.

The writers wish to express their appreciation to Dean A. H. Compton for his advice and encouragement in planning these experiments. It is a pleasure to acknowledge the generous assistance of the managers and men of the Isle Royale Mining Company. Mr. James Richards and Mr. William Boden were especially helpful in the maintenance of the equipment.

PHYSICAL REVIEW VOLUME 63, NUMBERS 5 AND 6 MARCH 1 AND 15, 1943

Cavitation in an Elastic Liquid

E. H. KENNARD
Cornell University, Ithaca, New York
(Received January 26, 1943)

An idealized theory of cavitation in the interior of a liquid is developed as an extension of the hydrodynamics of irrotational motion. It is assumed that cavitation occurs whenever the pressure sinks to a fixed breaking-pressure and that the pressure then rises at once to a fixed cavity pressure. The boundary of the cavitated region either advances as a breaking-front, moving with supersonic velocity, or remains stationary as a free surface, or recedes toward the cavitated region as a closing-front. The relevant formulas are obtained.

CAVITATION has been studied most extensively at the interface between a liquid and a solid, but apparently it may occur also within the liquid itself. The latter type of cavitation should be influenced by the elasticity of the liquid and should present certain hydrodynamical features of interest. In the present paper a contribution is offered to the theory of cavitation as a hydrodynamical phenomenon. The theory may also find application to the motion of liquids in pipes, even if the cavitation is actually initiated at the walls.[1]

1. FUNDAMENTAL ASSUMPTIONS

In order to develop a tractable analytical theory, it will be assumed that the liquid cavitates whenever its pressure sinks to a fixed *breaking-pressure* p_b, and that the pressure then rises at once to a definite cavity pressure p_c, the two pressures being such that

$$p_b \leqq p_c. \tag{1}$$

The pressure p_b represents the minimum pressure that the liquid can stand; and, as a special case, it may equal p_c. In actual cases cavitation within a liquid takes the form of small bubbles, and these commonly contain a variable amount of air or other gases in addition to the vapor of the liquid; as the bubbles collapse, the foreign gas tends not to redissolve entirely, and for this reason the pressure in the bubbles is not constant. Such complications will be ignored here. It may be assumed that the bubbles are indefinitely small and contain only vapor of the liquid, so that p_c is equal to the vapor pressure. The discussion will be limited to irrotational motion in a homogeneous liquid whose density remains almost but not quite constant. The one-dimensional case is easily treated completely and will be taken up first.

[1] Cf. Kennard, Phys. Rev. **35**, 428 (1930).

2. PLANE BREAKING-FRONTS

For one-dimensional motion the usual acoustic equations may be written

$$\frac{\partial u}{\partial t} = -\frac{1}{\rho}\frac{\partial p}{\partial x}, \quad \frac{\partial p}{\partial t} = -\rho c^2 \frac{\partial u}{\partial x}, \tag{2a, b}$$

where p = excess of pressure above the hydrostatic pressure, u = particle velocity, t = time, x = space coordinate, ρ = undisturbed density, and c = velocity of sound in the liquid. The derivatives occurring here will be assumed to be continuous functions. The equations are ordinarily assumed to hold only for small particle velocities, but they may also be applied generally to the relative motion of the liquid in the neighborhood of any point, that is, provided uniformly moving axes are employed relative to which the velocity of the liquid near the point is small.

Cavitation will obviously start where the pressure first sinks to p_b, hence at a point at which

$$p = p_b, \quad (\partial p/\partial t) < 0, \quad \text{or} \quad (\partial u/\partial x) > 0 \tag{3a, b, c}$$

by (2b). From this point, a *breaking-front* will advance toward both sides; that moving toward $+x$ or toward the right advances into regions where $\partial p/\partial x \geqq 0$, while the other, moving toward $-x$ or toward the left, advances into regions where $\partial p/\partial x \leqq 0$. Just ahead of each front, conditions (3a, b, c) must continue to hold.

To find the rate of advance of the breaking-

fronts, consider what happens as a front moving toward the right traverses, during a time dt, a layer of liquid of thickness dx (Fig. 1). At the beginning of dt, the pressure in the unbroken liquid is p_b over the left-hand face of the layer F_1 and is, therefore,

$$p_b+(\partial p/\partial x)dx$$

over the right-hand face F_2, whereas at the end of dt it has sunk to p_b at F_2 also. Thus the change in p at F_2 during dt is $(-\partial p/\partial x)dx$; or, if U_b denotes the speed of the front relative to the liquid, so that $dx=U_b dt$, the change is $-U_b(\partial p/\partial x)dt$. If, for the moment, axes moving with the unbroken liquid are employed, this change can also be written $(\partial p/\partial t)dt$, the derivative being evaluated at F_2. Equating the last two expressions and using (2b), we obtain

$$U_b=\rho c^2(\partial u/\partial x)/(\partial p/\partial x). \tag{4}$$

Here U_b is the velocity of the front relative to the liquid, which may itself be in motion; but in evaluating the space derivatives axes moving in any manner may be employed.

At the front there is a discontinuity in the pressure. To find its impulsive effect, consider the motion of the layer of liquid of thickness dx (Fig. 1). On the right-hand face F_2 the pressure is nearly equal to the breaking-pressure p_b. It sinks to this value as the front comes up to the face, whereas on the left-hand face there is acting the steady cavity pressure p_c. The momentum in the layer changes, therefore, during dt by $(p_c-p_b)dt$ per unit area. Let u_b denote the particle velocity just ahead of the front, u_c that just behind it. Then the velocity changes impulsively from u_b to u_c as the front passes, and since $dx=U_b dt$,

$$(p_c-p_b)dt=(u_c-u_b)\rho dx=(u_c-u_b)\rho U_b dt,$$

$$u_c=u_b+\frac{p_c-p_b}{\rho U_b}=u_b+\frac{p_c-p_b}{\rho^2 c^2}\frac{\partial p/\partial x}{\partial u/\partial x}, \tag{5}$$

from (4).

The same equations are obtained for a breaking-front advancing toward the left. In view of (3c), Eq. (4) makes U_b positive where $\partial p/\partial x>0$ and negative where $\partial p/\partial x<0$, the two signs referring to fronts traveling in opposite directions. The sign of u_c-u_b is likewise opposite in the two cases, the liquid being accelerated in the direction of advance of the front. At the initial point, where p first sinks to p_b, $\partial p/\partial x=0$ and $U_b=\pm\infty$.

It remains to be shown, however, that the motion of the liquid represented by u_c as defined by Eq. (5) is a hydrodynamically possible one. In doing this, an additional condition for the propagation of a breaking-front is obtained. The argument takes very different courses according as $p_c=p_b$ or $p_c>p_b$.

If $p_c=p_b$, by (5) $u_c=u_b$, the liquid being left at each point with that particle velocity which it happens to possess at the instant of arrival of the front. It is necessary that the liquid be not left with a motion of contraction; hence the values of u_c left behind the front can only vary in such a way that

$$(\partial u_c/\partial x)\geqq 0. \tag{6}$$

Now, if u has the value u_{b1} at the left-hand face F_1 of a layer of thickness dx (Fig. 1), at the instant when a front moving toward the right passes this face, then, at the same instant, at the right-hand face F_2,

$$u=u_{b1}+(\partial u/\partial x)dx.$$

Let uniformly moving axes be employed such that momentarily u_{b1} is zero or small. Then, by the time that the front has reached F_2, u will have changed at F_2 to

$$u_{b2}=u_{b1}+(\partial u/\partial x)dx+(\partial u/\partial t)dt.$$

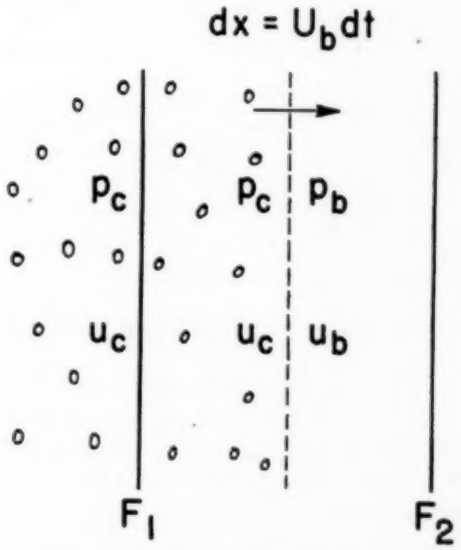

FIG. 1. Motion of a breaking-front.

After the passage of the front, u does not change with time because of the absence of a pressure gradient in the cavitated region. Hence the difference, $u_{b2}-u_{b1}$, is also the difference between the values of u_c at F_1 and at F_2, or du_c, so that

$$du_c = u_{b2}-u_{b1} = (\partial u/\partial x)dx + (\partial u/\partial t)dt,$$

or, by (2a) and the relation $dx = U_b dt$,

$$du_c = [U_b(\partial u/\partial x) - (1/\rho)(\partial p/\partial x)]dt.$$

The condition expressed by (6) now requires that

$$U_b \geqq (1/\rho)(\partial p/\partial x)/(\partial u/\partial x), \qquad (7)$$

since $\partial u/\partial x > 0$. Multiplication of this inequality by Eq. (4) gives

$$U_b^2 \geqq c^2; \qquad (8)$$

and division of this latter inequality by Eq. (4) squared gives

$$1 \geqq (1/\rho^2 c^2)[(\partial p/\partial x)/(\partial u/\partial x)]^2, \qquad (9)$$

whence

$$|\partial p/\partial x| \leqq \rho c(\partial u/\partial x). \qquad (10)$$

The same results are obtained for fronts moving toward the left.

If, on the other hand, $p_c > p_b$, the argument just given does not apply, because by Eq. (5) $u_c \neq u_b$ at the front. The situation appears to be essentially different. For a front running to the right ($\partial u/\partial x > 0$, $\partial p/\partial x > 0$), $u_c > u_b$, so that the liquid behind the front tends to overrun that just ahead of it, which is physically impossible. The condition that prevents this happening can be found as follows.

While the front is traversing the layer of thickness dx (Fig. 1), during a time dt, the face F_2 of the layer advances a distance $u_b dt$ (to the first order), whereas the other face F_1 advances a distance $u_c dt$. The volume occupied by the layer, per unit area, thus decreases by

$$(u_c - u_b)dt = [(p_c - p_b)/(\rho U_b)]dt \qquad (11)$$

by (5). During the same time, however, the liquid in the layer contracts, as its pressure rises suddenly from p_b to p_c. The elasticity being ρc^2, the contraction decreases the volume actually occupied by liquid by the amount

$$(1/\rho c^2)(p_c - p_b)dx = (1/\rho c^2)(p_c - p_b)U_b dt. \qquad (12)$$

Hence the liquid can continue to fit into the space allowed for it, with or without the occurrence of cavitation, provided

$$(1/\rho c^2)(p_c - p_b)U_b \geqq [(p_c - p_b)/\rho U_b],\ U_b^2 \geqq c^2.$$

Thus expressions (8) and (10) are obtained again.

In case $p_c > p_b$, however, it is not possible to show that necessarily $\partial u_c/\partial x \geqq 0$. Apparently it can happen that behind a front $\partial u_c/\partial x < 0$; in this case, any cavitation bubbles that may have been formed at the instant of passage of the front will proceed to decrease in size and ultimately to disappear again.

According to Eq. (8) as written it can happen that $U_b = \pm c$. It is easily seen, however, that if $U_b = \pm c$ for a finite length of time, cavitation does not actually occur. Thus *a true breaking-front travels always at a speed exceeding that of sound in the liquid*. The conditions found for its propagation, including (10), may be summarized as follows:

$$p = p_b, \quad (\partial u/\partial x) > 0, \qquad |\partial p/\partial x| < \rho c(\partial u/\partial x); \qquad (13a, b, c)$$

in addition, it is necessary that $\partial p/\partial x \geqq 0$ for propagation toward $+x$ or $\partial p/\partial x \leqq 0$ for propagation toward $-x$. In these expressions the derivatives are to be evaluated in the unbroken liquid just ahead of the breaking-front. These values are not affected in any way by the approach of the front; for no hydrodynamic influence of the first order can be propagated through a fluid at a speed exceeding that of sound.

Once started, a breaking-front will travel until it arrives at a point beyond which the necessary conditions are not satisfied. At a point where $\partial p/\partial x = 0$, the front may meet another one coming from the opposite direction, whereupon both fronts will disappear. At a point where $|\partial p/\partial x|$ becomes equal to $\rho c \partial u/\partial x$, with larger values beyond, the front, approaching at speed c relative to the liquid (provided $\partial u/\partial x > 0$), must suddenly stop advancing. What happens next at such a point will be considered presently.

A simpler rule than that just stated might have been supposed to be preferable, namely, that the front travels as far as pressures so low as p_b occur. This statement, however, although true, is less convenient than the conditions just stated, be-

cause the occurrence of cavitation results indirectly in a contraction of the region within which the pressure sinks to p_b. This results from the fact that the pressure is higher in the cavitated region than it would have been if cavitation had not occurred, and, after the breaking-front has ceased advancing, propagation of this higher pressure into adjoining regions prevents the occurrence of pressures so low as p_b at some points where such pressures would otherwise have occurred. It is impossible, in fact, for the breaking-front to touch the surface which, in the absence of cavitation would be the boundary of the region of pressures below p_b; for, at this surface, when $p=p_b$, $\partial p/\partial t=0$, else p would sink to p_b at points outside the surface as well (provided $\partial p/\partial t$ is continuous), and then by (2b) $\partial u/\partial x=0$ and condition (13c) is not satisfied.

3. THE CAVITATED REGION

In the cavitated region the pressure is assumed to be uniformly equal to p_c, so that there is no pressure gradient; hence the particle velocity u_c at each point remains as it was left by the passage of the breaking-front. Let η denote the fraction of the space which is occupied by bubbles. If $p_c=p_b$, η is zero immediately back of the breaking-front. If $p_c>p_b$, however, η starts from an initial value η_0 representing the difference between the space freed by compression from pressure p_b to p_c and the space filled by incoming liquid. When a front travels toward $+x$, the intial free space in a layer dx thick just back of the front equals the difference between expressions (12) and (11), so that, since $dx=U_b dt$,

$$\eta_0 dx=(1/\rho c^2)(p_c-p_b)U_b dt-[(p_c-p_b)/\rho U_b]dt,$$

$$\eta_0=[(p_c-p_b)/\rho c^2][1-(c^2/U_b^2)]. \qquad (14)$$

The same result is obtained for fronts traveling toward $-x$. Thereafter η changes at the rate $\partial u_c/\partial x$. Hence, at any time t subsequent to the passage of the front at time t_b,

$$\eta=\int_{t_b}^{t}(\partial u_c/\partial x)dt + [(p_c-p_b)/\rho c^2][1-(c^2/U_b^2)]. \qquad (15)$$

The value of η may vary from point to point in the cavitated region. The initial value η_0 will be small, in accordance with the assumption that the pressure remains within the linear range; but subsequently η may increase to any magnitude.

4. MOTION OF PLANE BREAKING-FRONTS IN TERMS OF WAVE TRAINS

Since no influence can be propagated with supersonic velocity past a breaking-front, the pressure and particle velocity ahead of the front will be determined by initial or boundary conditions elsewhere; hence, in the above formulas the values of p and u may be regarded as given. When, however, the boundary of the cavitated region moves more slowly than the speed of sound, the presence of cavitation is able to influence the values of p and u in the nearby unbroken liquid. In such cases analysis in terms of fundamental wave trains is convenient. It will be worth while to restate, also, the conditions for the propagation of a breaking-front in terms of such trains.

Any one-dimensional disturbance in unbroken liquid can be resolved into a train of waves traveling at speed c toward $+x$ and another traveling toward $-x$; if p_1, p_2 denote the corresponding pressures and u_1 and u_2, particle velocities, then

$$p_1=\rho c u_1, \qquad p_2=-\rho c u_2, \qquad (16a, b)$$

$$p=p_1+p_2, \qquad u=u_1+u_2, \qquad (17a, b)$$

$$p_1=\tfrac{1}{2}(p+\rho c u), \quad p_2=\tfrac{1}{2}(p-\rho c u). \qquad (18a, b)$$

Here the significance of p_1 and p_2 is really only mathematical, hence u_1, u_2, and u need not be restricted to be small. Substitution from these equations for u in (13b) gives

$$(\partial p_1/\partial x)-(\partial p_2/\partial x)>0,$$

and substitution in (13c) squared gives

$$[(\partial p_1/\partial x)+(\partial p_2/\partial x)]^2<[(\partial p_1/\partial x)-(\partial p_2/\partial x)]^2,$$

$$(\partial p_1/\partial x)(\partial p_2/\partial x)<0.$$

The first and last of these inequalities can be satisfied simultaneously only if $\partial p_1/\partial x$ is positive and $\partial p_2/\partial x$ negative. Hence the conditions for the propagation of a breaking front and Eqs. (4)

and (5) for U_b and u_c can be written, since $u_b = u$,

$$p_1 + p_2 = p_b, \quad (\partial p_1/\partial x) > 0, \quad (\partial p_2/\partial x) < 0; \tag{19a, b, c}$$

and, for travel toward $+x$,

$$(\partial p_1/\partial x) \geqq -(\partial p_2/\partial x), \tag{20a}$$

or, for travel toward $-x$,

$$(\partial p_1/\partial x) \leqq -(\partial p_2/\partial x); \tag{20b}$$

$$U_b = c\frac{(\partial p_1/\partial x) - (\partial p_2/\partial x)}{(\partial p_1/\partial x) + (\partial p_2/\partial x)}, \tag{21}$$

$$u_c = \frac{1}{\rho c}\left[p_1 - p_2 + (p_c - p_b) \times \frac{(\partial p_1/\partial x) + (\partial p_2/\partial x)}{(\partial p_1/\partial x) - (\partial p_2/\partial x)} \right]. \tag{22}$$

Equations (19a, b, c) lead to the useful conclusion that a wave of tension can give rise to cavitation only where it overruns a wave of *decreasing* pressure traveling in the opposite direction.

5. PLANE RESTING BOUNDARIES AND CLOSING-FRONTS

The next question to consider is the behavior of the boundary of a cavitated region when it cannot advance as a breaking front. It may stand still, relatively to the liquid, or it may advance into the cavitated region, leaving the liquid unbroken again behind it; in the latter case, the boundary may be called a *closing-front*. Which alternative occurs will depend, in general, both upon conditions in the cavitated region and upon the magnitude of the wave that is incident from the unbroken side.

Let p' denote pressure in the component wave train that approaches the boundary in the unbroken liquid and p'' that in the receding train; let u denote the particle velocity on the unbroken side and u_c that on the cavitated side, but let the positive direction for velocity be taken now always toward the cavitated region. As before, let p_c denote the uniform pressure in the cavitated region and η the fraction of the space that is occupied by bubbles.

Whether the boundary remains at rest or advances is found to depend upon the magnitudes

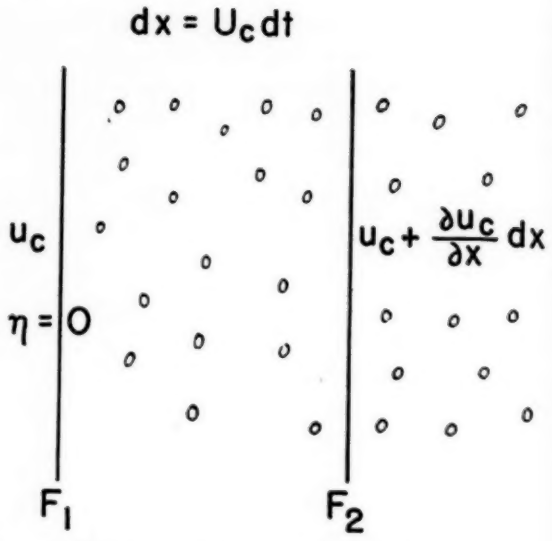

FIG. 2. Layer of cavitated liquid dx thick.

of p', u_c, $\partial u_c/\partial x$, and η. These quantities may be regarded as given; p'' is then determined by conditions at the boundary, and p and u are given by the relations, obtained from (17a, b) and (16a, b),

$$p = p' + p'', \quad u = (1/\rho c)(p' - p''), \tag{23a, b}$$

whence

$$p + \rho c u = 2p'. \tag{23c}$$

Four cases may be distinguished.

(1) Intrinsic Closing-Fronts

$$\eta = 0, \quad \partial u_c/\partial x < 0, \quad -\partial u_c/\partial x \geqq c\partial\eta/\partial x > 0. \tag{24a, b, c}$$

Here x denotes distance measured from the boundary into the cavitated region, and the relations refer to conditions at the boundary.

Because of (24a, b), the cavitation will proceed to disappear in the layers next to the boundary; hence the boundary will advance into the cavitated region as a closing-front, leaving unbroken liquid behind it. A front of this type, being propelled by conditions inside the cavitated region, may be called an *intrinsic* closing-front.

To find its speed of advance, consider a layer of the cavitated liquid dx thick (Fig. 2). If the particle velocity is u_c over the face toward $-x$ or F_1, that over the other face F_2 is

$$u_c + (\partial u_c/\partial x)dx.$$

Hence during a time dt the volume of the layer changes by $(\partial u_c/\partial x)dxdt$, for each unit of area of its faces and, since the pressure is constant, the change must occur in the cavitated space and not in the liquid itself. Hence,

$$(\partial u_c/\partial x)dxdt=(\partial/\partial t)(\eta dx)dt, \qquad \partial\eta/\partial t=\partial u_c/\partial x, \tag{25}$$

in which the time derivative is to be evaluated at a point moving with the liquid.

On the other hand, if U_c is the velocity of advance of the boundary relatively to the liquid, $dx=U_c dt$. At the beginning of dt, $\eta=0$ at F_1, hence at F_2 $\eta=(\partial\eta/\partial x)dx$; whereas at the end of dt, $\eta=0$ at F_2. Hence, during dt, η changes at F_2 by $d\eta=-(\partial\eta/\partial x)dx$. This can also be written $d\eta=(\partial\eta/\partial t)\partial t$. Hence, using $dx=U_c dt$, we obtain

$$(\partial\eta/\partial t)=-U_c(\partial\eta/\partial x), \tag{26}$$

and

$$U_c=-(\partial\eta/\partial t)/(\partial\eta/\partial x) \qquad =-(\partial u_c/\partial x)/(\partial\eta/\partial x) \tag{27}$$

by (25). Here the positive directions for x and u_c are taken toward the cavitated region and the signs of the derivatives are such as to make U_c positive.

So far as can be seen, the value of U_c as given by (27) might be either greater or less than c. If it is greater than c, everything is satisfactory. The advancing front leaves behind it a region in which $p=p_c$ and $u=u_c$, u_c being the local value of the particle velocity as encountered by the advancing front. The two component wave trains in the unbroken liquid are thereby progressively built out in accord with the equations

$$p'=\tfrac{1}{2}(p+\rho cu)=\tfrac{1}{2}(p_c+\rho cu_c), \tag{28a}$$

$$p''=\tfrac{1}{2}(p-\rho cu)=\tfrac{1}{2}(p_c-\rho cu_c). \tag{28b}$$

The part of the p' wave train that is already established and is moving toward the front is unable to overtake it. Even if $U_c=c$, there is no difficulty, although in this case a fixed discontinuity in p and u may occur at the front.

If, however, the value of U_c as defined by Eq. (27) is less than c, a front moving at speed U_c would be overtaken continually by values of p' coming out of the unbroken region. In such cases conditions at the boundary must be determined in part by the arriving values of p', and they will usually not be such as to satisfy Eqs. (28a, b). A different type of action must then occur at the boundary. Thus *intrinsic closing-fronts, when they occur, move through the liquid at velocities not less than that of sound.*

(2) Resting boundary

$$2p'\leqq p_c+\rho cu_c. \tag{29}$$

Let it be assumed that the pressure is continuous at the boundary and equal, therefore, to p_c. Then a wave train must be reflected from the boundary of such magnitude that, by (23a, c)

$$p''=p_c-p', \quad u=(1/\rho c)(2p'-p_c). \tag{30a, b}$$

These equations represent a possible motion provided $u\leqq u_c$, so that the unbroken liquid does not collide with the cavitated liquid; and this condition, in turn, is met provided p' is such that (29) holds. It may be concluded that, whenever (29) holds but the boundary cannot advance as an intrinsic closing-front moving at supersonic velocity, the boundary will remain stationary and the incident waves will be reflected from it in accord with Eq. (30a).

If $2p'$ is actually less than $p_c+\rho cu_c$, so that by (30b) $u<u_c$, separation of the two portions of the liquid must occur, with formation of a crevasse or a special layer of expanding bubbles. If $2p'=p_c+\rho cu_c$, the unbroken liquid remains in peaceful contact with the cavitated liquid.

If, however, (29) does not hold, no solution of the type just described is possible and a different process must occur.

(3) Forced Closing-Fronts

$$2p'>p_c+\rho cu_c, \quad \eta>0. \tag{31a, b}$$

When condition (31a) obtains, the incident waves are so strong that the boundary advances into the cavitated region, closing up the bubbles. The action is one of successive impacts, a finite discontinuity of pressure occurring at the moving boundary if $\eta>0$. A boundary moving in this manner may be called a *forced closing-front.*

Let U_c be the speed of advance of the front relative to the cavitated liquid ahead of it.

Then, during a time dt, a layer of cavitated liquid of thickness dx becomes consolidated. The argument is now similar to that in Section 2.

The mass $(1-\eta)\rho dx$ of liquid per unit area is accelerated from u_c to u; the added momentum is supplied by the action of a pressure p on one face and p_c on the other face. Hence,

$$(1-\eta)\rho(u-u_c)dx=(p-p_c)dt,$$

and since $dx=U_c dt$,

$$p-p_c=(1-\eta)\rho U_c(u-u_c), \tag{32}$$

where p and u denote pressure and particle velocity in the unbroken liquid just behind the front.

Furthermore, since one face of the layer moves at speed u and the other at u_c, its thickness changes during dt by $(u_c-u)dt$. Part of this change is taken up by compression of actual liquid from p_c to p, which changes the total thickness of liquid, initially equal to $(1-\eta)dx$, by the amount

$$-[(p-p_c)/\rho c^2](1-\eta)dx,$$

ρc^2 representing the elasticity. In addition, cavitated spaces of total thickness ηdx are closed up. Hence,

$$\begin{aligned}(u_c-u)dt&=-[(p-p_c)/\rho c^2](1-\eta)dx-\eta dx,\\ \rho c^2(u-u_c)&=[\rho c^2\eta+(1-\eta)(p-p_c)]U_c.\end{aligned} \tag{33}$$

In addition, there is Eq. (23c) or

$$p+\rho cu=2p'. \tag{34}$$

Equations (32), (33), and (34) suffice to fix U_c, p, and u. The solution can be written in a convenient explicit form by introducing the auxiliary quantity

$$v=(1/\rho c)(2p'-p_c)-u_c.$$

According to (31a) v is positive; it may be regarded as known. Then

$$U_c=cv/[v+(c-v)\eta], \tag{35}$$

$$\begin{aligned}p-p_c&=\frac{(1-\eta)\rho cv^2}{2v+(c-2v)\eta},\\ u-u_c&=v\frac{v+(c-v)\eta}{2v+(c-2v)\eta}.\end{aligned} \tag{36a, b}$$

In these equations, as in all equations not referring to breaking-fronts, u and u_c are taken positive toward the cavitated region.

Since $v>0$ and $1\geqq\eta>0$, these formulas make $p>p_c$ and $u>u_c$, as is obviously necessary for physical reasons. Furthermore, from (35) it is clear that $U_c<c$. Or, if we consider the velocity of the front relative to the unbroken liquid behind it or $U_c'=U_c-(u-u_c)$, we find that $U_c'<c$. Thus the front cannot run away but must remain subject to influences propagated up to it from behind at speed c. To sum up, *all forced closing-fronts move at a speed less than that of sound relative either to the unbroken liquid behind them or to the cavitated liquid in front.*

The requirement, $\eta>0$, has been included in the definition of forced closing-fronts because boundaries at which $\eta=0$ appear to constitute a singular class. One type of such boundaries has already been discussed.

(4) Boundaries at which $\eta=0$

If $2p'>p_c+\rho cu_c$, a little consideration shows that the boundary will advance as a closing-front of the intrinsic type if it can do so, otherwise as one of the forced type; in the latter case, its velocity of advance is initially equal to c, so that any tendency to form a front closing by intrinsic action but advancing at a speed below c is cut short. The front will usually advance at once into regions where $\eta>0$.

If, however, $2p'<p_c+\rho cu_c$, a resting boundary as described by Eqs. (30a, b) should certainly occur, accompanied by a finite discontinuity in the particle velocity and by the formation of a gap or a special layer of bubbles lying between the unbroken and the cavitated parts of the liquid. It appears, however, that the opposite side of this gap may also advance into the cavitated region as a closing-front, so that the original boundary splits into three, two resting boundaries separated by a gap and a closing-front.

The principal type of boundary at which $\eta=0$ is the boundary that has just ceased moving as a breaking-front. For there, usually, the inequality expressed by (13c) has just failed to exist because its members have momentarily become equal; hence by (4) at this instant, $U_b^2=c^2$ and by (14) $\eta=\eta_0=0$. At this instant, furthermore, Eq. (5)

becomes, after reversal of the signs of u_c and u_b because of the difference in the direction chosen here for positive velocities,

$$u_c = u_b - (p_c - p_b)/\rho c,$$

and insertion of the value of u_b given by this equation for u and of $p = p_b$ in (23c) gives

$$2p' = p_c + \rho c u_c.$$

The slightest increase in p' will thus cause the boundary to start back as a closing-front. Otherwise it remains as a resting boundary.

6. THREE-DIMENSIONAL CAVITATION

Insofar as the three-dimensional theory can be formulated in compact form, it is easily written out as a generalization of the one-dimensional theory.

Equations (2a, b) are replaced by

$$\partial \mathbf{u}/\partial t = -\nabla p, \quad \partial p/\partial t = -\rho c^2 \operatorname{div} \mathbf{u}. \quad (37a, b)$$

It is clear that wherever $\partial u/\partial x$ occurs in the one-dimensional formulas as the equivalent of $\partial p/\partial t$, it is to be replaced by div $\mathbf{u}$. The theory of boundaries as given above then becomes applicable to three-dimensional cavitation, provided x in the one-dimensional equations is interpreted as distance along the normal to the boundary, and provided u is replaced by the component of the particle velocity taken in the direction of this normal. In addition, it is to be assumed that, as a boundary moves, no change occurs in any component of the particle velocity tangential to it, the impulsive changes being confined to the normal component.

Cavitation will begin at a point where a local minimum of pressure sinks to the breaking pressure p_b, and from this point a breaking-front will spread out in the form of a closed surface surrounding the point of initiation and enclosing a cavitated region. In the unbroken liquid this surface, at which $p = p_b$, constitutes a surface of uniform pressure, hence the normal to the surface lies everywhere in the direction of ∇p. The conditions to be satisfied in the unbroken liquid in order that such a front may advance can at once be written down as a generalization of Eqs. (13a, b, c):

$$p = p_b, \quad \operatorname{div} \mathbf{u} > 0,$$
$$0 \leqq (\partial p/\partial n) < \rho c \operatorname{div} \mathbf{u}, \quad (38a, b, c)$$

where n stands for distance measured into the unbroken liquid along the normal to the boundary. As before, the front cannot travel to the boundary of the region in which, in the absence of cavitation, the pressure would sink to p_b, at least provided all derivatives of p are continuous functions of the space variables. For U_b, the velocity of propagation of the front along its normal relative to the unbroken liquid ahead, Eqs. (4) and (8) are replaced by

$$U_b = \rho c^2 \left(\frac{\partial u_x}{\partial x} + \frac{\partial u_y}{\partial y} + \frac{\partial u_z}{\partial z} \right) \Big/ \left(\frac{\partial p}{\partial n} \right) \geqq c. \quad (39)$$

In the same way the theory of the cavitated region, as developed in Section 3, can at once be generalized. Those components of the particle velocity which are tangential to the breaking-front are unaltered by the passage of the front, whereas the component perpendicular to the front, taken positive toward the unbroken liquid, is changed from u_{bn} to u_{cn} where

$$u_{cn} = u_{bn} + (p_c - p_b)/\rho U_b. \quad (40)$$

The fractional cavitation η, or the fraction of the space that is occupied by bubbles, is left by the passage of the front at the value stated in Eq. (14) or

$$\eta_0 = [(p_c - p_b)/\rho c^2][1 - (c^2/U_b^2)]; \quad (41)$$

after the lapse of a further time $t - t_b$ it becomes

$$\eta = \int_{t_b}^{t} \operatorname{div} \mathbf{u}_c dt + [(p_c - p_b)/\rho c^2] \times [1 - (c^2/U_b^2)]. \quad (42)$$

Here $\mathbf{u}_c$ is the particle velocity in the cavitated region, which remains constant in time as long as the cavitation lasts.

From the physical standpoint, the behavior of resting boundaries and of closing-fronts, also, is essentially the same as in the one-dimensional case. For intrinsic closing-fronts the mathematical theory likewise is similar and can at once be written down. Equation (27) for the propagation velocity of such a front, relative to the

cavitated liquid, is replaced by

$$U_c = -(\text{div } \mathbf{u}_c)/(\partial\eta/\partial n). \tag{43}$$

For a forced closing-front, the analogs of Eqs. (32) and (33) can at once be written:

$$p - p_c = (1-\eta)\rho U_c(u_n - u_{cn}), \tag{44}$$

$$\rho c^2(u_n - u_{cn}) = [\rho c^2\eta + (1-\eta)(p-p_c)]U_c. \tag{45}$$

Here p and u denote pressure and particle velocity on the unbroken side of the front and the subscript n denotes the component normal to the boundary, taken positive when directed toward the side of cavitation. Components of velocity tangential to the front are unaffected by its passage. Difficulty is encountered, however, in attempting to obtain a third equation in order to determine p, u, and U_c, if η and u_{cn} are assumed known. Even the condition for the distinction between resting boundaries and forced closing-fronts cannot easily be formulated in the general case. The disturbance in the unbroken liquid might, indeed, be resolved into an infinitude of plane waves; but the treatment of these waves at a curved boundary is rendered very complicated by the occurrence of diffraction. All that can readily be stated is that existing conditions in the unbroken liquid, which in turn depend in part upon conditions at distant boundaries, in combination with the existing distribution of the values of η and of the particle velocity in the cavitated region, will determine whether the boundary advances or remains at rest; and, if the boundary advances, those conditions in the unbroken liquid combine with Eqs. (44) and (45) to fix the values of p, u_n, and U_c.

It is unfortunate that the three-dimensional theory cannot be carried further in simple form.

A concluding comment may be added, however, concerning the special case of spherical waves.

Let

$$p_1 = \frac{1}{r} f(ct - r)$$

represent the pressure in a train of waves diverging from a fixed center, r being the distance from the center and f any differentiable function. Let these waves be superposed upon other waves of small amplitude represented as a whole by $p_2(x, y, z, t)$.

In this case relation (38c) may conveniently be written, by means of (37b) and the relation, $p = p_1 + p_2$,

$$-\frac{\partial p_1}{\partial t} - \frac{\partial p_2}{\partial t} > c\left(\frac{\partial p_1}{\partial n} + \frac{\partial p_2}{\partial n}\right) \geqq 0.$$

If the normal along which n is measured makes an angle θ with the direction of r,

$$\frac{\partial p_1}{\partial n} = \frac{\partial p_1}{\partial r}\cos\theta = -\left(\frac{1}{c}\frac{\partial p_1}{\partial t} + \frac{p_1}{r}\right)\cos\theta;$$

hence, the preceding equation, expressing the necessary condition for the propagation of a breaking-front, may be written

$$-(1-\cos\theta)\frac{\partial p_1}{\partial t} + \frac{cp_1}{r}\cos\theta > \frac{\partial p_2}{\partial t} + c\frac{\partial p_2}{\partial n}. \tag{46}$$

From this result it is clear that a breaking-front cannot follow a diverging spherical wave of tension into quiescent liquid ($p_1 < 0$, $p_2 = 0$); for in such a case $\theta = 0$, since over the front $p = p_b = p_1$. To cause cavitation, a spherical wave of tension must overrun other waves of such character that the right-hand member of Eq. (46) has sufficiently large negative values.

7. ENERGETIC AND THERMODYNAMICAL CONSIDERATIONS

The preceding equations have been based solely upon the conservation of matter and of momentum. An investigation, of which no details will be given, reveals, however, that, if $p_b < p_c$, the passage of either a breaking-front or a forced closing-front is likely to leave behind it a greater amount of energy than is accounted for by the elastic and kinetic energy of the cavitated water. Upon closer examination of the cavitation process, it appears probable that this excess energy is either dissipated or radiated away in consequence of local oscillations associated with the impulsive production or destruction of bubbles. Thus the theory involves no conflict with thermodynamics.

A difference between the breaking-pressure p_b and the cavity pressure p_c implies, however, an instability of the liquid which might seem to open the way for other types of action than those assumed above. There exists in fact, no hydrodynamic or thermodynamic reason why cavita-

tion should not occur at any pressure below p_c. An analogy might be expected with the behavior of moderately supercooled liquid, in which freezing must be initiated by external causes but, once started, spreads rapidly until the temperature of the mass has been raised to the freezing point. It might be anticipated, therefore, that a breaking-front, if unable to advance further at the pressure of spontaneous cavitation, p_b, would continue to advance at higher pressure p_b' until it encountered a pressure equal to p_c.

Against such an assumption the following objection may be raised. It can be shown that even on this alternative hypothesis a breaking-front must advance through the liquid at supersonic velocity. But the advance into regions of pressure higher than p_b would necessarily occur, not as a consequence of automatic changes in the unbroken liquid ahead, but as an effect propagated out of the region already cavitated; and it seems unlikely, although certainly not impossible, that such an effect could be propagated at a speed exceeding that of sound.

Which assumption corresponds more nearly with the behavior of actual liquids remains to be discovered by experiment.

PHYSICAL REVIEW VOLUME 63, NUMBERS 5 AND 6 MARCH 1 AND 15, 1943

Thermal Diffusion with Ammonia

W. W. WATSON AND D. WOERNLEY
Sloane Physics Laboratory, Yale University, New Haven, Connecticut

(Received February 2, 1943)

With a "two-bulb" thermal diffusion experiment in which is used NH_3 having about a 15 percent N^{15} content to increase the accuracy of the mass spectrometer analyses, it has been found that with decreasing temperature the thermal diffusion constant α of ammonia changes from + to − values at about room temperature. The value of α varies linearly with the logarithm of the absolute temperature, the rate of decrease being, however, nearly eight times that for neon and argon. A qualitative discussion is presented, attributing this effect largely to the strong first-order dipole-dipole intermolecular forces which are proportional to $1/R^4$.

IN general the phenomenon of thermal diffusion operates to produce an increased concentration of the heavier component in a binary gas mixture in the colder portion of the apparatus, while the lighter component tends to concentrate in the warmer part. For these cases there is a positive thermal diffusion constant α in the equation $D_T/D=\alpha c_1 c_2$, where D_T is the coefficient of thermal diffusion, D is the coefficient of ordinary diffusion, and c_1 and c_2 are the relative concentrations of the light and heavy components, respectively. In fact, until just recently no instance where thermal diffusion proceeds with a negative thermal diffusion constant had been reported. Grew[1] has now found a reversal in the sign of α with change in the composition of a neon-ammonia mixture. Between 0 and 75 percent neon, the heavier molecule, neon, tends to concentrate at the upper end of a Clusius-Dickel column. This indicates that the α is negative. Above 75 percent neon, the neon concentrates at the lower end, so that in this range α is positive. The theoretical possibility of such a reversal had been pointed out by Chapman.[2]

A definite temperature variation of the positive α for neon was found by Nier,[3] the value of α decreasing with the lowering of the mean temperature. Jones[4] has shown theoretically that a variation similar to that reported by Nier is to be expected for either the Sutherland or the Lennard-Jones 9,5 molecular models. This theoretical investigation indicated that, for tem-

[1] K. E. Grew, Nature **150**, 320 (1942).

[2] S. Chapman, Proc. Roy. Soc. **A177**, 38 (1940).
[3] A. O. Nier, Phys. Rev. **57**, 338 (1940).
[4] R. Clark Jones, Phys. Rev. **59**, 1019 (1941).

peratures near the critical temperature for a gas whose molecules are spherically symmetrical, the thermal diffusion constant might be negative. Recently Stier[5] has made measurements for α for argon over a number of temperature ranges in the two lowest of which α should be negative according to the Lennard-Jones 9,5 model. The observed α's are positive, however.

The present investigation with ammonia was initiated with the object of finding an experimental case where, with decreasing temperature, a reversal in the sign of the thermal diffusion effect occurs. Ammonia was considered to be a good possibility because (1) predictions from viscosity data indicate that α should be negative in the lower temperature ranges,[6] (2) it is possible to work well below the critical temperature, 132°C, and (3) it is known that long-range intermolecular forces are particularly strong where the molecules are symmetrical tops with a relatively large dipole moment.[7] Since the ammonia molecule is not spherically symmetrical and since there is the possibility of an interchange of energy between the external and internal degrees of freedom, most of the theoretical equations which have been developed for the thermal diffusion effect do not strictly apply. But thermal diffusion depends strongly on the intermolecular forces between the molecules involved, and hence any measurements of controlled variations of this phenomenon should contribute to our better understanding of these forces.

EXPERIMENTAL PROCEDURE

The experiments have been performed with an all-glass "two-bulb" apparatus, both bulbs being of large volume, 2 liters, in order to have a sufficient amount of gas for a number of cycles of operation in spite of the low initial pressure of 4.6 cm of Hg set by the temperature of the cold bulb, −76°C. The two bulbs were connected by a 1-cm bore tube 34 cm long, containing a three-way stopcock also of 1-cm bore. Appropriate temperature baths maintained the bulbs at the required constant temperatures during each experiment. After some trials good data were obtained for the temperature intervals 197°K–298°K, 197°K–373°K, and 298°K–457°K. These results are presented below.

Both to overwhelm any residual $N^{14}H$ mass peak (all NH_3 samples were converted to N_2 and analyzed for the N^{15}/N^{14} ratio) in the mass spectrometer and to develop larger changes in concentration in the thermal diffusion experiments, ammonia gas was prepared from samples of NH_4NO_3 in which the N of the ammonium radical was enriched in the N^{15} isotope. This "heavy" NH_4NO_3 was obtained from the Eastman Kodak Company and was diluted in every case with ordinary ammonium nitrate so that the prepared ammonia contained from 13 to 15 atom percent N^{15}. The NH_3 was obtained by slowly adding a concentrated solution of NaOH, the reaction taking place in a vacuum. The gas was condensed in a dry-ice trap and then thoroughly dried by vacuum distillations and drying agents. A sample of this ammonia was then taken for mass spectrometer analysis, and the two-bulb apparatus filled with the gas to a pressure of 4.6 cm of Hg. The hot and cold bulbs were then interconnected and allowed to come to equilibrium.

It can be shown that the relaxation time τ for this process is

$$\tau \cong (Vl/DA)[T_c/(T_h+T_c)], \qquad (1)$$

where V is the volume of one of the bulbs, l is the length, and A the cross section of the connecting tube, D is the coefficient of ordinary diffusion, and T_c and T_h are the temperatures of the cold and hot bulbs, respectively. For $T_c=197°$ and $T_h=373°$, τ is 3.2 hours. To insure that equilibrium was reached, the first thermal diffusion was continued for about five times this value of τ. The cold bulb was then isolated, and the ammonia pumped out of the hot bulb. Next, the connection between the two bulbs was reestablished and the process repeated. Since D is inversely proportional to the density, τ decreases

TABLE I. Values of α and R_T for ammonia.

T_c °K	T_h °K	c_1^0	c_1^0	$c_2-c_1^0$	α	R_T
298	457	0.1379	0.8621	+0.0017	+0.0105±0.0051	+0.41±0.20
197	373	0.1525	0.8475	−0.0009	−0.0039±0.0035	−0.15±0.14
197	298	0.1419	0.8581	−0.0016	−0.0100±0.0063	−0.39±0.25

[5] L. G. Stier, Phys. Rev. **62**, 548 (1942).
[6] H. Brown, Phys. Rev. **57**, 242 (1940).
[7] H. Margenau and D. T. Warren, Phys. Rev. **51**, 748 (1937).

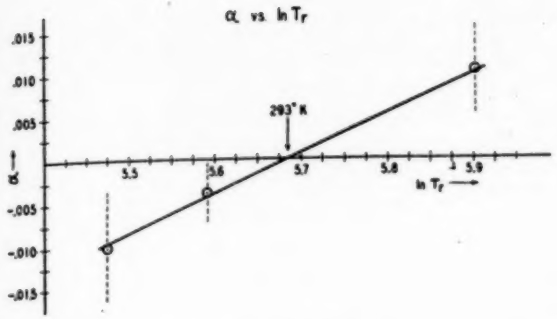

FIG. 1. Variation of the thermal diffusion constant α for ammonia with the logarithm of the absolute temperature.

proportionally with the pressure drop each time. This cycle of operations was repeated eight times in each experiment. For greater accuracy it would have been desirable to have repeated this process more than eight times, but there was a limitation on the initial amount of gas set by the vapor pressure of NH_3 at $-76°C$, and in the conversion to N_2 before analysis the pressure of the N_2 is only half that of the NH_3 converted. Before analysis we found it necessary to have this nitrogen in contact with a liquid-air trap for about 12 hours in order to condense all water vapor evolved in the conversion and any remaining non-oxidized ammonia.

The N^{15}/N^{14} ratios in the original and changed samples of gas were obtained by identical procedures using a modified Nier-type 60° mass spectrometer. Our modifications of Nier's original specifications[8] have been made to increase the stability of the instrument and to facilitate its operation. In order to be able to replace a burned-out filament more quickly, the filament stem is introduced into the side of the ion source. The electrometer tube is placed in a metal case in the evacuated system, with the ion collector placed at the top of the grid of the tube. The connections to the elements of the electrometer tube are brought into the case through the base of a 6L6 tube soldered into the metal case. Since this case may not be raised to as high a temperature as the other parts of the system during the preliminary baking out, its walls are cooled with water, ice, or dry ice to a constant lower temperature while in operation.

[8] A. O. Nier, Rev. Sci. Inst. **11**, 212 (1940).

RESULTS

The experimental values of α may be calculated from the equilibrium concentrations of the two isotopic molecules in such a two-bulb experiment from the relation

$$\alpha=\frac{c_2-c_2^0}{c_2^0c_1^0n}\times\frac{T_h/T_c+1}{\ln\,(T_h/T_c)}, \tag{2}$$

where c_2 is the concentration of N^{15} in the cold bulb, c_2^0 and c_1^0 are the concentrations of N^{15} and N^{14}, respectively, in the gas before the thermal diffusion began, n is the number of cycles of operation, and T_h and T_c are the temperatures of hot and cold bulbs, respectively. R_T, the index of intermolecular force, is taken to be the ratio of this experimental α to the hard sphere value $(105/118)[(m_1-m_2)/(m_1+m_2)]$. The latter is 0.0254 for this $N^{15}H_3$, $N^{14}H_3$ mixture. The measured concentrations and calculated α and R_T values are given in Table I.

The magnitude of the maximum possible error assigned to each of these α's needs explanation. For each temperature range only one thermal diffusion experiment is represented; the concentrations given are the average of at least ten determinations of the N^{15}/N^{14} abundance ratio in each case. The average deviation from the mean for this ratio in each case is about 0.0004, which makes the possible error for each $c_2-c_2^0$ difference ±0.0008. Improvement in this accuracy could have been made by averaging in data from additional runs, of course, but we feel that our values of α are considerably more accurate than would seem to be indicated by these tabulated possible errors. For in Fig. 1 in which these α's are plotted against ln T_r, where

$$T_r=\frac{T_hT_c}{T_h-T_c}\ln\frac{T_h}{T_c} \tag{3}$$

is the correct mean temperature[9] for the temperature interval T_h-T_c, it is evident that a linear relationship holds just as for neon and argon.[5] If Fig. 1 is changed into a R_T *vs.* ln T_r plot, the equation fitting the resulting straight line is

$$R_T=1.9\ln\,(T_r/293). \tag{4}$$

[9] H. Brown, Phys. Rev. **58**, 661 (1940).

TABLE II. Comparison of R_T values.

T_r	R_T obs.	$R_T(n)$ viscosity	R_T(Suth.) $C=500°$	R_T(Suth.) $C=370°$	R_T(L-J 9,5) $\epsilon/k=333°K$
366°	+0.41		−0.15	0	−0.27
268°	−0.15	−0.17	−0.30	−0.13	−0.41
239°	−0.39		−0.33	−0.22	−0.42

Of chief interest are the observed reversal in the sign of R_T at 293°K, the linear variation of R_T with $\ln T_r$ even though NH_3 is far from being a spherically symmetrical "hard" molecule like neon, and the size of the slope, 1.9, in Eq. (4) as compared to 0.25 for neon and argon.[5] These observations indicate a very rapid "softening" of the NH_3 molecule as the temperature decreases.

DISCUSSION

The temperature dependence of R_T as predicted by viscosity data and by the Sutherland and Lennard-Jones 9,5 molecular models has been considered by Jones.[4] Since the predictions on these models have been shown to be rather poor for neon and argon,[5] they could hardly be expected to hold for a polyatomic molecule such as ammonia. There is reason to believe, however, that the 9,5 model might be a fair approximation to the real intermolecular forces existing in ammonia. Comparison of such predicted R_T values with our observed values is made in Table II. For the theoretical relations upon which these calculations are based reference should be made to the paper by R. C. Jones.[4] The exponent n of T to give the coefficient of viscosity is taken to be approximately 1.1 in this entire temperature range.[10] From this a negative value of R_T close to that observed for our intermediate T_r is predicted. The Sutherland constant, $C=500°$, which appears in the equation for the viscosity, is also taken from reference 10, but Edwards' [11] experimental value, $C\cong 370°$, for the range 15°C to 184°C yields values of R_T agreeing somewhat better with the observations. As for the Lennard-Jones 9,5 model, the prediction that $R_T=0$ for a temperature of 1.54 T_c or 625°K is in marked disagreement with the observed $T_r=293°$K for the reversal point.

To describe adequately the intermolecular forces between dipole molecules such as ammonia no simple model would suffice. For there are in addition to the attractive forces arising from the dispersion effect which are common to all molecules and which vary as $1/R^7$, R being the distance between interacting molecules, (1) the dipole induction effect ($f\alpha 1/R^7$), (2) the alignment effect which depends on the rotational quantum number and hence on the temperature distribution of the molecules ($f\alpha\pm 1/R^7$ for large R but $\alpha 1/R^4$ for close approach), (3) resonance forces due to the possibility of exchange of a quantum of radiation if the interacting molecules have rotational quantum numbers differing by ± 1 ($f\alpha\pm 1/R^4$), and (4) the first-order forces between symmetrical top molecules carrying a dipole along their figure axis ($f\alpha\pm 1/R^4$). It has been shown by Margenau and Warren[7] that for NH_3 ($\mu=1.5\times 10^{-18}$ e.s.u.) these first-order forces (4) are greater than the second-order effect for linear dipoles over the main part of the range of the latter. And since for the repulsive part of these first-order forces the index is less than the critical value 5 for the Maxwellian case, for which the thermal diffusion effect is zero, they would have the tendency to make the thermal diffusion constant negative. Furthermore, all of these dipole-dipole forces (1)–(4) are temperature dependent, becoming more effective as the temperature is lowered because of lower molecular speeds and the concentration of the molecules into the few lower rotational quantum states.

Qualitatively it is thus clear why the thermal diffusion constant of ammonia becomes negative and why the molecule "softens" at such a rapid rate with decreasing temperature. More such measurements might yield considerable information about certain long-range van der Waals forces. It would be of interest, for example, to have similar data for a linear dipole molecule such as HCN for which the dipole moment is large but for which the symmetrical top effect is missing.

We wish to thank Professor L. Onsager for stimulating discussions about thermal diffusion.

[10] M. Trantz and R. Heberling, Ann. d. Physik **10**, 155 (1931).

[11] R. S. Edwards and B. Worswick, Proc. Phys. Soc. **38**, 16 (1925).

Suggestions for a Theory of the Coastal Refraction

G. GRÜNBERG
Academy of Sciences of the U.S.S.R., Moscow, U.S.S.R.
(Received October 16, 1942)

1.

ALTHOUGH the problem of the propagation of electromagnetic waves along a plane separating two dissimilar isotropic homogeneous media can be at present considered completely solved through the work by Sommerfeld and his followers, the more difficult case of three or more different media seems not yet to have been successfully attacked. Such an investigation would, however, be of considerable interest, both theoretical and practical. In particular, the theory of the coastal refraction, i.e., of the peculiar way in which electromagnetic waves are reflected and refracted when passing from the sea to the shore, relates to the case of three different media (air, water, soil, see Fig. 1).

We appreciate the difficulty of this last problem when we recall that even the much simpler problem of the diffraction of electromagnetic waves by a simple wedge of finite conductivity has not yet been solved exactly. We therefore cannot expect that the much more difficult problem of the coastal refraction, which in its simplest form (when the boundaries OA, OB, OC of the different media are planes) corresponds to the case of two such wedges with different properties, can be solved exactly.[1]

In such circumstances it seems to be advisable to seek for some approximate method of approach to the problem under consideration. Such a method can be based on the well-known fact that an electromagnetic field varying with the time can penetrate but little into a sufficiently good conductor. This leads to the possibility of formulating a certain approximate boundary condition at the surface of separation of two media, one of which has a much higher conductivity than the other.

Let us derive this boundary condition as follows: Consider the propagation of electromagnetic waves along a plane separating two dissimilar homogeneous isotropic media and let x, y, z be a set of rectangular coordinates whose origin lies in the plane of separation and whose z axis is directed upwards. Then the equation

$$\Delta E_j'^{(2)}=\frac{\epsilon_2\mu_2}{c^2}\frac{\partial^2 E_j'^{(2)}}{\partial t^2}+\frac{4\pi\mu_2\sigma_2}{c^2}\frac{\partial E_j'^{(2)}}{\partial t} \qquad (1)$$

holds where $E_j'^{(2)}$ denotes one of the components of the electric vector in the second medium. Confining ourselves to the case of simple harmonic oscillations and putting consequently $E_j'^{(2)}=E_j^{(2)}e^{-i\omega t}$, we find Eq. (1) assumes the form

$$\frac{\partial^2 E_j^{(2)}}{\partial x^2}+\frac{\partial^2 E_j^{(2)}}{\partial y^2}+\frac{\partial^2 E_j^{(2)}}{\partial z^2}=-k_2^2 E_j^{(2)}, \qquad (2)$$

where

$$k_2^2=\frac{(\epsilon_2\omega+4\pi\sigma_2 i)\mu_2\omega}{c^2}.$$

If the medium (2) possesses a sufficiently high conductivity, the electric field must rapidly decrease in the direction of the negative z axis, its rate of decrease being greater for greater conductivity σ_2 of the medium. On the other hand in the directions x and y, i.e., along the surface of separation, the field varies relatively slowly.[2] It follows, therefore, that under the

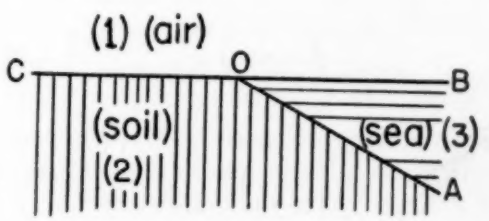

FIG. 1.

[1] It might be of interest to note that the corresponding electrostatic and related problems allow of an exact solution (in quadratures) in the case of an arbitrary number of such wedges, the vertices of which are in contact with each other. See G. Grünberg, Tech. Phys. U.S.S.R. **5**, 525 (1938); G. Grünberg, J. Phys. U.S.S.R. **2**, 213 (1940); G. Grünberg, J. Phys. U.S.S.R. **3**, 401 (1940); G. Grünberg and I. Zuckermann, J. Tech. Phys. (russ.) **12**, 36 (1942).

[2] E_x and E_y vary continuously on passing through the surface of separation, and $E_x^{(1)}$ and $E_x^{(2)}$ are proportional to each other [see Eq. (5)]. Therefore, their variation along the earth's surface is in the main determined by the wave-length $\lambda\cong 2\pi c/\omega$ in the air.

conditions stated the derivatives $\partial^2 E_j^{(2)}/\partial x^2$ and $\partial^2 E_j^{(2)}/\partial y^2$ will be small in comparison with $\partial^2 E_j^{(2)}/\partial z^2$. Neglecting them, therefore, in Eq. (2) we get approximately

$$d^2 E_j^{(2)}/dz^2 = -k_2^2 E_j^{(2)};$$

hence

$$E_j^{(2)} = A \exp(-ik_2 z) + B \exp(ik_2 z).$$

For $z = -\infty$ one must have $E_j^{(2)} = 0$; consequently if k_2 is so chosen that $R(ik_2) < 0$, then $B = 0$ and

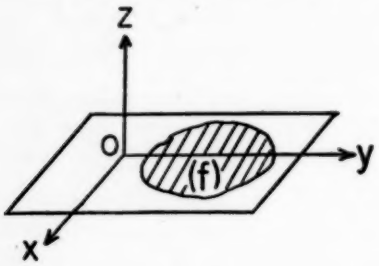

FIG. 2.

$$E_j^{(2)} = A \exp(-ik_2 z) = (E_j^{(2)})_{z=0} \cdot \exp(-ik_2 z). \quad (3)$$

This solution has been derived under the assumption that $\partial^2 E_j^{(2)}/\partial x^2$ and $\partial^2 E_j^{(2)}/\partial y^2$ are relatively small in comparison with $\partial^2 E_j^{(2)}/\partial z^2$. But insofar as orders of magnitude alone are concerned, one has

$$\partial^2 E_j^{(2)}/\partial x^2 \approx (2\pi/\lambda)^2 E_j^{(2)},$$
$$\partial^2 E_j^{(2)}/\partial y^2 \approx (2\pi/\lambda)^2 E_j^{(2)},$$

where λ denotes the wave-length in air. Hence, using Eq. (3) we find that the condition for the validity of Eq. (3) is

$$\left(\frac{2\pi}{\lambda |k_2|}\right)^2 \ll 1. \quad (4)$$

We are now in a position to formulate the boundary condition in question, which we shall write down only for the vertical component E_z of the field. We start with the two exact boundary conditions

$$(\epsilon_1\omega + 4\pi\sigma_1 i) E_z^{(1)} = (\epsilon_2\omega + 4\pi\sigma_2 i) E_z^{(2)}, \quad (5)$$

$$\partial E_z^{(1)}/\partial z = \partial E_z^{(2)}/\partial z, \quad (6)$$

which hold at the plane $z = 0$ of separation, the first of them expressing, as usual, the continuity of the normal component of the total current and the second one being an immediate consequence of the fact that in both media $\operatorname{div} \mathbf{E} = 0$ and at the surface of separation itself $\partial E_x^{(1)}/\partial x = \partial E_x^{(2)}/\partial x$ and $\partial E_y^{(1)}/\partial y = \partial E_y^{(2)}/\partial y$.[3] Inserting now into Eq. (6) the value $(\partial E_z^{(2)}/\partial z)_{z=0} = -ik_2 (E_z^{(2)})_{z=0}$ from Eq. (4) and using Eq. (5), we at once get:

$$\left.\frac{\partial E_z^{(1)}}{\partial z}\right|_{z=0} = -2\pi\alpha E_z^{(1)}\Big|_{z=0}, \qquad \alpha = \frac{i\mu_2\omega(\epsilon_1\omega + 4\pi\sigma_1 i)}{2\pi k_2 c}, \quad (7)$$

which is the condition required. Its validity is connected with the degree of accuracy of Eq. (3), which in its turn depends on the smallness of the quantity $(2\pi/\lambda|k_2|)^2$. If the displacement current in the ground can be neglected, inequality (4) assumes the form:

$$\frac{1}{2}\left(\frac{2\pi d}{\lambda}\right)^2 \ll 1,$$

where $d = c/(2\pi\mu_2\sigma_2\omega)^{\frac{1}{2}}$. In this case

$$\alpha = \pi d \mu_2 \epsilon_1 (1+i)/\lambda^2,$$

and $E_z^{(2)} = (E_z^{(2)})_{z=0} \cdot \exp[(i-1)z/d]$, so that d determines the thickness of the layer of the ground within which the field differs sensibly from zero. For example, when $\lambda = 3\times 10^4$ cm, $\sigma_2 = 5\times 10^7$, $\mu_2 = 1$, the ratio of the displacement current to the conduction current is about 0.01 and $d \leqq 0.02\lambda$, $\frac{1}{2}(2\pi d/\lambda)^2 = 4\times 10^{-3}$. For greater wave-lengths and the same conductivity of the soil, conditions for the application of Eq. (7) are even more favorable. It should also be noted that for $\sigma_2 = \infty$ Eq. (7) gives

$$(\partial E_z^{(1)}/\partial z)_{z=0} = 0, \quad (8)$$

[3] For $E_x^{(1)} = E_x^{(2)}$ and $E_y^{(1)} = E_y^{(2)}$ at all points of the plane $z = 0$. It might be of interest to note that if the surface of separation were not plane, then introducing appropriate curvilinear coordinates and transforming the equation $\operatorname{div} \mathbf{E} = 0$ into them, we could find, taking into account the continuity of the tangential components of the field, the corresponding generalization of Eq. (6). A similar condition holds for the normal component H_n of the magnetic field.

and this is readily seen to be the exact boundary condition for perfectly conducting ground.

2.

In order to apply the results obtained to the solution of the problem of the coastal refraction, let us consider the following idealization of the problem in question: *Given an island (f) on a perfectly conducting sea, the surface of the island being strictly horizontal and at sea level. At the surface of the island condition (7) holds while at the sea surface $(\partial E_z/\partial z)_{z=0}=0$. Find the electromagnetic field produced in the upper half-space (air, $z>0$, see Fig. 2) by a given distribution of oscillators placed within this half-space.*

Such an idealization evidently can be used only when the surface of the island is sufficiently flat, horizontal, and does not protrude much from the sea. Moreover, the boundary condition (7) certainly cannot be correct in the immediate neighborhood of the coast line. Still it seems one may be allowed to use it even there in consequence of the supposed smallness of the ratio d/λ, which shows that already at a small distance off the coast line (of the order of a small fraction of the wave-length λ) condition (7) can be safely applied.[4]

We are now in a position to derive the fundamental integral equation of the problem. To that end let us apply Green's theorem

$$\int_{(v)}(\psi\Delta\varphi-\varphi\Delta\psi)dv=\int_{(F)}\left(\psi\frac{\partial\varphi}{\partial n}-\varphi\frac{\partial\psi}{\partial n}\right)dF \quad (9)$$

to a hemisphere of radius $R\to\infty$, lying in the upper half-space, its center coinciding with the origin of coordinates (Fig. 3).

Putting here

$$\varphi=E_z,\quad \psi=\exp(ik_1r)/r,$$

$$r=((x-\xi)^2+(y-\eta)^2+(z-\zeta)^2)^{\frac{1}{2}},$$

excluding the point $M(x, y, z)$ (where $r=0$) from the range of integration by means of a small sphere of radius $\rho\to 0$, and taking into account that $\Delta E_z+k_1^2E_z=-4\pi f_z$, where f_z is a given function determined by the distribution of the "primary" currents in space, we easily get

$$\left.\begin{aligned}4\pi(E_z)_M=4\pi(E_z^0)_M+\int_{(AB)}\left\{\frac{\partial E_z}{\partial n}\frac{\exp(ik_1r)}{r}\right.\\ \left.-E_z\frac{\partial}{\partial n}\left(\frac{\exp(ik_1r)}{r}\right)\right\}df_{AB},\\ E_z^0=\int_{(v)}\frac{f_z\exp(ik_1r)}{r}dv\end{aligned}\right\} \quad (10)$$

where the subscript M denotes that the corresponding quantity pertains to the point M. The integral on the right in (10) is extended over the whole plane AB,[5] and E_z^0 is the "primary" field, which would be produced by the given sources in the absence of the surface of separation, i.e., if the air were to fill in the whole space. On applying formula (10) to a point M which lies on the earth's surface and thus makes $Z\to 0$, we readily find

$$-\int_{(AB)}E_z\frac{\partial}{\partial n}\left(\frac{\exp(ik_1r)}{r}\right)df_{AB}=2\pi E_z.$$

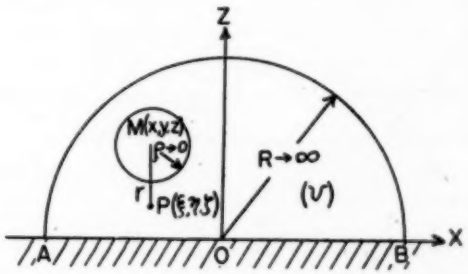

FIG. 3.

When we introduce this into Eq. (10) and use the boundary conditions (7) and (8), we obtain

$$(E_z)_{z=0}=2(E_z^0)_{z=0}+\alpha\int_{(f)}(E_z)_{z=0}\cdot\frac{\exp(ik_1r)}{r}df. \quad (11)$$

This is the integral equation in question. From the derivation just given it follows that Eq. (11) applies just as well to the case of several islands present, if (f) denotes their total area. It should

[4] The thickness of the layer of the ground, beneath which the field is practically zero, is of the order of d. It is, therefore, to be expected that at a distance of the order of a few d, say $3d$ or $4d$, condition (7) holds sufficiently well. If, as in the case considered above, $d/\lambda\leqslant 0.02$, then $3d\leqslant 0.06\lambda$, which proves our assertion.

[5] The surface integral extended over the outer hemisphere of radius $R\to\infty$ disappears (at least if we take into account the conductivity of the air).

be noted that for perfectly conducting ground, i.e., when $\alpha=0$, Eq. (11) gives $(E_z)_{z=0}=2(E_z^0)_{z=0}$. The normal component of the actual field at the surface of a perfectly conducting ground has, therefore, only in the absence of the ground, double the value of the normal component of the "primary" field due to the given sources. This corresponds evidently to the usual "reflection" rule for a perfectly conducting plane.

3.

Let us apply Eq. (11) to the case when the region (f) occupied by the dry land is a half-plane (Fig. 4). It suffices to consider the case of a primary field $(E_z^0)_{z=0}$ having the form $(E_z^0)_{z=0}=f(x)e^{isy}$ [where Y is the direction of the coast line (Fig. 4) and s is a constant], for an arbitrary primary field can always be resolved into such components by means of a Fourier integral.

Putting consequently $(E_z)_{z=0}=F(x)e^{isy}$ we obtain Eq. (11).

$$F(x)=2f(x)+\alpha\int_0^\infty F(\xi)d\xi \times\int_{-\infty}^{+\infty}\frac{\exp\left[i\{s\eta+k_1[(x-\xi)^2+\eta^2]^{\frac{1}{2}}\}\right]}{[(x-\xi)^2+\eta^2]^{\frac{1}{2}}}d\eta, \quad (12)$$

or using the formula

$$\int_{-\infty}^{+\infty}\frac{\exp\left[i\{s\eta+k_1[(x-\xi)^2+\eta^2]^{\frac{1}{2}}\}\right]}{[(x-\xi)^2+\eta^2]^{\frac{1}{2}}}d\eta =i\pi H_0^{(1)}[(k_1^2-s^2)^{\frac{1}{2}}|x-\xi|], \quad (13)$$

where $H_0^{(1)}$ denotes the Hankel function of the first kind and of zero order, we find

$$F(x)=2f(x)+\pi\alpha i\int_0^\infty F(\xi)H_0^{(1)}(m|x-\xi|)d\xi, \quad (14)$$

$$m=(k_1^2-s^2)^{\frac{1}{2}}.$$

This equation allows for an exact solution (in quadratures).[6] This shows that in those cases when the approximate boundary condition (7) proves to be sufficiently accurate, the solution

[6] By a method of Hopf and Wiener; see Titchmarsh *Introduction to the Theory of Fourier Integrals* (Oxford, 1937), p. 339, and generalized by E. Reissner, J. Math. and Phys. [5], **20**, 219 (August 1941).

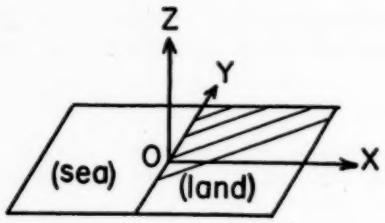

FIG. 4.

of the problem of the coastal refraction can be given in quadratures for an arbitrary primary field. We intend to give this general solution in a subsequent paper as soon as possible. Here we shall confine ourselves to the consideration of the case of a plane wave propagated from the sea, its direction making an angle θ with the X axis. Then $f(x)=e^{imx}$, and if we put $F(x)=2e^{imx}\psi(x)$ in Eq. (14) we obtain:

$$\psi(x)=1+\pi\alpha i\int_0^\infty e^{-im(x-\xi)}H_0^{(1)}(m|x-\xi|)\cdot\psi(\xi)d\xi$$

$$=1+\pi\alpha i\left\{\int_0^x e^{-im(x-\xi)}H_0^{(1)}[m(x-\xi)]\psi(\xi)d\xi +\int_x^\infty e^{im(\xi-x)}H_0^{(1)}[m(\xi-x)]\psi(\xi)d\xi\right\}. \quad (15)$$

Instead of solving this equation exactly, basing on the remark that $\psi(x)$ is a function which in general varies but slowly in comparison to e^{imx}, we shall give here its approximate solution.[7] This enables us to put approximately[8]

[7] For perfectly conducting ground $\psi(x)=1$. If the ground is not perfectly conducting but possesses a sufficiently high conductivity, then at a distance of the order of a few wave-lengths off the coast line, the wave must be propagated much in the same way as for perfectly conducting ground, its amplitude and phase varying but slowly in the direction of propagation. This proves our assertion if only θ is not near 90°, i.e., if the incident wave (primary) is not a glancing one. It should also be noted that in the neighborhood of the coast line $\psi(x)$ cannot differ appreciably from unity, the difference being of the order of the (small) quantity α/m.

[8] For $e^{ims}H_0^{(1)}(mz)$ is a nearly twice as rapidly varying function as e^{ims} and, moreover, rapidly decreasing. This can be seen from the asymptotic expression $H_0^{(1)}(mz)\approx(2/\pi mz)^{\frac{1}{2}}e^{i(mz-\frac{1}{4}\pi)}$, which gives a good approximation at arguments of the order of a few units and which shows that $e^{ims}H_0^{(1)}(mz)\approx(2/\pi mz)^{\frac{1}{2}}e^{i(2ms-\frac{1}{4}\pi)}$. In contradistinction, it is not possible to use this kind of argument for a similar simplification of the first member on the right of Eq. (15), for asymptotically

$$e^{-ims}H_0^{(1)}(mz)\approx(2/\pi mz)^{\frac{1}{2}}e^{-i\frac{1}{4}\pi},$$

which is not at all a rapidly varying function.

$$\int_x^\infty e^{im(\xi-x)}H_0^{(1)}[m(\xi-x)]\psi(\xi)d\xi$$

$$\cong\psi(x)\int_0^\infty e^{imu}H_0^{(1)}(mu)du=(2/\pi m)\psi(x), \quad (16)$$

the last result being a consequence, for $x=\infty$, of the formula

$$\int_0^x e^{\pm imu}H_0^{(1)}(mu)du=\frac{1}{m}\left\{\pm\frac{2}{\pi}+mxe^{\pm imx}\times[H_0^{(1)}(mx)\mp iH_1^{(1)}(mx)]\right.,$$

which may be easily verified by differentiation.[9]

According to Eq. (16) the second member on the right-hand side of Eq. (15) is approximately equal to $(2\alpha i/m)\psi(x)$. This is usually not more than a small fraction of the member $\psi(x)$, which stands on the left of (15). For instance when $\lambda=3\times10^4$ cm, $\sigma_2=5\times10^7$, $\mu_2=1$, we find that $d/\lambda\cong2\times10^{-2}$ and $m=(\omega\cos\theta)/c=(2\pi/\lambda)\cos\theta$, $2\alpha i/m=(d/\lambda\cos\theta)(i-1)$, which, for $0\leqslant\theta\leqslant60°$, yields $d/\lambda\cos\theta\leqslant4\times10^{-2}$. It is therefore clear that even a relatively high error involved in the approximate evaluation of the integral (16) cannot affect considerably the determination of $\psi(x)$ from Eq. (15) if, instead of this last equation, its approximate form

$$\left.\begin{aligned} U\psi(x)&=1+\pi\alpha i\int_0^x K(x-\xi)\psi(\xi)d\xi,\\ U&=1-(2\alpha i/m),\\ K(z)&=e^{-imz}H_0^{(1)}(mz),\end{aligned}\right\} \quad (18)$$

is used. This is an integral equation of Volterra type, which can be solved readily by means of Laplace transforms. Its solution can be shown to be

$$\left.\begin{aligned}\psi(x)&=\frac{e^{-imx}}{2\pi Ui}\int_{\sigma-i\infty}^{\sigma+i\infty}\frac{e^{mxz}dz}{(z-i)\left\{1+\beta\dfrac{\{1-(2i/\pi)\lg[z+(z^2+1)^{\frac{1}{2}}]\}}{(z^2+1)^{\frac{1}{2}}}\right\}},\\ \beta&=-\pi\alpha i/Um,\quad \sigma>0,\end{aligned}\right\} \quad (19)$$

where the path of integration is a straight line, lying in the right half-plane z, parallel to the imaginary axis; and the values of the radical and the logarithm are uniquely determined by the condition that they both are real and positive on the positive part of the real axis.

A detailed investigation of the solution (19) will be given in a paper which is to appear in the *Journal of Physics of the U.S.S.R.* (under the same title as above). It should only be noted that at a sufficiently great distance from the coastline formula (19) gives approximately:

$$\psi(x)\cong\frac{e^{i\frac{1}{4}\pi}}{U(2\pi mx)^{\frac{1}{2}}\beta}=\frac{\lambda^{\frac{1}{2}}(\cos\theta)^{\frac{1}{2}}}{2\pi^2d\sqrt{x}}, \quad (x\to\infty), \quad (20)$$

which in particular shows that at such distances the direction of propagation of the "refracted" wave coincides asymptotically with that of the primary one, its amplitude being a slowly varying function of x in accordance with the assumption made above.

[9] This formula is a special case of a series of general formulae relating to Bessel functions of any kind, which we intend to publish elsewhere.

Electronic Energy Bands in Body-Centered Iron

MILLARD F. MANNING*
University of Pittsburgh, Pittsburgh, Pennsylvania
(Received December 19, 1942)

Calculations of the electronic energy bands in body-centered iron by the Wigner-Seitz-Slater method are reported. There are found to be two filled and four partially-filled bands. The lowest two filled bands are responsible for the cohesion; the next three partially-filled bands for the ferromagnetism; and the highest band is responsible for the electrical conduction. The width of the occupied levels is about 0.6 Rydberg but the density of states is high for only about 0.4 Rydberg in good agreement with the data obtained from x-ray emission bands. The density of states is calculated as a function of the energy and compared with similar results obtained by Greene for face-centered iron. The density of states at the highest occupied energy level is 17 electrons/atom-Rydberg compared with 11 electrons/atom-Rydberg for face-centered iron. This higher density of states accounts for the fact that body-centered iron is ferromagnetic, but face-centered iron is not. It also indicates a greater electronic specific heat for body-centered iron than for face-centered iron. This higher electronic specific heat is responsible for the high temperature change from a face-centered to a body-centered structure.

INTRODUCTION

THERE is considerable scientific interest in metallic iron because it is one of the few elements which show ferromagnetism and because of the phase changes from body-centered to face-centered and back to body-centered as the temperature is raised.

The method of calculating the electronic energy levels reported in this paper is that developed by Wigner and Seitz[1] and extended by Slater[2] and others.[3] The essential feature of this method is that the wave function within the polyhedron surrounding any one atom is expressed as a sum of terms (fourteen for the body-centered lattice) each of which consists of a spherical harmonic multiplied by the appropriate radial function. The radial functions are found by a modified Hartree procedure and the arbitrary coefficients in the linear combination are chosen so that the wave functions satisfy the Bloch[4] periodicity condition and join smoothly in passing from one atom to its eight nearest and six next-nearest neighbors. It turns out that these conditions impose a determinantal relationship between the energy of an electron and the components of the momentum or wave number vector **k**. For a general direction of **k** the determinantal relations become very complicated, but for a number of symmetrical directions, simpler relations are obtained. For the body-centered lattice the results of the expansion of the determinant for the special directions are given in reference 3. The directions of **k** for which solutions have been obtained are indicated in Fig. 1, which is a drawing of the first Brillouin zone corresponding to a body-centered structure.[5]

RESULTS

In the calculations the first step was the determination of an effective field for the calculation of the radial factors of the different wave

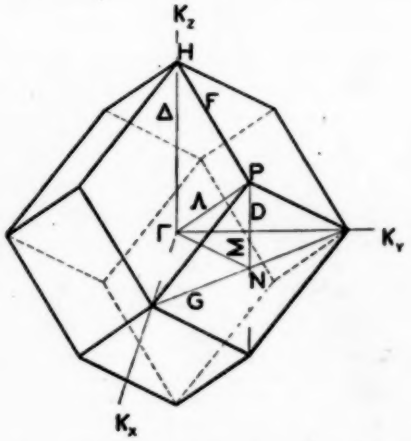

FIG. 1. The first Brillouin zone for the body-centered lattice.

* Deceased June 1, 1942.

[1] E. Wigner and F. Seitz, Phys. Rev. **43**, 804 (1933); Phys. Rev. **46**, 509 (1934).

[2] J. C. Slater, Phys. Rev. **45**, 794 (1934).

[3] M. I. Chodorow and M. F. Manning, Phys. Rev. **52**, 731 (1937). For a list of other applications of this method, see M. F. Manning and M. I. Chodorow, Phys. Rev. **56**, 787 (1939).

[4] F. Bloch, Zeits. f. Physik **52**, 555 (1928).

[5] The notation is that of L. Bouckeart, R. Smoluchowski, and E. Wigner, Phys. Rev. **50**, 58 (1936).

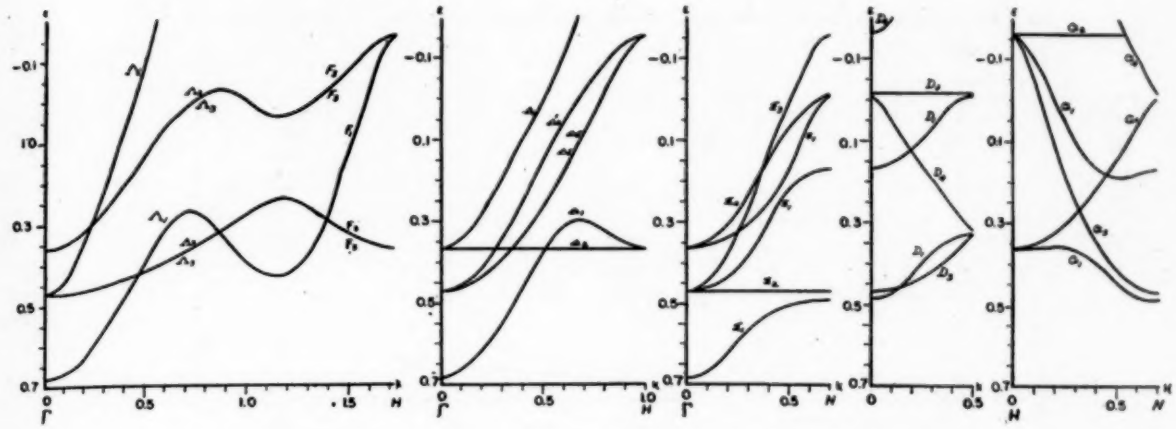

FIG. 2. Energy ϵ *vs.* momentum K for the different directions of propagation.

functions. In determining the effective field for the metal, the charge-densities for $1s$ to $3p$ electrons were assumed the same as found for the iron atom by Manning and Goldberg.[6] The charge-densities for the $4s$ and $3d$ were renormalized to the volume of the atomic sphere in metallic iron and other readjustments made. Further details are given in Appendix I.

By use of the field so obtained, the radial wave functions were found by numerical integration as in the Hartree self-consistent field method for atoms. The values of the functions and their radial derivatives at the half-distances between nearest neighbors and between next-nearest neighbors were then determined by standard methods of interpolation and numerical differentiation. (For iron the lattice parameter at room temperature is 2.86A. The corresponding distance between nearest neighbors is 2.345 Bohr units and the distance between next-nearest neighbors is 2.71 Bohr units. The corresponding values of $\rho(\equiv \log_e 1000r)$ are 7.760 and 7.904.)

TABLE I. Values of ϵ for which certain important functions vanish. The notation is that of Chodorow and Manning (reference 3).

Function	ϵ
$3s_1'g_2'+2s_2'g_1'$	0.684
$2D_1D_2S_4+2D_2S_2+D_1S_3+S_1$	0.490
d_1'	0.470
d_2'	0.365
$D_1B_2+B_1$	0.325
$2D_1D_2S_4+2D_2S_2+D_1S_3+S_1$	0.165
B_1	−0.008
d_2	−0.015
d_1	−0.160

TABLE II. Maximum and minimum values of ϵ for each band and values of ϵ at the symmetry points (reference 3).

	I	II	III	IV	V	VI
Min. E	0.684	0.470	0.470	0.470	0.365	0.365
Max. E	0.292	0.240	−0.160	−0.160	−0.160	
Γ	0.684	0.470	0.470	0.470	0.365	0.365
P	0.325	0.325	0.325	−0.015	−0.015	
N	0.490	0.470	0.165	−0.008	−0.015	−0.160
H	0.365	0.365	−0.160	−0.160	−0.160	

The values of the functions and derivatives are then used to calculate the coefficients in the transcendental equations relating E and $\mathbf{k}$ given in reference 3. The procedure in solving these equations was very similar to that used in the calculations for metallic tungsten.[7] A few comments about slight modifications in the procedure are given in Appendix II. The results of the calculation of the energy as a function of the momentum are given in Fig. 2. It does not seem necessary to tabulate the numerical values from which the figures were plotted, but Table I gives the energies at which certain key combinations of functions and derivatives vanish, and Table II gives the maximum and minimum energies for each band and the energies at a number of special points in the Brillouin zone. In these tables and elsewhere in this paper ϵ is the negative of the energy expressed in Rydbergs.

Although energy-momentum relations are ob-

[6] M. F. Manning and L. Goldberg, Phys. Rev. **53**, 662 (1938).

[7] M. F. Manning and M. I. Chodorow, Phys. Rev. **56**, 787 (1939).

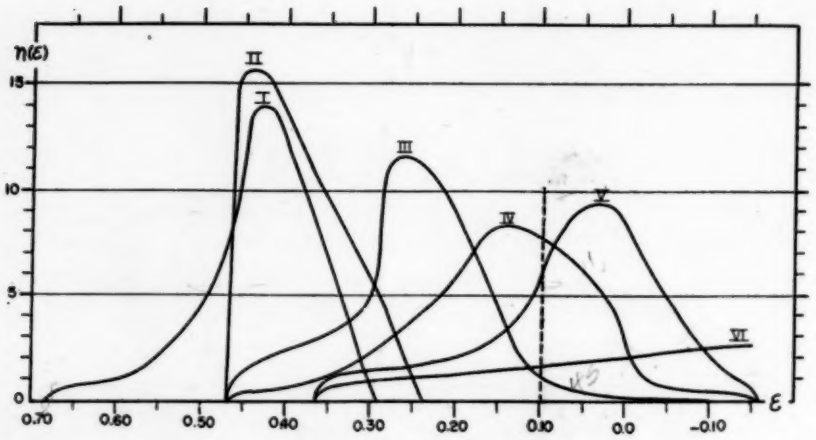

FIG. 3. $n(\epsilon)$ *vs.* ϵ for the separate bands. $n(\epsilon)$ = number of states per unit energy range.

tained directly for only a limited number of lines in **k** space, very plausible constant energy contours based on these known lines can be drawn for the principal planes in **k** space. By considering the contours in these planes as known, energy contours for a number of planes $K_z=0$, 0.1, 0.2, etc., can be interpolated. Each of the planes K_z=constant can be divided into a region in which the energy is greater than a particular value and a region in which the energy is less than this particular value. For each plane the area of the region with energy less than a particular energy was obtained by using a planimeter. This procedure was repeated for all of the planes and by numerical integration the volume in **k** space with energy less than a particular energy was determined. Since this volume is proportional to the number of electrons with energy less than the energy considered, the corresponding number of electrons can be found by using the normalizing relation that there are two electrons per atom in each energy band. In the present paper this quantity is designated by $N(\epsilon)$. The values of $N(\epsilon)$ for each of the energy bands and for the sum of the six bands are given in Table III. Since there are eight valence electrons per atom in iron, the highest occupied level at absolute zero in non-magnetic iron occurs at $\epsilon=0.105$.

From the values of $N(\epsilon)$, the values of $n(\epsilon)(\equiv -dN/d\epsilon)$ can be found by numerical differentiation. ($n(\epsilon)d\epsilon$ is the number of energy levels per atom with energy between ϵ and $\epsilon+d\epsilon$.) Since numerical differentiation is a process in which considerable accuracy is lost, the values of $n(\epsilon)$ found by differentiation were adjusted so that

$$\int_{\epsilon_1}^{\epsilon_2} n(\epsilon)d\epsilon$$

as found by a planimeter checked the corresponding increment in $N(\epsilon)$. The resulting values of $n(\epsilon)$ for the separate bands and for the total are given in Figs. 3 and 4.

TABLE III. Values of $N(\epsilon)$ as a function of ϵ.

ϵ	I	II	III	IV	V	VI	Total
0.70							
	0.003						
0.65	0.017						0.017
	0.032						
0.60	0.058						0.058
	0.090						
0.55	0.122						0.122
	0.199						
0.50	0.275						0.275
	0.456						
0.45	0.623	0.306	0.025	0.003			0.957
	1.003	0.599					
0.40	1.328	0.902	0.118	0.025			2.373
	1.614	1.138					
0.35	1.970	1.494	0.288	0.063	0.033		3.848
	2.000	1.651					
0.30	2.000	1.802	0.460	0.156	0.103	0.034	4.555
		1.969					
0.25	2.000	1.998	0.968	0.336	0.170	0.078	5.550
0.20		2.000	1.477	0.541	0.245	0.121	6.384
0.15		2.000	1.895	0.904	0.372	0.188	7.359
0.10			1.939	1.302	0.552	0.255	8.048
0.05			1.967	1.677	0.945	0.406	8.995
0.00			1.982	1.937	1.405	0.468	9.792
−0.05			1.992	1.971	1.747	0.589	10.299
−0.10			1.997	1.993	1.904	0.816	10.710
−0.15			2.000	1.998	1.979	0.882	10.859

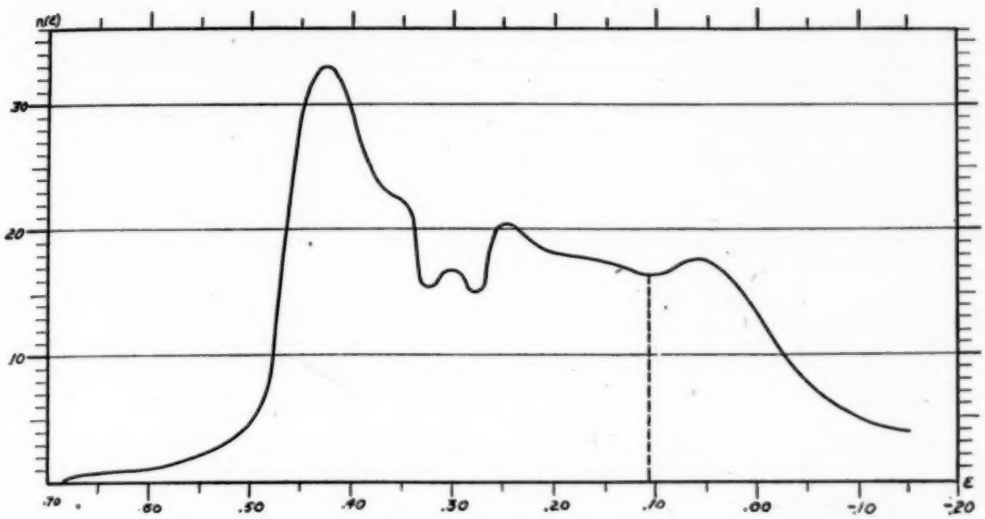

FIG. 4. $n(\epsilon)$ *vs.* ϵ for the sum of the six bands.

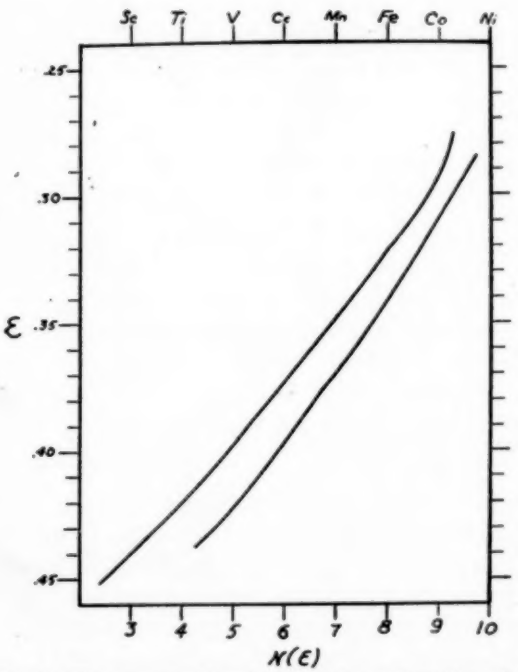

FIG. 5. The average Fermi energy $\bar{\epsilon}$ as a function of the number of electrons per atom. The upper curve is for body-centered iron, the lower one for face-centered.

From the results depicted in these figures, some general remarks about the electronic structure of metallic iron can be made. Bands I and II are completely filled in the metal and hence do not contribute to either the electrical conductivity or the ferromagnetic properties. Band VI is a wide band with a considerable admixture of s functions and probably accounts for most of the conductivity. Bands III, IV, and V are narrow bands with a high density of states and are the important bands in connection with ferromagnetism.

This model for the electronic structure of metallic iron combines many of the features of the "d" band model suggested by Mott[8] and the homopolar group of levels suggested by Pauling.[9]

The general features of the energy bands for body-centered iron are very similar to those found for tungsten.[7] The only important difference is that for tungsten the energy for which $3s_1'g_2'+2s_2'g_1'=0$ lies above the energies for which d_1' and d_2' are zero, while for iron this condition is fulfilled for an energy lower than the energies for which d_1' and d_2' vanish. (See Fig. 6.) The general results are also quite similar to those obtained by Greene[10] for face-centered iron. However, the lowest band in face-centered iron begins at the energy for which $s'=0$ and all five of the d bands start at the energy for which $d'=0$. (Actually this is due to an approximation in the theory as Bethe[11] and Chodorow[12] have pointed out that even at the center of the momentum cell the d level should split into a group of two levels and a group of three levels.)

[8] N. F. Mott, Proc. Phys. Soc. **47**, 571 (1935).
[9] L. Pauling, Phys. Rev. **54**, 899 (1938).
[10] J. B. Greene and M. F. Manning, Phys. Rev. **63**, 203 (1943).
[11] H. Bethe, Ann. d. Physik **87**, 55 (1928).
[12] M. I. Chodorow, Phys. Rev. **55**, 675 (1939) and M.I.T. thesis (1936).

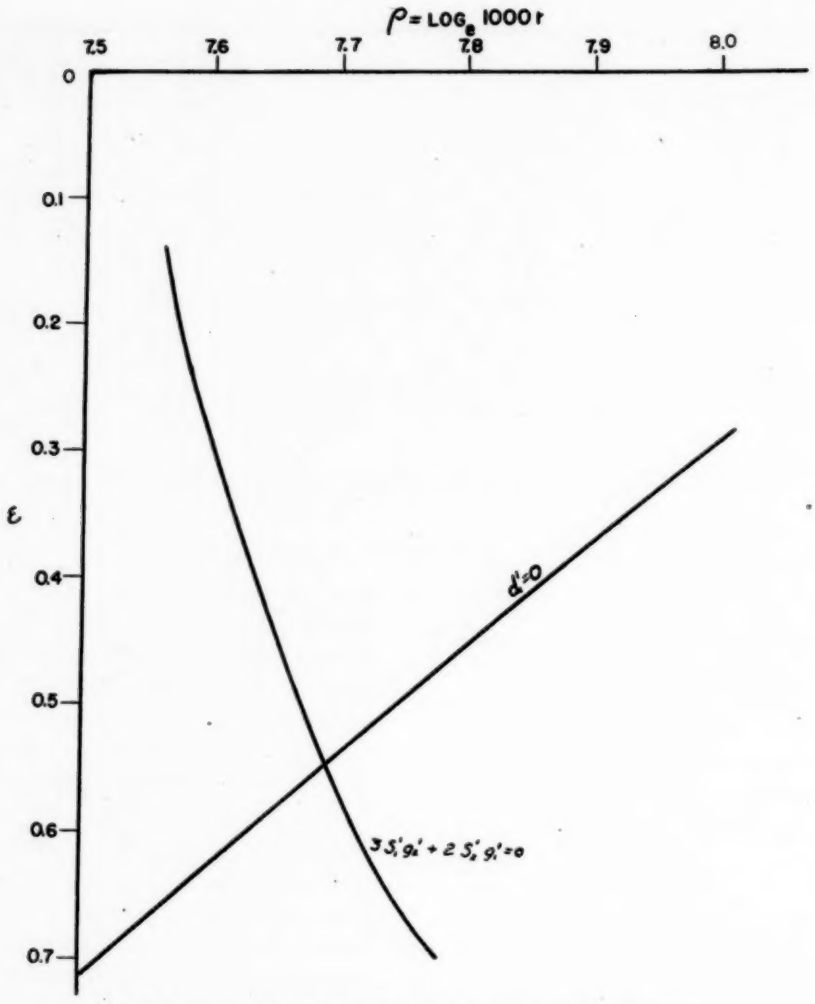

FIG. 6. The energy for which certain functions vanish *vs.* $\log_e r$. r is the interatomic distance in Bohr units.

APPLICATIONS

Energy Relations

A quantitative calculation of the binding energy of body-centered iron and its stability relative to the face-centered structure would require a consideration of the exchange and correlation energies which is not possible by the method used here. It is, however, interesting to compute the average Fermi energy as a function of the total number of electrons per atom and compare with the same results obtained for the face-centered structure.

The average Fermi energy is defined by the equation:

$$N(\epsilon_m)(\bar{\epsilon}-\epsilon_0) = -\int_{\epsilon_0}^{\epsilon_m} n(\epsilon)(\epsilon-\epsilon_0)d\epsilon, \qquad (1)$$

where ϵ_0 refers to the lowest level and ϵ_m to the highest level occupied at absolute zero. This integral could be evaluated from the information in Fig. 4, but since $n(\epsilon)$ is obtained only as the derivative of another function, it is preferable to integrate Eq. (1) by parts to obtain:

$$\bar{\epsilon} = \epsilon_m + \frac{1}{N(\epsilon_m)}\int_{\epsilon_0}^{\epsilon_m} N(\epsilon)d\epsilon. \qquad (2)$$

Although the results calculated are based on iron, they should be approximately valid for neighboring elements in the same row of the periodic table if the appropriate number of electrons per atom is used. Similar calculations have been made by Greene[10] for the face-centered structure and the results are plotted in Fig. 5. In

the neighborhood of iron the difference in mean Fermi energy is about 0.02 Rydberg/atom. Since the extra magnetic energy of the body-centered lattice is of this same order of magnitude and there are a number of other corrections which may be different for the two structures, it is easy to see why iron might show phase changes. In the neighborhood of ten electrons per atom the average Fermi energy for the body-centered structure rises much more rapidly than for the face-centered structure, thus indicating that for nickel the face-centered structure should be more stable. This gives no information about cobalt, although here the face-centered structure is favored over the body-centered structure by the magnetic energy.

The considerable concentration of states near the bottom of the d band has been found for all of the transition elements which have been studied[13,14,7] and may be considered responsible for their relatively high binding energies. This possibility has been emphasized by Manning and Chodorow[7] and by Seitz.[15,16]

The behavior of the lowest energy in each type of band is qualitatively similar to that found by Greene[10] for face-centered iron. However, the method used by Greene does not show the splitting of the d band at $\mathbf{k}=0$, and the lowest band for the face-centered lattice begins at the energy for which $s'=0$ while for the body-centered lattice the lowest band begins at the energy for $3s_1'g_2'+2s_2'g_1'=0$. It turns out that for the portion of the $s'=0$ curve inside of the minimum (it seems probable that this is always the important part for transition metals) the second condition corresponds to a curve shifted slightly toward smaller values of interatomic distance but otherwise similar. The behavior of the energies for which $d_1'=0$ and $3s_1'g_2'+2s_2'g_1'=0$ as a function of interatomic distance is shown in Fig. 6. It is interesting to note that for tungsten with its smaller number of d electrons and a recently-filled f shell, the normal interatomic distance corresponds to the $3s_1'g_2'+2s_2'g_1'$ curve, being higher than the d' curves.

[13] H. M. Krutter, Phys. Rev. **48**, 664 (1935).
[14] J. C. Slater, Phys. Rev. **49**, 537 (1936).
[15] F. Seitz, *Modern Theory of Solids* (McGraw-Hill, New York, 1940), p. 430 ff.
[16] F. Seitz and R. P. Johnson, J. App. Phys. **8**, 186 (1937).

Ferromagnetism

The relation of the ferromagnetic behavior of iron, cobalt, and nickel to the structure of their electronic energy bands has been discussed by Slater in a series of papers.[14,17,18] There are unsurmounted difficulties in the formulation of a complete theory of ferromagnetism, but certain general features can be discussed in terms of the present model.

In the non-magnetic state there are equal numbers of electrons with each spin, whereas in the magnetic state there are more electrons with positive than with negative spin. In the magnetized state the Fermi energy is of course greater, because in order to reverse the spins it is necessary to transfer electrons to higher vacant levels of the opposite spin. For substances which are ferromagnetic this increase in energy is more than compensated by the increase in the number of exchange integrals between electrons with parallel spin. Slater[14] showed that this change in exchange energy is proportional to the square of the number of uncompensated spins. The change in Fermi energy is also proportional to the square of the number of uncompensated spins if $n(\epsilon)$ can be regarded as constant. The actual relation is

$$\Delta\epsilon_f=\mu^2/2n(\epsilon_m), \tag{3}$$

where μ is the number of uncompensated spins expressed in Bohr magnetons per atom, $n(\epsilon_m)$ is the number of energy levels (both spins) per Rydberg unit of energy at the highest occupied level for the non-magnetic state, and $\Delta\epsilon_f$ is the change in Fermi energy upon reversing $\mu/2$ spins. For ferromagnetism $\Delta\epsilon_e$, the change in exchange energy accompanying the change to the magnetic state, must be larger numerically than $\Delta\epsilon_f$. Hence, it follows that only those substances are ferromagnetic for which $n(\epsilon)$ is large. In this connection it is interesting to note that Greene's results for face-centered iron indicate a much smaller density of states near ϵ_m than reported here for body-centered iron; therefore, it is quite understandable that face-centered iron should not be ferromagnetic.[19]

[17] J. C. Slater, Phys. Rev. **49**, 931 (1936).
[18] J. C. Slater, Phys. Rev. **52**, 198 (1937).
[19] Since face-centered iron is stable only at temperatures above the Curie point and cannot be retained at lower temperatures, no direct evidence about its ferromagnetism

If the number of states per unit energy range is not constant, the change in Fermi energy accompanying the change to the magnetic state is no longer given by Eq. (3) but can be found by using Eq. (1) for each direction of spin. In computing the change in Fermi energy, Bands I and II can be neglected because they are completely filled. Also, it is usually considered that Band VI can be neglected because of the low density of states and because the s and p functions which predominate in this band are concentrated further from the nucleus than the d functions which predominate in the other bands and hence contribute less to the exchange energy. The actual result of the computation of Fermi energy as a function of μ showed that the Fermi energy increased slightly more rapidly than proportional to the square of μ, but the difference from strict proportionality was not enough greater than the computational error to be significant.

For iron there are eight valence electrons per atom; four in the two lowest filled bands, and 0.25 electron in Band VI. There are thus 3.75 electrons per atom in the three bands which are assumed to contribute to the ferromagnetism. With only the three bands contributing to the ferromagnetism, the saturation magnetic moment is determined by one of three conditions:[20]

1. The number of negative spins per atom cannot be negative.
2. The number of positive spins per atom cannot be greater than three.
3. If $\Delta\epsilon_e$ increases less rapidly with μ^2 than $\Delta\epsilon_f$, the difference may vanish at some value of μ less than that determined by either of the above conditions.

There does not seem to be any element or alloy in the iron group for which the first condition is the determining one. The second would give a saturation moment of $3.00-0.75=2.25$ Bohr magnetons per atom. The experimental value is about 2.20 or 2.22 magnetons per atom. This small difference cannot be regarded as conclusive evidence against the assumption that the second condition is the important one. In order to say definitely about the third, it would be necessary to have more definite information about the variation of the Fermi and exchange energies with μ.

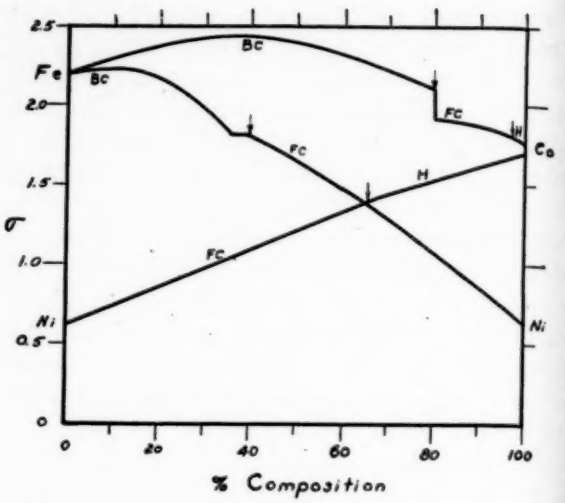

FIG. 7. Magnetic moments of Fe-Ni-Co alloys as a function of composition. (After Borelius.)

For the alloys of iron with manganese, chromium, and vanadium the saturation moments decrease with addition of alloying element[21] and the Curie point also decreases except for a slight initial rise in one or two cases. Since, according to Fig. 4, the $n(\epsilon_m)$ values increase with a decrease in the number of electrons per atom, the most likely explanation of the decreasing saturation moments and Curie temperatures is that they are due to a decrease in the exchange energy gained upon reversal of spin. This decrease in exchange energy is due to the fact that for atoms with smaller nuclear charge, the d functions are concentrated further from the nucleus and hence contribute a smaller exchange integral.[22]

For the Fe-Ni (Fig. 7) system the saturation moment increases slightly with the addition of Ni, and then decreases to the phase boundary[23] where the saturation moment is about 2.2 magnetons. Since the corresponding number of electrons per atom is 8.4, it is necessary to assign

can be obtained. However, any reasonable extrapolation of the high-temperature paramagnetic susceptibility of face-centered iron and the Curie points in the face-centered portion of the Fe-Ni alloy system indicate that face-centered iron would not be ferromagnetic.

[20] F. Seitz, reference 15, page 430.

[21] Data quoted by J. C. Slater, reference 17, page 935.

[22] J. C. Slater, reference 17, page 934.

[23] G. Borelius, *Handbuch der Metallphysik* (Leipzig, 1935), Vol. I, p. 291.

0.6 electron per atom in order to account for the observed moment.

For cobalt-iron alloys the saturation moment reaches a maximum of 2.4 magnetons at 8.4 electrons per atom and then decreases to 2.0 magnetons at the phase boundary which occurs at 8.8 electrons per atom. For both cases the corresponding number of electrons per atom in Band VI is equal to 0.80.

The number of electrons per atom in Band VI for nickel and cobalt alloys is much greater than the values extrapolated from the present calculations. Two possibilities of accounting for this difference can be suggested. It may be that for these elements the energy at the top of Band VI is much lower than for iron and the density of states is so much higher, that the number of electrons in Band VI can be as large as 0.80. (It is also possible that there is such an effect in iron and that the saturation moment is determined by a balance of exchange and Fermi terms.) It is also conceivable that Band VI contributes to the ferromagnetism. It would not be ferromagnetic by itself, but a net spin for this band might be produced by a coupling with the net spins in other bands.

Electronic Specific Heat[24]

The electronic contribution to the specific heat is given by the formula[25,26]

$$(C_v)_e = 0.209\times10^{-4} n(\epsilon_m) RT, \qquad (4)$$

where $(C_v)_e$ is in cal./g-atom C°, $n(\epsilon_m)$ is the number of energy levels per atom per Rydberg unit of energy at the top of the Fermi distribution, R is the universal gas constant, and T is the absolute temperature. For body-centered iron $n(\epsilon_m)$ is 17 for the non-magnetic state. Hence the corresponding electronic contribution to the specific heat is $6.9\times10^{-4}T$. This result is valid only at temperatures well above the Curie temperature. Any possibility of checking this against an excess of C_v above the Dulong and Petit value at high temperatures is made impossible by the phase change. At higher temperatures where the body-centered phase is again stable, there are no satisfactory data for determining the dilatation correction.

In one respect there is satisfactory agreement with experiment. As shown in detail in a later section the body-centered structure can become more stable than the face-centered structure at high temperatures only if the specific heat at constant pressure for this structure is higher in this region than the specific heat[27] for the face-centered structure. It is very probable (see reference 40) that the difference is due chiefly to electronic contributions and hence it is a qualitative check on the theory that the value found for body-centered iron is about one and a half times the value found by Greene for face-centered iron.

At low temperatures the distribution of electrons is different and the specific heat for each direction of spin must be computed separately. If the observed value of the saturation moment and the computed $n(\epsilon)$ curves are used to determine the correct values of $n(\epsilon_m)$ to use in Eq. (4), the computed electronic specific heat is found to be $4.6\times10^{-4}T$. Measurements by Duyckaerts[28] and Keesom and Kurrelmeyer[29] at liquid helium temperatures yielded a term $12\times10^{-4}T$ in the specific heat.

X-Ray Emission Bands[30]

The $K\beta_5$-emission band of iron has been studied

[24] In a previous paper (reference 7) Manning and Chodorow reported calculations of the electronic specific heat of metallic tungsten and tantalum. For both of these metals the computed electronic specific heat checked the excess of C_v above 6.0 cal./g-atom C°, at high temperatures within the accuracy of the $C_p - C_v$ correction. There were not then and are not yet available any low temperature data for tungsten. For tantalum the electronic specific heat had been computed from data on the effect of a magnetic field on the superconducting transition temperature and a result of approximately $27\times10^{-4}T$ had been obtained. More recent data by Keesom and Desirant [Proc. Roy. Soc. Ams. **42**, 536 (1939)] and by Mendelssohn [Nature **148**, 316 (1941)] yield a value $14\times10^{-4}T$ compared with the calculated value of $6\times10^{-4}T$.

[25] E. C. Stoner, Proc. Roy. Soc. **A154**, 656 (1936).

[26] H. Bethe, *Handbuch der Physik* (Julius Springer, Berlin), Vol. 24, Part 2, p. 430.

[27] J. B. Austin, Ind. and Eng. Chem. **24**, 1225 (1932).

[28] G. Duyckaerts, Physica **6**, 401 (1939).

[29] W. H. Keesom and B. Kurrelmeyer, Physica **6**, 633 (1939).

[30] Bearden and Snyder [Phys. Rev. **59**, 162 (1941)] have reported studies of x-ray emission and absorption of metallic tungsten and compared their results with the $n(\epsilon)$ curves calculated by Manning and Chodorow. Bearden and Snyder compute from their data that the range of occupied levels in the metal is about 6.5 or 7.0 ev. In comparing with the calculated values they use 10.0 ev. as the calculated width. The present author's estimate of this width is 6.0 ev. This is in considerably better agree-

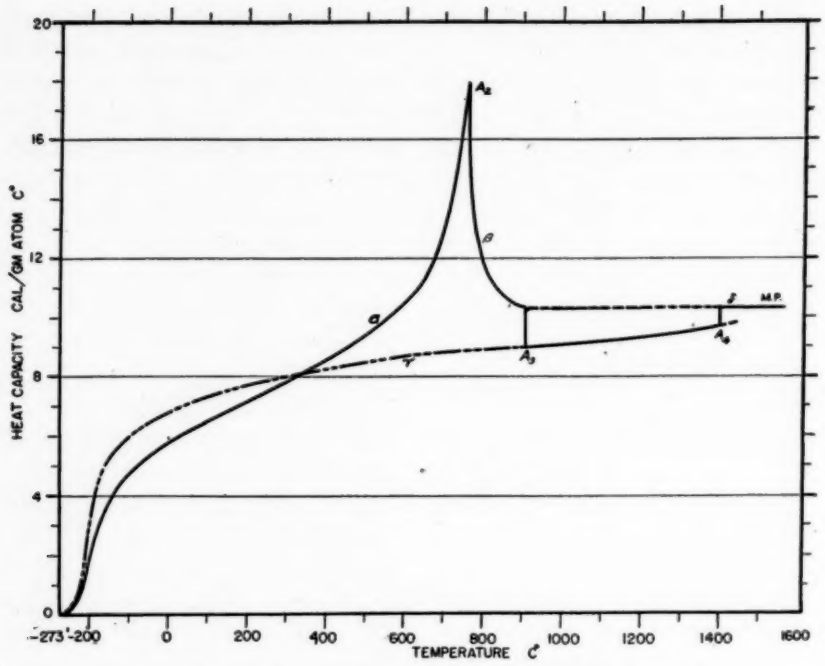

FIG. 8. Specific heat of Fe *vs.* temperature. (After Austin.)

by Beeman and Friedman[31] and the $L\alpha$ and $L\beta$ bands by Farineau.[32] Beeman and Friedman obtained a width of about 7 ev and Farineau obtained a width of about 5.5 ev. The width of the calculated $n(\epsilon)$ curve is about 5 or 5.5 ev depending upon how much weight is given to the low energy portion of the $n(\epsilon)$ curve. The agreement is probably better than should be expected, as the experimental lines are broadened by the finite width of the lower levels and the Auger effect.

Electrical Conductivity

At room temperatures the conductivity of iron is only about one-eighth of the conductivity of copper and only a small part of this difference can be accounted for by differences in Debye temperature and atomic volume. The lowest two bands can make no contribution to the conductivity and it is probably correct to assume that Bands III, IV, and V make little contribution to the conductivity because of the high effective mass of the electrons in these narrow bands. Most of the conductivity is therefore due to the electrons in Band VI. Since there is only 0.25 electron per atom in this band, a lower conductivity than for copper should be expected. Since the conductivity varies as the one-third power[33] of the number of conduction electrons per unit volume, the smaller number of conduction electrons in iron than in copper is responsible for an appreciable, but not a major part, of the difference in conductivity. Mott[8,34] has proposed that the low conductivity of the transition metals is due to the fact that the vacant states in the poorly-conducting bands increase the probability of scattering for the conduction electrons. This theory is able to account qualitatively for a number of features such as the thermoelectric power and high tem-

ment with the experimental results, but the question of addition of line widths probably needs special consideration when the $n(\epsilon)$ curves have such irregular shapes and when the relative proportions of the different types of wave function change with the energy.

The reason for the discrepancy between the 6 ev and the 10 ev has been explained to the author by Dr. Snyder in personal conversation. It arose because the meaning of the term "atomic unit of energy" was not stated carefully enough. In both that paper and this one the unit of energy is the Rydberg unit of energy—13.54 ev—and not twice this quantity which is frequently referred to as an atomic unit. The author regrets any misunderstanding which this may have caused.

[31] W. W. Beeman and H. Friedman, Phys. Rev. **56**, 392 (1939).

[32] J. Farineau, Comptes rendus **206**, 1011 (1938).

[33] F. Seitz, *Modern Theory of Solids* (McGraw-Hill, New York, 1940), p. 537.

[34] N. F. Mott, Proc. Roy. Soc. **A153**, 699 (1936); **A156**, 368 (1936).

perature variation of resistance of transition metals.[34,35] However, Wilson[36] has carried out a more detailed investigation in which he shows that transitions from one band to another can take place only if states represented by the same coordinates in the reduced zone scheme have energy differences of the order of magnitude of thermal energies. This is equivalent to assuming that the constant energy surfaces for the different bands intersect or are close together at a number of points in the reduced zone in order for Mott's model to be applicable.[37] The energy contours obtained in the present calculations have been examined to see if this condition is satisfied for any appreciable number of points in **k** space and it was found that the energy differences between corresponding points in different bands[38] were much larger than thermal energies at all points of the momentum cell. Hence either Mott's model is not applicable or the condition discussed by Wilson is not valid. Seitz[37] suggests that where *d* bands are involved the Δk selection rule used by Wilson may not be applicable.

Phase Changes in Metallic Iron

The phase changes which take place in iron as the temperature is raised are rather unusual. At low temperatures the stable structure is body-centered cubic, between 1179° and 1773°K the stable structure is face-centered cubic, and between 1773°K and the melting point the stable structure is again body-centered cubic.

The thermodynamic condition which determines the relative stability of two phases at constant pressure is that the Gibbs[39] free energy $U-TS+PV$ shall be a minimum. For phase changes in the solid state the PV term can usually be neglected. In the following discussion the body-centered phase will be denoted by the subscript 1 and the face-centered phase by the subscript 2. We then have at any temperature:

$$G_1(T)-G_2(T)=[U_1(0)-U_2(0)]+\int_0^T(C_1-C_2)dT-T\int_0^T(1/T)(C_1-C_2)dT, \quad (5)$$

where C_1 and C_2 stand for the specific heats at constant pressure.

If the right-hand side of this equation is negative at a given temperature the body-centered structure is stable, and if it is positive the face-centered structure is stable. The empirical specific heats[40] as chosen by Austin[27] are shown in Fig. 8. Since the face-centered structure cannot be retained at low temperatures by quenching, the specific heats for this structure are not obtained directly but by a process of extrapolation from a series of alloys for which the face-centered structure can be retained. At low temperatures it seems definite that the face-centered phase has the lower Debye temperature and hence the higher specific heat. At higher temperatures the specific heat associated with the disappearance of ferromagnetism gives the body-centered phase the higher specific heat. At the transition temperature the free energy of the two phases must be equal. To see how this happens Eq. (5) can be written

$$\begin{aligned}G_1(B)-G_2(B)=&[U_1(0)-U_2(0)]\\&+\int_0^{T_A}(C_1-C_2)dT\\&-T_A\int_0^{T_A}(1/T)(C_1-C_2)dT\\&+\int_{T_A}^{T_B}(C_1-C_2)[1-(T_B/T)]dT\\&+(T_B-T_A)\int_0^{T_A}(1/T)(C_2-C_1)dT. \quad (6)\end{aligned}$$

In this equation T_A is the temperature at which the specific heats of the two phases become equal,

[34] N. F. Mott and H. Jones, *Properties of Metals and Alloys* (Oxford, 1936), p. 267.
[36] A. H. Wilson, Proc. Roy. Soc. **167**, 580 (1938).
[37] F. Seitz, *Modern Theory of Solids*, page 540.
[38] This result can also be obtained by reference to Fig. 2. The condition could be satisfied only for energies near the energies.
[39] J. C. Slater, *Introduction to Chemical Physics* (McGraw-Hill, New York, 1939), p. 23.
[40] For more recent data and for a review of the literature subsequent to Austin's paper see J. W. Awberry and Ezer Griffiths, Proc. Roy. Soc. **A174**, 1 (1940). Although it seems probable that these data supersede those quoted by Austin, the data quoted by him are sufficiently accurate for the present arguments.

and T_B is the temperature of the transition from the body-centered to the face-centered structure. The sum of the first three terms on the right-hand side is just the difference in free energies at the temperature T_A. Since the body-centered structure is stable at T_A the sum of these three terms must be negative. The fourth term on the right is also negative, so that it is the fifth term which is responsible for making the free energy become positive above T_B. It is interesting to note that this term is merely the entropy at T_A multiplied by the temperature interval between T_A and T_B.

If T_C denotes the transition point at which the body-centered structure again becomes stable, we have:

$$G_1(C)-G_2(C)=(T_C-T_B)\times\left[\int_0^{T_B}(1/T)C_2dT-\int_0^{T_B}(1/T)C_1dT\right]-\int_{T_B}^{T_C}(C_1-C_2)[(T_C/T)-1]dT. \quad (7)$$

In the bracket the first term represents the entropy of the face-centered structure and the second integral represents the entropy of the body-centered structure at T_B. Since the body-centered structure is stable at 0°K, and the entropy term increases more rapidly with temperature than the energy, the only possibility of making the face-centered structure stable at T_B is for it to have a greater entropy. Hence the first term on the right-hand side of Eq. (7) must be positive. For the body-centered structure to be stable above T_C the second term must be negative and this can be true only if the specific heat at constant pressure is higher for the body-centered phase. Part of this difference in the specific heat might come from a difference in the dilatation correction, but it is probable that most of it comes from the higher electronic specific heat[41] in agreement with the calculations of this paper and the following one.[10]

A few remarks on the effect of alloying elements on the transition temperatures can be made. For some substances such as nickel and cobalt the face-centered structure is more stable than the body-centered structure at absolute zero. Hence if we assume that the energy difference between the phases varies monotomically with composition it follows that adding these elements to iron should widen the temperature range in which the face-centered or γ-phase is stable. In general the energy difference term will favor the face-centered structure whenever the added element has more electrons per atom because the spreading of the energy bands favors the face-centered structure. The Debye temperature will also be affected by alloying elements but general remarks are difficult to make. The variation of the Curie point with composition will also have a marked effect on the lower transition temperature because without the excess specific heat of demagnetization the face-centered structure would become stable at a much lower temperature. It is also true that because of the greater density of states at the top of the Fermi distribution for body-centered iron it becomes ferromagnetic and at absolute zero there is a magnetic term in the free energy which favors the body-centered structure. It thus follows that an element such as manganese which produces a marked lowering of the Curie point will, because of this effect, increase the range of stability of the γ-phase.

When there is such a close balance between opposing factors as has been indicated, the electronic contribution to the specific heat can have an appreciable effect on the transition temperature. This point has been discussed by Smoluchowski[42] who pointed out that if the addition of an alloying element shifted ϵ_m to a portion of the $n(\epsilon)$ curve where the density of states was decreased for the body-centered structure and increased for the face-centered structure, this would increase the stability range of the face-centered or gamma-structure. The $n(\epsilon)$ curves obtained in this paper and the following paper do not yield conclusive evidence in either agreement or disagreement with this theory. This may indicate either that the method used does not give sufficient detail to answer questions involving the

[41] The importance of the electronic specific heat in making the body-centered structure stable at high temperatures has been pointed out by Seitz in *Modern Theory of Solids*, page 488.

[42] R. Smoluchowski, Princeton Meeting of the American Physical Society, December, 1941. Abstract: Phys. Rev. **61**, 390 (1942). The author wishes to thank Dr. Smoluchowski for sending him a brief abstract of his talk and for other interesting correspondence on the subject.

TABLE IV. Values of $2rZ_p$ for metallic iron.

ρ	$2rZ_\rho$	ρ	$2rZ_\rho$	ρ	$2rZ_\rho$
0.0	0.0518	4.0	2.2936	6.0	7.524
0.2	0.0632	4.1	2.4875	6.1	7.711
0.4	0.0771	4.2	2.6937	6.2	7.835
0.6	0.0940	4.3	2.9122	6.3	7.886
0.8	0.1146	4.4	3.1423	6.4	7.858
1.0	0.1396	4.5	3.3835	6.5	7.753
1.2	0.1702	4.6	3.6349	6.6	7.581
1.4	0.2072	4.7	3.8953	6.7	7.351
1.6	0.2520	4.8	4.1629	6.8	7.105
1.8	0.3063	4.9	4.4367	6.9	6.845
2.0	0.3720	5.0	4.7145	7.0	6.571
2.2	0.4511	5.1	4.9975	7.1	6.312
2.4	0.5462	5.2	5.2809	7.2	6.063
2.6	0.6601	5.3	5.5699	7.3	5.821
2.8	0.7962	5.4	5.8909	7.4	5.587
3.0	0.9578	5.5	6.1544	7.5	5.363
3.2	1.1490	5.6	6.4492	7.6	5.169
3.4	1.3738	5.7	6.7419	7.7	5.053
3.6	1.6367	5.8	7.0255	7.8	5.089
3.8	1.9422	5.9	7.2906	7.9	5.111
4.0	2.2936	6.0	7.5244	8.0	5.130

change of $n(\epsilon)$ with ϵ or it may be that some of the other effects mentioned above may be important.

Acknowledgment

The author wishes to acknowledge a grant from the Permanent Science Fund of the American Academy of Arts and Sciences toward the purchase of the computing machine upon which most of the calculations of this paper were carried out.

APPENDIX I

Determination of Effective Field in the Metal

Since the method of finding the effective field to use in computing metallic wave functions is slightly different from that for the free atom, it will be described briefly. Atomic calculations are normally carried out in terms of quantities which Hartree denotes by Z and Z_p (Z/r^2 determines the effective force on an electron and Z_p/r determines the potential energy of an electron at a distance r from the nucleus). Z is determined by numerical evaluation of a definite integral and Z_p by solution of the differential equation:

$$dZ_p/d\rho = Z_p - Z \qquad (8)$$

which is integrated inwards subject to the boundary condition that Z_p approaches zero at large values of r. The effective field of a valence electron in the metal was assumed to be due to the nucleus, the *1s* to *3p* core, and to one *s* type and six *d* type functions. The field due to the inner electrons and the nucleus was taken to be the same as found by Manning and Goldberg[45] for the iron atom. As a first approximation to the charge distribution of the other valence electrons the atomic charge distributions were used except that they were normalized to the atomic volume characteristic of the metal. In computing the field due to such a charge distribution the ordinary method of inward integration of Eq. (8) is not satisfactory because of the difficulty in determining initial values of $2Z_p$. If the electronic charge due to the valence electrons within a sphere of radius r is designated by ζ, then $2\zeta/r^2$ is the force on one valence electron due to the remaining valence electrons, and the inward integration of this quantity with respect to r yields the potential energy due to the other valence electrons. This method is not applicable to inner shell electrons because of the rapid variation of $2\zeta/r^2$.

By use of the potential field thus found, integrations for *d* functions for a range of energies were carried out by the same methods as used in self-consistent field calculations.[43-45] The energy for which the radial factor of the *d* function became zero and also the energy at which the radial derivative became zero at the half distance between nearest neighbors were thus determined. Since the method by which the first approximation was found concentrated the charge too close to the nucleus, the charge densities for these new wave functions would be concentrated too far from the nucleus. An attempt was made to allow for this in a manner similar to that used in atomic calculation by choosing for the next approximation a field obtained by averaging the initial field with one found by using wave functions based upon that field. A weighting of six-tenths initial to four-tenths final has been used. For the final field six different charge distributions corresponding to energies between that for which $d_1'=0$ and that for which $d_1=0$ were used. Since previous experience with transition metals indicated a considerable concentration of levels near $d'=0$, additional weight was given to levels in this region. Two more approximations were made and at the end of the last approximation the total width of the *d* band checked the width at the end of the previous approximation within a tenth of a unit. It was therefore decided that approximations made in using this field would be less than other errors inherent in the general method.

Since the effective potential for metallic iron may be useful for other calculations, the values are given in Table IV.

APPENDIX II

Computational Procedure

After the wave functions and their radial derivatives at the half-distances between neighbors and next-nearest neighbors have been obtained, the next step is the solution of the transcendental equations which relate the energy and the components of the wave number vector **k**. The procedure was similar to that used in the calculations for

[43] D. R. Hartree, Proc. Roy. Soc. **A141**, 282 (1933); D. R. Hartree and W. Hartree, Proc. Roy. Soc. **A149**, 210 (1935).

[44] A. A. Bennett, W. E. Milne, and H. Bateman, *Numerical Integration of Differential Equations*, Bulletin of the National Research Council, No. 92 (1933).

[45] M. F. Manning and J. Millman, Phys. Rev. **53**, 673 (1938).

tungsten, but one change was made which seems worth recording. A typical example of the transcendental equations to be solved has the form:

$$A_1T_1^2T_2^2+A_2T_1T_2+A_3T_2^2+A_4T_1^2+A_5=0, \quad (9)$$

where $T_1=\tan(ka/4)$, $T_2=\tan(ka/2)$ and the A's are tabulated functions of the wave functions and their derivatives and hence of the energy. One method of solution is to evaluate the expression for two values of $ka/4$, interpolate or extrapolate for a value of $ka/4$ which makes the expression vanish; try another value of $ka/4$ and so forth until the desired accuracy is obtained. Another method is to express T_2 in terms of T_1 and thus obtain a polynomial in T_1^2 which can be evaluated very rapidly by the method of synthetic division.[46] This procedure was used for all of the transcendental equations except that for F_1 which has twelve different tangent factors. However, a table of these tangent factors as a function of the argument made by Dr. Chodorow in connection with the calculations for tungsten shortened the computations for this direction considerably. Details of the computational method for obtaining $n(\epsilon)$ and $N(\epsilon)$ are given in the appendix of the paper on tungsten.[3]

APPENDIX III

In reporting calculations such as these, some estimate of the approximations made is in order. The most obvious and probably the most important approximation is the neglect of all exchange effects. This precludes any detailed discussion of ferromagnetism. Correlation effects are also neglected. The neglect of exchange and correlation effects means that calculation of the binding energy cannot be made and remarks about the relative stability of different structures can be only qualitative. The net effect of exchange and correlation would be to make the energy bands narrower and hence $n(\epsilon_m)$ larger. It is to be expected that the effects of exchange and correlation will be greater for iron than for tungsten because of the smaller number of d electrons in tungsten and also because the incomplete shielding of the f electrons in tungsten makes the electrostatic contribution to the potential energy greater.

Another approximation is involved in the Slater method of fitting boundary conditions. Only fourteen functions are used and the continuity condition on functions and derivatives is satisfied only at fourteen points rather than over the entire surface of the Wigner-Seitz polyhedron. An attempt to estimate the magnitude of this error has been made by Shockley,[47] but it is not certain to what extent his results are applicable to the present problem. More elaborate methods of calculating energy levels in metals have been developed by Slater,[17] Chodorow,[12] and by Herring.[48,49] The present calculations yield a good general picture of the energy levels, and can serve as a starting point for more elaborate calculations.

Even within the method itself certain approximations are made. Without much more elaborate calculations it is not possible to determine a completely satisfactory charge distribution because the criterion for self-consistency is more difficult to apply in the case of a solid. Another approximation is made in using only known lines and interpolating contours. Similarly, when using sections 0.1 unit apart in finding $N(\epsilon)$ by a volume integration in $\mathbf{k}$ space, some detail in determining the $N(\epsilon)$ curves is lost. The method of determining $n(\epsilon)$ always leads to a further smoothing effect so that the net effect of the last three approximations mentioned is to make the $n(\epsilon)$ less irregular than might be the case if a more elaborate method of calculation were used.

In summary, it seems probable that the general features of the electronic structure of metallic iron as obtained by this method are essentially correct and that detailed numerical agreement is not possible without much more elaborate methods of calculation. It seems probable that the classification of the energy bands into two responsible for the binding, three responsible for the magnetic behavior, and one for conduction is fundamental to the problem. It is interesting to note that the markedly greater value (17 *vs.* 11) of $n(\epsilon_m)$ for the body-centered structure than for the face-centered structure is necessary in order to account for the observed differences in magnetic behavior and in electronic specific heat, and also to account for the high temperature phase change.

[46] I. S. and E. S. Sokolnikoff, *Higher Mathematics for Engineers and Physicists* (McGraw-Hill, New York, 1934), Chapter II.

[47] W. Shockley, Phys. Rev. **52**, 866 (1937).
[48] C. Herring, Phys. Rev. **57**, 1169 (1940).
[49] C. Herring and A. G. Hill, Phys. Rev. **58**, 132 (1940).

Electronic Energy Bands in Face-Centered Iron

JACK B. GREENE* AND MILLARD F. MANNING**
University of Pittsburgh, Pittsburgh, Pennsylvania
(Received December 19, 1942)

Calculations of the electronic energy bands for face-centered iron by the Wigner-Seitz-Slater method are reported. There are found to be two filled and four partially-filled bands. The density of states is calculated as a function of the energy; the curves of the density of states *vs.* energy appear quite similar to those calculated by Slater for copper but resemble more closely those for body-centered iron. The density of states at the highest occupied energy level at absolute zero is 11.4 states per Rydberg unit of energy per atom. These results have been used to calculate the average Fermi energy as a function of the total number of valence electrons; to investigate the ferromagnetism of Ni and Co by calculating the change in Fermi energy as a function of the number of uncompensated spins; and to calculate the electronic specific heat at an elevated temperature. The calculated electronic specific heat is found to agree fairly well with the difference from $3R$ of the experimentally-measured specific heat. There are no experimental data for the specific heat of face-centered iron at low temperatures.

INTRODUCTION AND PROCEDURE

AT ordinary temperatures metallic iron has a body-centered structure (α-iron), but from 870°C to 1390°C the face-centered structure (γ-iron) is the stable one. Above 1390°C the body-centered structure is again stable. γ-iron is of scientific interest principally because many of its properties are quite different from those of α-iron. The most important of these differences is that γ-iron is not ferromagnetic. Although γ-iron is stable only above the Curie temperature, all extrapolations to room temperature indicate that it would not be ferromagnetic. γ-iron does exist at ordinary temperatures in the form of austenitic steel, since the steel has been quenched from a temperature where γ-iron is the stable form.

The Wigner-Seitz-Slater cellular method of calculating energy bands in metals[1,2] has been applied to sodium,[2] to lithium,[3] to copper,[4] to calcium,[5] and to one transition metal, tungsten.[6] With modifications it has also been applied to some insulators.[7] In this paper it has been applied to face-centered iron. In applying this method one starts with the radial part of the wave function and the radial derivative of the wave function at a distance half-way between nearest atoms in the face-centered lattice. For face-centered iron the lattice parameter at 900°C is 3.63A and the corresponding distance r between nearest neighbors is 4.85 Bohr units. The corresponding value of $(\rho \equiv \log_e 1000r)$ is 7.79, where r is in Bohr units. These radial wave functions were found by a modified Hartree procedure in which the Schroedinger equation was integrated numerically, with the same effective field as that used by Manning[8] in the work on body-centered iron and explained fully by him in Appendix I of his report. These integrations were carried out for s, p, d, and f functions over a range of energy values wide enough to give six complete energy bands.

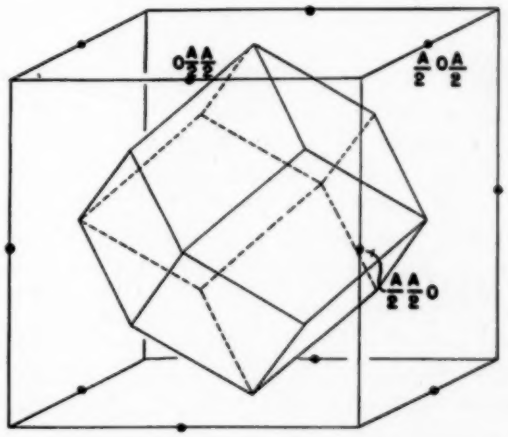

FIG. 1. The polyhedral cell for the face-centered lattice.

* Now at the University of Illinois, Urbana, Illinois.
** Deceased June 1, 1942.
[1] E. P. Wigner and F. Seitz, Phys. Rev. **43**, 804 (1933).
[2] J. C. Slater, Phys. Rev. **45**, 794 (1934).
[3] F. Seitz, Phys. Rev. **47**, 400 (1935).
[4] H. M. Krutter, Phys. Rev. **48**, 664 (1935).
[5] M. F. Manning and H. M. Krutter, Phys. Rev. **51**, 761 (1937).
[6] M. F. Manning and M. I. Chodorow, Phys. Rev. **56**, 787 (1939).
[7] M. F. Manning and M. I. Chodorow, Phys. Rev. **56**, footnote 2, p. 787 (1939).
[8] M. F. Manning, Phys. Rev. **63**, 190 (1943).

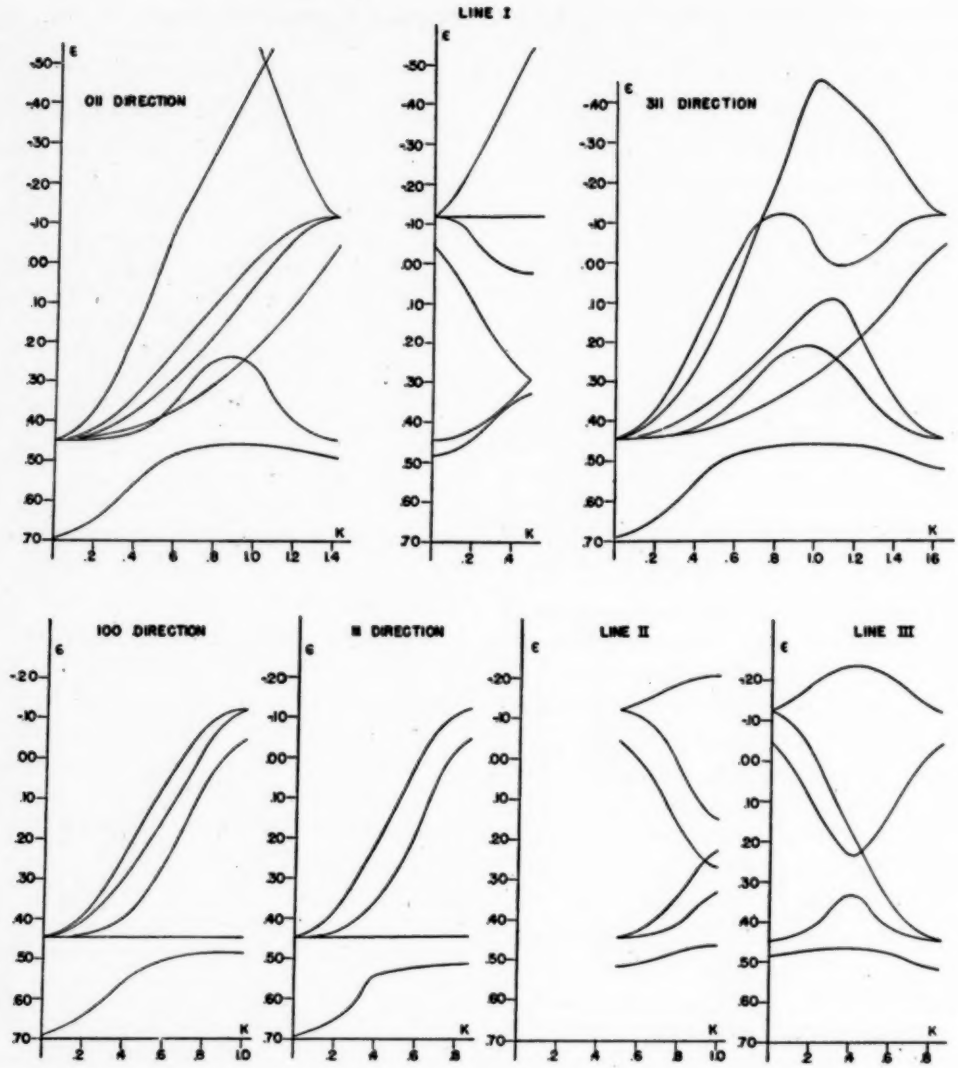

FIG. 2. Energy *vs.* momentum for the different directions of propagation.

The next step was to express the wave function within the polyhedron surrounding an atom in the face-centered lattice (see Fig. 1) as the sum of twelve terms (since there are twelve sides to this cell), each term being the product of a radial wave function times a spherical harmonic. The arbitrary coefficients of these terms must be chosen so that the wave functions satisfy the Bloch[9] periodicity condition and join smoothly in passing from one atom to its twelve nearest neighbors. The application of these conditions leads to a determinant, the solution of which gives the momentum of the electron in certain directions in terms of the radial wave functions and radial derivatives; this momentum of the electron is expressed by the wave number vector K. Since the radial wave functions are in turn functions of the energy, a relationship is established between the energy and the wave number vector or momentum in that particular direction. The solution of the determinant in the general direction is too laborious to attempt, but for a

[9] F. Bloch, Zeits. f. Physik **52**, 555 (1928).

TABLE I. Maximum and minimum energies for each band.

Band	I	II	III	IV	V	VI
Max. ϵ	0.688	0.443	0.443	0.443	0.443	0.443
Min. ϵ	0.327	0.240	−0.0475	−0.124	−0.124	−0.525

number of symmetrical directions the solution simplifies a great deal. For the face-centered lattice the results of the expansion of the determinant for a number of special directions have been given by Shockley.[10]

RESULTS

The results of the calculation of the energy as a function of the momentum are given in Fig. 2. In Table I the maximum and minimum energies for each band are given, and in Table II the energies at a number of special points in the first Brillouin zone (the momentum cell) are tabulated. Figure 3 shows the first Brillouin zone for the face-centered lattice with the location of these special points indicated. (The point O is the center of the cell but is not shown in this figure.) In these tables and elsewhere in this paper ϵ is the negative of the energy expressed in Rydbergs. The curves for the 011 direction, for the 100 direction, and for the 111 direction are quite similar to those for copper.[4] These were the only directions for copper available for comparison.

Using the energy-momentum relationships for the known lines in K space, one can draw fairly good energy contours for the principal planes in K space. One can then interpolate from these to get energy contours in the planes $K_z=0.1$, 0.2, $\cdots$1.0. In each of these planes the area enclosed

TABLE II. Values of ϵ for some points in the Brillouin zone.

Point	Band I	II	III	IV	V	VI
O	0.69	0.44	0.44	0.44	0.44	0.44
A	0.517	0.44	0.44	−0.0475	−0.125	−0.125
B	0.48	0.44	−0.0475	−0.125	−0.125	−0.125
C	0.46	0.31	0.18	0.01	−0.05	−0.45
D	0.325	0.29	0.29	0.02	−0.125	−0.55
E	0.46	0.31	0.18	0.01	−0.05	−0.45

by each constant-energy contour, within which the energy was less than (i.e., ϵ greater than) the value of the energy for this contour, was found by means of a planimeter. This was done for each of the ten planes and then the results integrated to get the volume enclosed by the surface of constant energy. This volume is then proportional to the number of electrons per atom or states per atom with energy less than

[10] W. Shockley, Phys. Rev. **51**, 129 (1937).

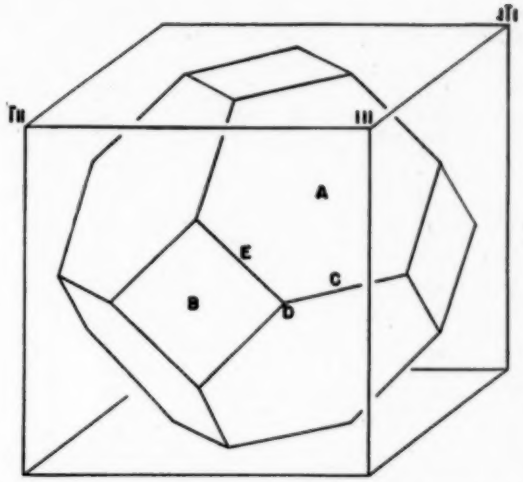

FIG. 3. The first Brillouin zone for the face-centered lattice, showing the points referred to in Table II.

the energy considered. The number of electrons with energy less than a given energy can be found by the normalizing condition that the total volume of the momentum cell represents two electrons per atom in each energy band. This quantity is called $N(\epsilon)$. The values of $N(\epsilon)$ for each of the energy bands and for the sum of the six bands are given in Tables IIIa and IIIb. It will be noticed that in the first three bands, values of $N(\epsilon)$ are tabulated every 0.025 unit of ϵ. For Bands IV and V they are tabulated every 0.05 unit of ϵ, and for Band VI every 0.10 unit of ϵ. This was done because the last three bands extended through a wider energy range and would have required more contours than it was felt the accuracy of the method justified.

From the values of $N(\epsilon)$ the values of $n(\epsilon)[=-(dN/d\epsilon)]$ can be found by numerical differentiation. $[n(\epsilon)d\epsilon$ is the number of energy levels per atom with energy between ϵ and $(\epsilon+d\epsilon).]$ The resulting values of $n(\epsilon)$ for the separate bands and the total value of $n(\epsilon)$ for all six bands as functions of ϵ are given in Fig. 4.

Bands I and II, being completely filled, would not be expected to contribute either to the electrical conductivity or to ferromagnetism. Bands III, IV, and V are the ones to be investigated to see why face-centered iron is not ferromagnetic. Band VI looks more like a band predicted from the "free electron" picture than any of the others. It probably accounts for the

TABLE IIIa. Number of states having energies less than a given energy.

Band I		Band II		Band III		Band IV		Band V		Band VI	
ϵ	$N(\epsilon)$	ϵ	$N(\epsilon)$	ϵ	$N(\epsilon)$	ϵ	$N(\epsilon)$	ϵ	$N(\epsilon)$	ϵ	$N(\epsilon)$
0.675	0.001	0.425	0.496	0.425	0.165	0.40	0.045	0.40	0.016	0.40	0.006
0.65	0.009	0.40	0.905	0.40	0.349	0.35	0.146	0.35	0.056	0.35	0.024
0.625	0.029	0.375	1.24	0.375	0.502	0.30	0.274	0.30	0.104	0.30	0.049
0.60	0.057	0.35	1.52	0.35	0.615	0.25	0.430	0.25	0.182	0.25	0.082
0.575	0.084	0.325	1.72	0.325	0.731	0.20	0.625	0.20	0.284	0.20	0.126
0.55	0.126	0.30	1.86	0.30	0.850	0.15	1.03	0.15	0.387	0.15	0.174
0.525	0.206	0.275	1.99	0.275	0.982	0.10	1.40	0.10	0.520	0.10	0.238
0.50	0.399	0.25	2.00	0.25	1.21	0.05	1.62	0.05	0.684	0.05	0.304
0.475	0.850			0.225	1.64	0.00	1.88	0.00	0.859	0.00	0.394
0.45	1.57			0.20	1.74	−0.05	1.96	−0.05	1.13	−0.10	0.642
0.425	1.77			0.175	1.82	−0.10	1.99	−0.10	1.60	−0.20	1.05
0.40	1.89			0.15	1.87					−0.30	1.47
0.375	1.95			0.125	1.91					−0.40	1.82
0.35	1.99			0.10	1.94					−0.50	1.99
				0.075	1.96						
				0.05	1.98						
				0.025	1.99						
				0.00	2.00						

electrical conductivity. Band VI also is the widest band of those investigated. In general features the energy bands for face-centered iron resemble those of body-centered iron[8] more than any other metal that has been investigated. In general features the total $n(\epsilon)$ curve resembles that for copper,[11] but since the energy units are different for the two cases, closer comparison is difficult. Band VI in copper is very much like Band VI for face-centered iron; that is the only single energy band shown for copper.[11]

Since there are eight valence electrons per atom in face-centered iron, reference to Table IIIb shows that the highest occupied level at absolute zero in face-centered iron occurs at $\epsilon=0.117$. The corresponding value of $n(\epsilon)$ is 11.4. Thus the density of states at the edge of the Fermi distribution is 11.4 states per atom per Rydberg unit of energy.

APPLICATIONS

Energy Relations

The average Fermi energy has been computed as a function of the total number of valence electrons per atom. The average Fermi energy $\bar{\epsilon}$ is defined by the equation

$$N(\epsilon_m)(\bar{\epsilon}-\epsilon_0)=-\int_{\epsilon_0}^{\epsilon_m} n(\epsilon)(\epsilon-\epsilon_0)d\epsilon, \qquad (1)$$

where ϵ_0 refers to the lowest level occupied at absolute zero and ϵ_m to the highest. Equation (1) can be integrated by parts, giving

$$\bar{\epsilon}=\epsilon_m+\frac{1}{N(\epsilon_m)}\int_{\epsilon_0}^{\epsilon_m} N(\epsilon)d\epsilon.$$

This avoids the inaccuracies that arose when $N(\epsilon)$ was differentiated numerically to give $n(\epsilon)$. The results of these computations for the face-centered lattice are shown in Fig. 5; the average Fermi energy is plotted against the total number of valence electrons per atom. In the preceding paper,[8] Manning has discussed the average Fermi energy for the two kinds of iron and the possible extrapolations to predict the structure of the other neighboring elements in the periodic table.

For the face-centered lattice the lowest band begins at the energy for which $s'=0$ and the other five bands begin at the energy for which $d'=0$. The behavior of the energies for which

TABLE IIIb. Summation of $N(\epsilon)$ values for all bands.

ϵ	$\Sigma N(\epsilon)$	ϵ	$\Sigma N(\epsilon)$
0.675	0.001	0.30	5.14
0.65	0.009	0.25	5.90
0.625	0.029	0.20	6.78
0.60	0.057	0.15	7.46
0.575	0.084	0.10	8.10
0.55	0.126	0.05	8.59
0.525	0.206	0.00	9.13
0.50	0.399	−0.10	10.2
0.475	0.850	−0.20	11.0
0.45	1.57	−0.30	11.5
0.425	2.43	−0.40	11.8
0.40	3.21	−0.50	12.0
0.35	4.35		

[11] J. C. Slater, Phys. Rev. 49, 537 (1936).

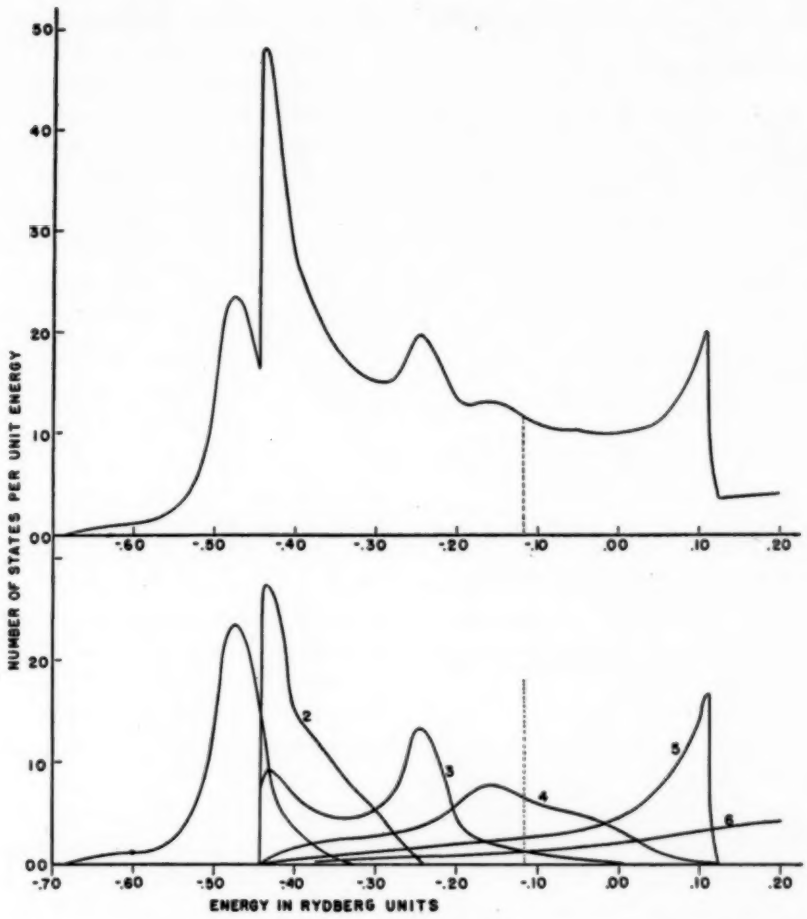

FIG. 4. Number of states per unit energy range *vs.* energy. The upper curve is the sum of the six lower curves.

$s'=0$ and for which $d'=0$ as a function of interatomic distance is shown in Fig. 6. It should be noted that the abscissa is r, the actual interatomic distance, and not ρ, the $\log_e$ of the interatomic distance.

Magnetism

It is interesting to see whether these calculations can offer at least a qualitative explanation of why body-centered iron is ferromagnetic and face-centered iron is not. According to the discussion of ferromagnetism in the paper on body-centered iron,[8] when a substance changes from a non-magnetic state to a magnetic state there is an increase in the Fermi energy, and an increase in the binding energy due to the increase in the number of exchange integrals between electrons of parallel spin. A ferromagnetic substance is one in which the change in Fermi energy is more than compensated for by the increase in the number of exchange integrals. Slater[11] showed that this change in exchange energy is proportional to the square of the number of uncompensated spins. The change in Fermi energy is also proportional to the square of the number of uncompensated spins if $n(\epsilon)$ can be regarded as constant, the expression for the change in Fermi energy being

$$\Delta\epsilon_F=\mu^2/2n(\epsilon_m), \qquad (2)$$

where μ is the number of uncompensated spins in Bohr magnetons, and $n(\epsilon_m)$ is the number of energy levels of both spins per Rydberg unit of energy at the highest occupied level for the non-magnetic state, and $\Delta\epsilon_F$ is the change in Fermi energy upon reversing $\mu/2$ spins. The smaller $\Delta\epsilon_F$ is, the more likely it is to be compensated for by the increase in exchange integrals;

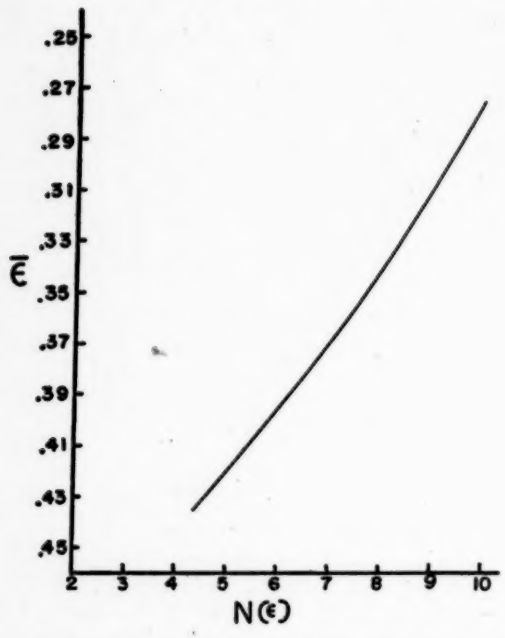

FIG. 5. Average Fermi energy *vs.* total number of valence electrons per atom.

hence, the larger $n(\epsilon_m)$ is, the more likely the metal is to be ferromagnetic. For body-centered iron $n(\epsilon_m)$ is 17 and for face-centered iron $n(\epsilon_m)$ is 11.4. Hence the body-centered metal would be more likely to be ferromagnetic.

If the number of states per unit energy range is not constant, the change in Fermi energy is no longer given by Eq. (2), but must be found by using Eq. (1) for each direction of spin. In computing this change Bands I and II, being closed bands, are neglected, and Band VI, being concentrated relatively far from the nucleus, is also neglected. In the hope of applying these calculations to the neighboring ferromagnetic metals, cobalt and nickel, the change in Fermi energy as μ increases was computed for the total number of valence electrons equal to 8.0, 8.5, 9.0, 9.5, and 10.0, respectively. Equation (1) was used for each direction of spin, and it was applied only to Bands III, IV, and V. In general, the Fermi energy increased less rapidly than did μ^2 but there were some fluctuations which indicated the computational error was rather large.

The saturation magnetic moment of a ferromagnetic metal is determined by one of the following conditions:[8]

(1) The number of negative spins per atom cannot be negative.
(2) The number of positive spins per atom cannot be greater than three.
(3) If the exchange contribution to the energy increases less rapidly with μ^2 than does the increase in the Fermi energy, the difference between the two may vanish at some value of μ less than that determined by either of the other two conditions.

The first condition never seems to occur in any atom or alloy involving iron group elements. Since, for face-centered iron, the Fermi energy did not increase as rapidly as μ^2 for the total number of valence electrons equal to 8.0, 8.5, 9.0, 9.5, and 10.0, it would indicate that condition (3) did not determine the maximum value of μ. Then the number of positive spins per atom must be equal to three; i.e., all the levels with plus spins are filled. Table IV shows a comparison of the value of the saturation magnetic moment calculated on this assumption and the experimentally-observed value[12] for Ni and Co.

The calculated magnetic moment for Ni is arrived at in the following way: There are 10 outside electrons, of which 4 are in Bands I and II; from the results for face-centered iron there are 0.64 electron in Band VI. Thus there are 5.36 electrons in the bands that contribute to magnetism. If there are 3 electrons with plus spin there are 2.36 electrons with minus spin and the magnetic moment is 0.64 spin per atom. This agrees fairly well with the observed value

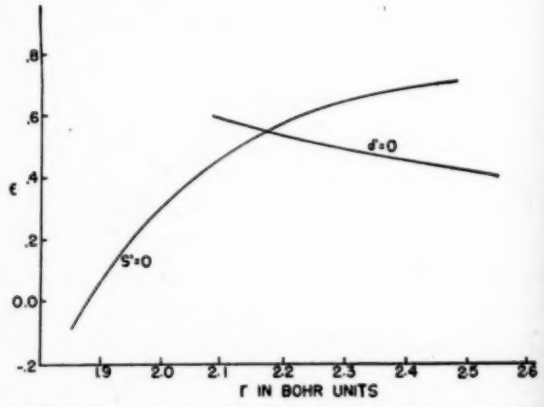

FIG. 6. The energy for which $d'=0$ and the energy for which $s'=0$ as a function of interatomic distance.

[12] E. C. Stoner, *Magnetism and Matter* (Methuen and Company, Ltd., London, 1934), p. 366.

of the saturation magnetic moment, but the value calculated in the same way for cobalt is somewhat different from the observed value. This might be due to the fact that the results for face-centered iron cannot be applied to hexagonal cobalt; it might be due to errors in these calculations; or possibly, the levels with plus spin are not filled. If one uses the observed saturation magnetic moment and assumes the levels of plus spin are all filled, then one finds that the corresponding number of electrons in Band VI has to be 0.71. This value is much larger than the value indicated by the calculations for face-centered iron. Manning[8] found this same difficulty with cobalt-iron alloys. He suggested the possibility that the electrons in Band VI, by coupling with electrons in other bands, contribute to the magnetic moment.

Electronic Specific Heat

The electronic contribution to the specific heat may be computed from the formula[13]

$$(C_v)_e=(5.670/27.08)\times10^{-4}n(\epsilon_m)RT, \quad (3)$$

where $(C_v)_e$ is the electronic contribution to the specific heat per gram atom, R is the universal gas constant, T is the absolute temperature, and $n(\epsilon_m)$ is the number of states of both spins per Rydberg unit of energy at the edge of the Fermi distribution.

It is only at very high and very low temperatures that the electronic contribution to the specific heat is appreciable. The contribution at very low temperatures was not computed because there are no experimental data available for comparison. For high temperatures it was decided to compare the theoretical contribution to the specific heat with that computed from experimental data at a particular temperature. The temperature of 960°C is well above the transition temperature from α- to γ-iron and there are very good data for the specific heat of iron at this point.

Specific heat measurements are made at constant pressure, but for comparison purposes one needs to have the specific heat at constant volume, C_v. This is generally computed from the equation

$$C_p-C_v=9\alpha^2VT/\beta, \quad (4)$$

where 3α is the thermal coefficient of volume expansion per degree centigrade, V is the specific volume, T is the absolute temperature, and β is the compressibility. All the quantities except β are available at the required temperature. β is ordinarily measured at room temperature and extrapolated to higher temperatures,

TABLE IV. Saturation magnetic moments for nickel and cobalt.

Element	Calculated magnetic moment	Observed magnetic moment
Co	1.39	1.71
Ni	0.64	0.61

but face-centered iron is unstable at room temperature. However, if we make use of Grüneisen's law,

$$\gamma=3\alpha V/C_v\beta, \quad (5)$$

where γ has an approximately constant value for all temperatures,[14] then, writing Eq. (4) in terms of γ, we get

$$C_p/C_v=1+3\gamma\alpha T. \quad (6)$$

The value of γ used[15] is an extrapolated value, since there is no experimental one available for face-centered iron. The value of γ does not vary much from metal to metal; for α-iron it is 1.68; for copper, 1.96; for nickel, 2.2; and for cobalt, 2.1. Since copper and nickel both have face-centered structures, the value for face-centered iron should be about 2.0.

Substituting the following values[16] of C_p, α, γ, and T in Eq. (6):

$$(C_p)_{960°C}=7.94 \text{ cal./g atom °C},$$

$$(\alpha)_{960°C}=25\times10^{-6} \text{ per °C},$$

$$\gamma=2.0,$$

$$T=1233°\text{A},$$

[13] E. C. Stoner, Proc. Roy. Soc. **154**, 656 (1936); also H. Bethe, *Handbuch der Physik* (J. Springer, Berlin, 1933), Vol. 24, Part 2, p. 430.

[14] See F. Seitz, *Modern Theory of Solids* (McGraw-Hill Book Company, Inc., New York, 1940), p. 138.

[15] Values of γ are from J. C. Slater, Phys. Rev. **57**, 744 (1940).

[16] Value of $(C_p)_{960°C}$ is an experimentally-determined value, reported by E. Lapp, Ann. de physique **6**, 826–855 (1936); Value of $(\alpha)_{960°C}$ is from *Metals Handbook* (American Society for Metals, Cleveland. 1939), p. 434.

one gets[17]

$$C_v = 6.70 \text{ cal./g atom °C.}$$

If one assumes that the specific heat due to the lattice vibrations at this temperature is the Dulong and Petit value of $3R$, then the quantity

$$C_v - 3R = 0.73 \text{ cal./g atom °C}$$

represents the electronic specific heat at this temperature. The theoretical value of the electronic specific heat computed by Eq. (3) is 0.59 cal./g atom °C, and the agreement between these two values is very good.

It is to be expected that the theoretical value of the electronic specific heat would be smaller than the other value. If the lattice vibrations were not entirely harmonic the value of $(C_v - 3R)$ would contain contributions due to the anharmonicity as well as the contribution of the electronic specific heat. Furthermore, the method of calculating the electronic energy bands reported here did not consider such corrections as exchange and correlation, which would tend to make the total spread in energy smaller and hence $n(\epsilon)$ larger. This would make the electronic contribution greater than that found here.

Qualitatively one can see that the electronic specific heat of body-centered iron would be greater than that of face-centered iron because $n(\epsilon_m)$ is greater for the body-centered iron. Manning[8] has already pointed out that it is because of this high electronic specific heat for the body-centered phase that this phase again becomes stable as the temperature increases.

In conclusion it should be pointed out that the same approximations have been made in the calculations for face-centered iron as were made for body-centered iron. A detailed discussion of these approximations and their accuracy has been given by Manning[8] in Appendix III of the paper on body-centered iron.

[17] By a method involving an extrapolation of β, Mme. Lapp has calculated a value of C_v to be 7.66 cal./g atom °C; see reference 16.

PHYSICAL REVIEW VOLUME 63, NUMBERS 5 AND 6 MARCH 1 AND 15, 1943

The Nature of the Primary Particles Responsible for Cosmic-Ray Phenomena

W. F. G. SWANN
Bartol Research Foundation of The Franklin Institute, Swarthmore, Pennsylvania

(Received January 21, 1943)

LATITUDE EFFECT CONSIDERATIONS

As a preliminary, we notice that if $\beta = v/c$, the minimum value for vertical entry through the earth's magnetic field H of a particle of mass m and charge ne is given by

$$(m/n)[\beta_m/(1-\beta_m^2)^{\frac{1}{2}}] = ef(H), \qquad (1)$$

where $f(H)$ involves only the field and terrestrial dimensions, and e is the electronic charge.

We note, therefore, that if subscripts (1) and (2) refer to magnetic latitudes φ_1 and φ_2

$$\frac{\beta_{m1}}{(1-\beta_{m1}^2)^{\frac{1}{2}}} \frac{(1-\beta_{m2}^2)^{\frac{1}{2}}}{\beta_{m2}} = \frac{f(H_1)}{f(H_2)}. \qquad (2)$$

We note further that if the primary particle splits into mesotrons which are born at rest in the frame of reference of the primary particles, then the value of β for the primary particle is equal to that for the corresponding mesotrons, and (2) applies for the minimum velocities of the mesotrons at the two latitudes.

Now the writer has shown[1] that if $F(E)dE$ represents the energy distribution of the vertically directed mesotrons at the point of production, then the number of mesotrons at a distance x below this point, and resulting from the group representing the integrated value of $F(E)dE$, is N_x where

$$N_x = \int_{E_m}^{\infty} \{[1+A/(\gamma+1)]e^{-\lambda x} - A/(\gamma+1)\}^{[\lambda c\tau_0(\gamma+1+A)]^{-1}} F(E)dE, \qquad (3)$$

[1] W. F. G. Swann, Phys. Rev. **60**, 470 (1941).

with $$A \equiv \alpha\rho_0/\lambda m_0 c^2,$$

and $$\gamma \equiv E/m_0c^2 = [1/(1-\beta^2)^{\frac{1}{2}} - 1];$$

m_0, τ_0, ρ_0, α, E_m being, respectively, the rest mass of the mesotron, its mean life at rest, the ratio of the atmospheric density at $x=0$ to that at sea level, the ionization energy loss per unit of mass (per unit area) traversed, the minimum energy for entry, and where λ is the constant in the expression $\rho=\rho_0 \exp[\lambda x]$ for the relative atmospheric density at the depth x.

Now if R_{12} is the ratio of the values of N_x at the latitudes φ_1 and φ_2, we see from (3) that R_{12} at sea level depends only upon $(1-\beta_{m1}^2)$, $(1-\beta_{m2}^2)$, and the altitude of production. We can express $(1-\beta_{m2}^2)$ in terms $(1-\beta_{m1}^2)$ by (2) and then, R_{12} depends only upon β_{m1} and the altitude of production.

If now we repeat the process for the *latitude ratio* R'_{12} at another altitude, we shall find another set of values of $(1-\beta_{m1}^2)$ with corresponding altitudes of production necessary to fit the facts. There will be only one value of $(1-\beta_{m1}^2)$ which fits the values of R_{12} and R'_{12} for the same altitude of production. On submitting the matter to calculation, using the sea-level data[2] for latitudes and 0°, and A. H. Compton's data[3] for an altitude of 13,000 feet, we find $(1-\beta_{m1}^2)=0.028$ for the latitude 40°. Using this in Eq. (1), and realizing that $f(H)$ is known for the latitude in question, we find that m/n equals the proton mass. Thus the conditions are satisfied by a primary particle of proton mass and single electronic charge splitting into 10 mesotrons,[4] since the mesotron mass is approximately one tenth that of the proton. Moreover there is no other value of n which would lead to a particle having the mass of any known particle.

[2] E.g., A. H. Compton and R. N. Turner, Phys. Rev. **52**, 799 (1937); T. H. Johnson, Rev. Mod. Phys. **10**, 194 (1938).

[3] A. H. Compton, Rev. Sci. Inst. **7**, 71 (1936); R. T. Young and J. C. Street, Phys. Rev. **51**, 386 (1937).

[4] In the writer's previous paper, Phys. Rev. **60**, 470 (1941), a value 5 instead of 10 was reached. This resulted from considerations founded upon an erroneous value taken for the vertical magnetic cut-off energy.

CONSEQUENCES OF INTENSITY-ZENITH ANGLE CONSIDERATIONS

The writer has called attention[5] to the fact that the flatness of the intensity-zenith angle curves at high altitudes points to a decay of low energy mesotrons, with the creation of electrons whose directions of motion show wide angles with the directions of the primaries.

In an unpublished memorandum, the writer has shown that if electrons are born from mesotrons in such manner that they travel out on the average equally in all directions in the frame of reference of the mesotrons, then viewed from stationary axes they perpetuate the direction of the mesotrons to such an extent that the ratio of the electron intensity in a direction perpendicular to a mesotron stream to that in the direction parallel to it is, in the case of mesotrons of constant velocity βc, given by $1-\beta^2$. If the ratio has to be as great as 50 percent at high altitudes, as experimental data demand, we must have $1-\beta^2$ not much less than 0.5.

Now the value of $1-\beta^2$ which evolves from the foregoing latitude considerations, and appropriate to the mesotrons from protons as primaries is 0.028. Such a value for the mesotrons would result in inappreciable horizontal electron intensity. If, however, we consider singly charged helium atoms as primaries, the value of $1-\beta^2$ for the minimum energy of entry at latitude 40° is 0.45. Such a value of $1-\beta^2$ can provide, therefore, for an appreciable horizontal intensity in the resulting electrons. The inference is, therefore, that there may be two types of primaries—protons which are responsible for the generation of the mesotrons observable at sea level and at semi-high altitudes, and in addition, heavier particles, possibly singly ionized helium atoms which, through their offspring electrons, result in the special features pertinent to the broad intensity-zenith angle curves for high altitudes.

I wish to thank Mr. Paul Weisz for his discriminating computation of the data in this paper.

[5] W. F. G. Swann, Rev. Mod. Phys. **11**, 242 (1939); Phys. Rev. **59**, 770 (1941).

Letters to the Editor

PROMPT publication of brief reports of important discoveries in physics may be secured by addressing them to this department. The closing date for this department is the third of the month. Because of the late closing date for the section no proof can be shown to authors. The Board of Editors does not hold itself responsible for the opinions expressed by the correspondents. Communications should not in general exceed 600 words in length.

The Probable Accuracy of the General Physical Constants

FRANK BENFORD
Research Laboratory, General Electric Company, Schenectady, New York
December 7, 1942

THE general constants used in chemistry and physics are a closely knit group. Physical equations, derived from theory, connect most of these constants in numerous ways and hence there are different ways of mathematically deriving and experimentally determining some of the more fundamental constants. These various values have been closely studied for accuracy and the published lists of the weighted averages of these constants usually have attached to each constant a value for the assumed probable error. To illustrate, the 1929 value assigned to c, the velocity of light, was:

$$c = (2.99796 \pm 0.00004)10^{10} \text{ cm sec.}^{-1}.$$

From these limits it is to be assumed that a determination of c made with equal equipment and competence would have a 50-50 chance of giving a value between 2.99792 and 2.99800 for the significant figures. The latest published value[1] however, is $(2.99776 \pm 0.00004)10^{10}$ and here the departure from the previous value is 0.00020 or 5 times the original probable error. Consulting a table of probability functions one finds that the odds against this deviation, considered as a random event, is 1341 to 1. But this new value of c is based on too much data to be considered as a single event, and certainly the forethought and care that go into a determination of the speed entitle it to a better adjective than random; therefore, it might be expected to be in better agreement. It thus becomes apparent that the assigned probable limits do not apply to the absolute accuracy of c, but only to its accuracy as judged by internal evidence of the experiments. If there are systematic errors of conception or execution the whole group will be shifted away from the true value without increasing the apparent probable error. The given probable error then is no longer a real measure of accuracy, but is reduced to being an indicator of the consistency of the data that went into the computation of the assigned value. The distinction between consistency and accuracy is important, and it should not be overlooked.

The writer has been working in radiation and using the radiation constants c_1 and c_2 and also Wien's displacement constant A and the Stefan-Boltzmann constant σ. It is these particular constants that have suffered the greatest proportional change in Dr. Birge's latest summary, as is illustrated in Table I. Here only significant figures have been retained, the various appended values of 10^n and the zeros preceding the probable errors being dropped for better readability. The selection of constants was intended to cover those of personal interest and a few of the more important fundamental ones.

The main contributing factor to the changes between the 1929 and 1941 list is the new value assigned to the electronic charge. In 1929 it was 4.7700 ± 50 and in 1941 it was 4.8025 ± 10, a difference of 325 as compared to the probable error of 50. The change is 6.5 times as great as the probable error, and the chances against such a change are 100,000 to 1, on the basis of the 1929 figures. It is here again evident that the assigned limits refer to the consistency of the data from which 4.7700 ± 50 was derived, and the present value would, in 1929, have seemed impossible from the internal evidence.

One possible criterion of the accuracy of the constants would be to note in successive lists the number of the new values that fall within the preceding limits. If half are within and half without then the limits are becoming true indicators of accuracy, and the truth is being approached by steps similar to the sum of the series $\frac{1}{2}+\frac{1}{4}+\frac{1}{8}+\cdots$ which after an infinite number of terms (lists) will approach 1, the symbol of perfection.

TABLE I. Probable values of the general physical constants (from Birge).

		1929		1941		Change / 1929 P.E.	Chance 1 to
Velocity of light	c	2.99796	±4	2.99776	±4	5.0	$1.3 \cdot 10^6$
Gravitational constant	G	6.664	2	6.670	5	3.0	$2.0 \cdot 10^3$
Volume of ideal gas	V_0	22.4141	8	22.4146	6	0.6	<1
International ohm	P	1.00051	2	1.00048	2	1.5	$2.0 \cdot 10^2$
Ice point	T_0	273.18	3	273.16	1	0.7	<1
Joule eq. (mech.)	J_{15}	4.1852	6	4.1855	4	0.5	<1
Joule eq. (elec.)	J_{15}'	4.1835	7	4.1847	3	1.7	$3.0 \cdot 10^2$
Faraday constant (chem.)	F	96.494	5	96.501	10	1.4	$2.0 \cdot 10^2$
Faraday constant (phys.)	F	96.489	7	96.514	10	3.6	$6.5 \cdot 10^4$
Electronic charge	e'	4.7700	50	4.8025	10	6.5	$1.0 \cdot 10^{11}$
Spec. E.C. (spectroscopic)	e/m	1.7610	10	1.7592	5	1.8	$3.0 \cdot 10^2$
Spec. E.C. (deflection)	e/m	5.3034	60	5.2736	15	5.0	$1.3 \cdot 10^6$
Planck constant	h	6.5470	80	6.6242	24	9.6	$1.0 \cdot 10^{20}$
Ratio *es* to *em* units	c'	2.99790	10	2.99776	4	1.4	$2.0 \cdot 10^2$
Rydberg constant	R_H	109677.758	50	109677.581	7	3.5	$5.4 \cdot 10^4$
Avogadro's number	N_0	6.0644	60	6.0228	11	7.0	$4.0 \cdot 10^9$
Boltzmann constant	K	1.37089	140	1.38047	26	6.8	$1.0 \cdot 10^9$
Stefan-Boltzmann	σ	5.7139	60	5.6728	37	6.9	$1.0 \cdot 10^9$
Wien's displacement	A	2.8836	11	2.8972	7	12.4	$1.0 \cdot 10^{33}$
First radiation const.	c_1	4.9330	60	4.9907	—	9.6	$1.0 \cdot 10^{20}$
Second radiation const.	c_2	1.43170	60	1.43848	34	11.3	$1.0 \cdot 10^{34}$

The debt of chemists and physicists to Dr. Birge is great, and I hope that he will, in future lists, increase this indebtedness by pointing out the distinction between consistency and accuracy.

[1] Raymond T. Birge, Rev. Mod. Phys. 13, 233 (1941).

Comments on "The Probable Accuracy of the General Physical Constants"

RAYMOND T. BIRGE
Department of Physics, University of California, Berkeley, California
February 17, 1943

IN the preceding paper by Dr. Frank Benford, attention is called to the important distinction between consistency and accuracy. The recent large and wholly unanticipated changes in the measured values of many of the general physical constants have been noted and discussed in numerous papers and it would be superfluous to make further comments, were it not for the fact that Dr. Benford's paper concludes with the remark, "I hope he will, in future lists, increase this indebtedness by pointing out the distinction between consistency and accuracy."

For many years now I have attempted to emphasize just this distinction. Unfortunately the true value of any physical magnitude can never be known. Hence the absolute accuracy of a measured result cannot be determined and we can only note the difference, if any, between the *internal* and *external* consistency of the data. In 1932 I initiated a discussion[1] of these two important concepts and noted certain relations and facts that had hitherto been generally overlooked.

Previous to the time that I began publishing critical values of the general physical constants, it was rather exceptional to attach a probable error, or other measure of reliability, to suggested "most probable" values. It seemed to me, however, desirable to attempt such an estimate, even in cases where the estimate was admittedly almost a pure guess. On the other hand, as I have noted,[2] F. W. Clarke, whose calculated atomic weight values were considered authoritative, prior to the formation of national and international committees on the subject, regularly published probable errors. Unfortunately he ignored all discrepancies between internal and external consistency and as a result adopted a system of weighting that seems quite unjustified and misleading.

The table published by Dr. Benford shows that the average change of value, between 1929 and 1941, is some five times the 1929 published probable error. But in Clarke's work on atomic weights, I found that the probable error based on external consistency averaged fully *ten* times that based on internal consistency and in at least one case was *one hundred* times as large. In other words, atomic weight determinations prior to 1920 were afflicted with unknown and unsuspected systematic errors that averaged fully ten times the assumed experimental errors.

It is unfortunate that even the most carefully conducted precision work on physical constants seems, with rare exceptions, to contain errors considerably larger than any suspected by the experimenters themselves. No one has better reason to realize and to regret this fact than the present writer. I cannot, however, refrain from pointing out that I have always tried, in my estimates of probable error, to make allowance for systematic errors, and have also more than once noted and made correction for errors overlooked by the original authors. As a result of the diversity of methods now used in determining most of the general constants, and of the greater attention being paid to the question of systematic errors, I feel that the values and probable errors of the 1941 list can be accepted with considerably greater confidence than in the case of any earlier list. One may hope that never again will it be necessary to base an adopted value of an important constant on the results of a single method, carried out chiefly by a single experimenter.

[1] R. T. Birge, Phys. Rev. **40**, 207 (1932). See pp. 213–223. Further pertinent material on the general subject matter of this note appears on pp. 122–123 of the paper by W. E. Deming and R. T. Birge, Rev. Mod. Phys. **6**, 119 (1934), and in the Introduction (pp. 1–8) of my 1929 paper on the general constants, Rev. Mod. Phys. **1**, 1 (1929). My detailed discussion of the 1941 list of constants appears in *Reports on Progress in Physics* **8**, 90–134 (1941).
[2] Page 221 of first reference of footnote 1.

Cosmic-Ray Stars at 10,000 Feet

WAYNE E. HAZEN
University of California, Berkeley, California
February 23, 1943

A PRELIMINARY survey of the stars observed in a cylindrical cloud chamber (30×30 cm) at Tioga Pass, Yosemite National Park, has been completed. The chamber contained eight 0.7-cm lead plates separated by 2.5-cm air spaces. Out of 9100 expansions, none of which was counter controlled, approximately 8500 useful photographs were obtained.

A total of 58 stars were observed, two of which originated in the gas and the others in the lead plates. The number of penetrating particles that occurred in the same volume and about the same time was 19,000. At 14,000 ft. with similar apparatus Powell[1] observed 156 stars and 9840 penetrating particles. A direct comparison indicates a de-

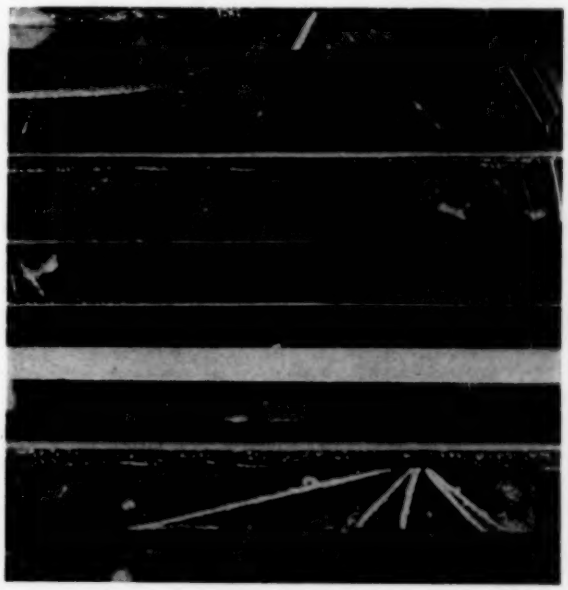

FIG. 1. Photographs of stars that occurred slightly before the chamber expansion. The star in the upper photograph contains both long and short range particles while the one in the lower photograph contains only short range particles.

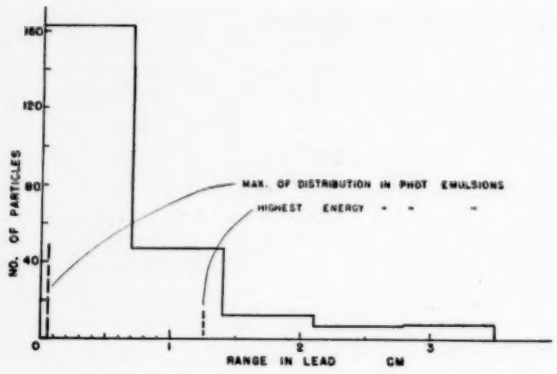

FIG. 2. Range distribution of the particles that occurred in 58 star showers at 10,000 ft.

crease in the relative abundance of stars by a factor of five in going from 14,000 feet down to 10,000 feet, whereas the soft component decreases by only a factor of two. It is entirely possible, however, that the conditions of observation were sufficiently different in the two cases so that the factor for decrease in relative abundance of stars might also be nearer two.

Thirty-one of the stars contained only particles with range less than 0.7 cm of lead and consisted of 3.3 particles on the average. Only one or two of these stars appeared to be initiated by an ionizing ray and none of them was associated with cascade showers. The remaining twenty-seven stars contained particles with range greater than 0.7 cm of lead in addition to shorter range particles and consisted of 5.1 particles on the average. Eight of this latter group of stars apparently were initiated by ionizing rays but again none of them was associated with cascade processes. Photographs of typical stars are reproduced in Fig. 1.

The only previously reported data on the range distribution of star particles have been obtained from tracks in photographic emulsions.[2] In Fig. 2 the range distribution of particles from the present observations is compared with the results of Widhalm's observations with photographic emulsions. Most, if not all, of the long range particles observed with the cloud-chamber technique could not be detected in photographic emulsions for two reasons: First, since the ionization of the long-range particles was not much greater than the minimum, they probably could not be observed in the emulsion, and secondly, most of them would pass out of the emulsion before coming to rest. The last four blocks in the diagram of Fig. 2 should be increased by factors of about 1.3, 2, 3, and 4, respectively, in order to take into account the decreasing solid angle subtended by the final plate as we proceed away from the star's origin. When this correction is included we find that nearly half of all the star particles have ranges exceeding 0.7 cm of lead.

The number of star particles that might be interpreted as electrons is extremely small, certainly less than ten for all particles and less than five for particles of range greater than 0.7 cm of lead, while the number of particles in the latter group that are most likely to be electrons is even smaller. The infrequency of occurrence of particles in stars that are most likely to have been electrons is in essential agreement with the few previous observations of star showers employing a technique capable of ascertaining the nature of the particles. The present evidence indicates that most of the stars are probably initiated by neutrons, the others by penetrating rays (mesotrons or protons).

The above work was made possible through the helpfulness of F. A. Kittredge, Superintendent of Yosemite National Park.

[1] W. M. Powell, Phys. Rev. **61**, 670 (1942).
[2] A. Widhalm, Zeits. f. Physik **115**, 481 (1940).

Proceedings of the American Physical Society

"Annual Meeting of 1942," New York, January 22–23, 1943

THE "Annual Meeting of 1942," postponed from December, 1942 because of the congestion of trains expected to prevail during the holiday season, was held at Columbia University in New York City on January 22–23, 1943. The American Association of Physics Teachers (AAPT) and the American Society for X-Ray and Electron Diffraction (ASXRED), having postponed their meetings as we did ours, met on the same days and shared in some of our meetings, extending to us a reciprocal hospitality. Notwithstanding the sudden and belated change to a time normally regarded as much less favorable, the meeting was surprisingly and delightfully successful, ranking in size of attendance with the best winter meetings of the past. Nearly three hundred of our members registered, and another hundred who were members of the AAPT or the ASXRED or simply guests. The joint dinner of the three societies was attended by nearly two hundred. Excellent arrangements were made by H. W. Webb as Chairman of the Local Committee.

The special features of the meetings, attended by all three societies, comprised the Retiring Presidential Address of President P. W. Bridgman of the Physical Society; the presentation of the Oersted Medal of the AAPT to G. W. Stewart, the response of Mr. Stewart, and the Richtmyer Memorial Lecture delivered by G. F. Hull, Sr.; and an address by P. Debye, arranged by the ASXRED, on the topic "Recent Developments in X-Ray and Electron Diffraction." Forty-three ten-minute papers were contributed, of which the abstracts are appended (five of them coming by way of the ASXRED); those numbered 5, 18, 39, 40, 41, 42, and 43 were read by title.

At the Business Meeting of the Society, short reports were made by or in the name of the Secretary (who gave the present membership of the Society as 4112, comprising 917 Fellows and 4 Honorary Members); the Treasurer (whose full report will soon be sent to the membership); and the Acting Editor (who said that it is planned to continue issuing one number per month of the Physical Review for the present). The Secretary also announced that the membership list to be issued in 1943 will be confined to the names of members elected since the last previous list was issued. The Tellers of the recent election (R. T. Cox and F. C. Nix) reported through Mr. Cox the election of the following officers: *President*, A. W. Hull; *Vice President*, A. J. Dempster; *Secretary*, K. K. Darrow; *Treasurer*, G. B. Pegram; *Members of the Council:* R. B. Lindsay, Alpheus W. Smith; *Members of the Board of Editors:* M. Phillips, B. Rossi, W. H. Zachariasen. These entered upon their terms at the end of the meeting.

The Council met on Thursday evening, January 21, and again on Saturday evening. Two Members were advanced to Fellowship; two candidates not previously Members were elected to Fellowship; 60 candidates were elected to Membership. The names of all these are appended. The Council appointed G. B. Pegram to succeed himself as Member of the Governing Board of the American Institute of Physics.

A Joint Resolution originating from the American Institute of Physics was submitted to the Business Meeting of the Society by the Council thereof, and to the corresponding meeting of the AAPT by the authorities thereof, and passed by both Societies. The text of this resolution is appended. It has since been transmitted to the officials named in its text and to many others.

The Society has lost through death the following Fellows and Members: H. G. Beutler of the University of Chicago, noted in spectroscopy; C. A. Hall of the Electrical Storage Battery Company in Philadelphia; James E. Ives formerly of the U. S. Public Health Service; G. B. Karelitz of Columbia University.

Members advanced to Fellowship: Arthur Adel, Frank Morgan.

Other candidates elected to Fellowship: Pierre Auger, S. Chandrasekhar.

Candidates elected to Membership: James Henry

Awbery, Arnold M. Bass, J. G. Bennett, Seymour Benzer, Daniel Bershader, William H. Billhartz, John Markus Blatt, Lyle B. Borst, Robert Stephen Burpo, Jr., Owen Chamberlain, Rev. Ernest Clarke, Alden P. Cleaves, Howard S. Coleman, Norman Davids, Pauline V. Davidson, James J. Donoghue, Bernard Epstein, Herman Theodore Epstein, Vincent Fitzgerald, Elizabeth F. Focht, Edward M. Fryer, Donald N. Gideon, Gerhart Groetzinger, Harold Palmer Hanson, Rudolph G. E. Hutter, J. Wesley Kemp, Capt. Paul J. Kopp, Louis W. Labaw, Robert W. Leonard, John Holton McGinn, Arthur E. Middleton, Elliott W. Montroll, Thomas M. Moore, Herbert C. Muether, Raymond L. Murray, Edward J. Nagy, J. Burton Nichols, Newton Hays Odell, William Elwood Ogle, H. Lowell Olsen, Francis Perrin, Fritz Pordes, H. Eugene Powell, Paul P. Reichertz, Dale W. Rinehart, Salomon Rosenblum, H. Gunther Rudenberg, Noel W. Scott, Gerald Lionel Simard, William Warner Sleator, Jr., John B. Smyth, A. O. Stanesby, Richard G. Stephenson, Rodolphus A. Swan, Jr., Vernon Thornton, Charles B. Vance, George Warfield, Richard Nicholas Work, Kenneth P. Yates, Ignace Zlotowski.

Joint resolution of the American Physical Society and the American Association of Physics Teachers:

WHEREAS the Army and Navy College Training Programs as so far announced provide for the training of technical personnel for use almost solely, if not entirely, within the Armed Forces, and

WHEREAS other war agencies, whose effective functioning is essential to the support of the Armed Forces in expediting the prosecution of the war, also need technically trained personnel in large numbers, and

WHEREAS these other war agencies, such as war industry, war research, and war training staffs are now confronted with the closing off of the usual avenues of supply of technically trained personnel from the same groups now being drawn upon through induction and enlistment.

THEREFORE BE IT RESOLVED that the American Physical Society and the American Association of Physics Teachers in joint session in New York City on January 23, 1943, urge that effective steps be taken at the earliest possible date to provide an over-all War Training Program to meet *all* of the needs of the Army, of the Navy, of War industry, and of war research in scientific and technological fields.

That in such a program adequate provision be made to insure such a flow, of personnel trained in the field of physics into war research, into war industry, and into training staffs, as will be necessary to prevent serious impairment of the critical war services to be rendered by these agencies. That copies of these resolutions be sent to the Chairman of the War Manpower Commission, to the Secretary of War, to the Secretary of the Navy, to the Chairman of the War Production Board, to the Director of the Office of Scientific Research and Development and the Chairman of the National Defense Research Committee.

KARL K. DARROW, *Secretary,*
American Physical Society
Columbia University, New York, New York

ABSTRACTS OF CONTRIBUTED PAPERS

1. Decomposition of Matter Through the Magnet (Magnetolysis). FELIX EHRENHAFT.—I have stated already that microscopic bodies, especially of ferromagnetic elements, do move in homogeneous magnetic fields, reversing their direction with the reversal of the field. In the spirit of M. Faraday and J. C. Maxwell one must therefore conclude that these test bodies carry an excess of north- or south-magnetic charge and consequently have to be called magnetic ions. Therefore we have to establish the equation; Div $B \gtrless 0$. A consequence of these facts is the phenomenon of magnetophoresis already published.* Lately I have discovered that the magnet causes chemical composition and decomposition of matter in several cases. The quantity of gas, originated in certain chemical processes occuring between the magnetrodes and the magnetolyte (e.g., acidulated water) is considerably increased by the application of the magnetic field. The gas created is a mixture of hydrogen and oxygen. Herewith is proved that the poles of a magnet break up water through magnetolysis, the same as electric poles break up water by electrolysis. Now the way is open to measure the intensity of the magnetic current.

It should be mentioned that the same electric potential of the magnetrodes is secured, be it by using one piece of metal for the magnet, or two pieces which are metallically connected.

* Science **94**, 232 (1941): **96**, 228 (1942); Phys. Rev. **61**, 733 (1942).

2. The Effect of Oblique Incidence on the Conditions for Single Scattering of Electrons by Thin Foils. GERALD GOERTZEL AND R. T. COX, *New York University.*—In setting up and applying criteria for the single scattering of electrons by thin foils, it has been usual to assume that the principal deviations from single scattering are caused by the combination of small deflections with one large one. It is here shown that with electrons obliquely incident on

the foil much more serious deviations may be caused by the combination of two deflections of the same order of magnitude. It is concluded that the difference observed by Chase and Cox[1] between the scattering at 90° to the two sides of a foil on which electrons are incident at 45° may be ascribed to this cause. The bearing of this factor on the negative result of Dymond's[2] experiment on the polarization of electrons is also considered.

[1] Chase and Cox, Phys. Rev. **58**, 243 (1940).
[2] Dymond, Proc. Roy. Soc. **A145**, 657 (1934).

3. The Small Angle Scattering of Electrons by Aluminum. BOWEN C. DEES AND BERNARD HAMERMESH, *New York University.*—The angular distribution of scattering of 46 kv electrons scattered by an aluminum foil of $1.3 \cdot 10^{-5}$ cm thickness has been studied in the angular range between 0° and 10°. The mean projected angle of scattering was determined experimentally for the cases of normal and 45° incidence, and the resulting experimental values were compared with the values predicted by a theoretical treatment given by Goudsmit and Saunderson.[1] Agreement with theory was found in each case. Attempted comparison with the theoretical treatment given by Williams[2] led to results which showed that his treatment was inapplicable to the circumstances of this experiment, and forced the conclusion that the scattering observed in this experiment was multiple for a very small angular range at most. Finally, investigation showed that the scattering found did not approach single scattering even at the largest angles of observation, and led to the conclusion that the observed scattering was mainly plural.

[1] Goudsmit and Saunderson, Phys. Rev. **57**, 24 (1940); **58**, 36 (1940).
[2] E. J. Williams, Proc. Roy. Soc. **169A**, 531 (1939); Phys. Rev. **58**, 292 (1940).

4. Motion of the Copper Arc in Transverse Magnetic Field. CHARLES G. SMITH,* *Raytheon Mfg. Co.*—An arc between equal parallel rings of copper is subjected to a transverse radial magnetic field. With lower ring as cathode and south pole at center, the arc viewed from above rotates counter-clockwise at atmospheric pressure, but below a critical pressure it rotates clockwise. The pressure for reversal varies approximately inversely as the distance between rings. Critical air pressures ranging from 36 to 3 cm were observed. The peculiar clockwise rotation results from the thermomotive force or Righi-Leduc factor operative in the solid cathode, according to one emission theory[1] of the mobile arc cathode. Mass movement of ionized gas caused by electromagnetic force tends to drive the arc around counter-clockwise. This tendency becomes less at reduced pressure since viscosity factors increase due to spreading of the arc column. Below the critical pressure, phenomena in the solid cathode predominate. The observations apparently extend the emission theory to include the copper arc over a wide range of pressure.

* Experiments performed at Harvard University.
[1] C. G. Smith, Phys. Rev. **62**, 48 (1942).

5. The Adsorption of Thorium on Tantalum. CHARLES J. GALLAGHER, *University of Notre Dame.*—It is known that thorium adsorbed on the surface of tungsten or molybdenum results in a decrease in the work function and also a decrease in the value of A, the emission constant.[1] The behavior of thorium on tantalum was investigated and similar effects were noted. Thorium was evaporated from thoriated tungsten onto a well-outgassed tantalum ribbon and the thermionic emission at 1390K studied as a function of the time of evaporation. The work function of the tantalum changed from 4.07 volts to 2.52 volts, while A decreased by a factor of thirty. The ribbon was then held at 1550K and the emission from the two sides studied separately. The emission from the activated side decreased, while that of the clean side increased until both reached the same final level after about twenty hours. This indicates that the adsorbed thorium had migrated around the edges of the ribbon and distributed itself uniformly over the emitting surface.

[1] A. L. Reimann, *Thermionic Emission* (John Wiley and Sons, New York, 1934) pp. 99, 134.

6. The Action of Oxygen, Nitrogen and Hydrogen in Lowering the Photoelectric Work Function of Zirconium, Titanium and Thorium. H. C. RENTSCHLER AND D. E. HENRY, *Westinghouse Lamp Division.*—Pure wire surfaces of zirconium, titanium and thorium were made by thermal decomposition of the iodides. Photoelectric surfaces of the pure metals were prepared by the method previously described[1] and the work functions of these metals were determined from the photoelectric threshold wave-lengths. Zirconium and titanium when heated in pure oxygen, nitrogen or hydrogen dissolve considerable amounts of these gases. The photoelectric work functions of surfaces similarly prepared from the metals with the dissolved gases were found to be appreciably lower than for the corresponding pure metals and the photoelectric response from such surfaces is as constant as that from the pure metal. Thorium reacts with these same gases to a lesser extent and the shift in the photoelectric response is similar to that for zirconium and titanium.

[1] Rev. Sci. Inst. **3**, 794 (1932).

7. The Photoconductance of Evaporated Bismuth Films. A. H. WEBER AND L. M. FRIEDERICH, S. J., *St. Louis University.*—Observations were made of the dark conductance and photoconductance* of films deposited on Pyrex in high vacuum, continuously and discontinuously, both at room temperature and at liquid-air temperature. A photoconductance effect, observed in all the films deposited, disappeared in every instance at a critical thickness, 11 to 292 atom layers depending on the conditions of deposition. Films deposited continuously, both at room temperature and at liquid-air temperature, attained a greater respective thickness (2 to 3 times) before the photoconductance effect disappeared than did those deposited discontinuously. Films deposited at room temperature lost the photoconductance effect at a much greater film thickness (8 to 15 times) than did those deposited at liquid-air temperature. A film no longer exhibiting photoconductance at liquid-air temperature, when allowed to warm to room temperature, again showed a photoconductance effect. These observations lead to the conclusion that bismuth films exhibiting

the photoconductance effects have a patch structure and that the increased electrical conductance when illuminated is not *true* photoconductance, but photoelectric emission from patch to patch.

* Defined as the electrical conductance of the films when illuminated.

8. The Compensation of Random Fluctuations in a D.C. Bridge Amplifier. J. C. M. BRENTANO AND E. R. SCHLEIGER, *Northwestern University.*—In measuring small potential differences or currents it is sometimes necessary to use d.c. amplification. Instances are the measurement of weak ionization currents or photoelectric phenomena involving delay actions where a.c. amplification cannot readily be adopted. A compensated symmetrical bridge using two thermionic tubes has the advantage over single tube circuits that it is easy to control; with it all disturbances and fluctuations can be eliminated very effectively, except fluctuations due to random changes of filament emission which actually set the limit to the ultimate amplification attainable. In a bridge* comprising two vacuum tubes, essentially of tetrode type, the intermediate grids acting as control grids, compensation for such fluctuations can be obtained by a system of cross connections between the inner grids and plates by which an emission fluctuation of one filament produces similar changes in the symmetrical halves of the bridge. The unsteadiness level can thus be reduced by a factor of thirty.

* Brit. Pat. 526869.

9. Graphical Treatment of Non-Linear Circuits. P. I. WOLD, *Union College.*—With the increase in the use of circuits containing non-linear elements, it becomes important to make calculations as to the behavior of any such circuit. Most non-linear elements have a volt-ampere characteristic which can be given by an infinite series only. The analytical treatment, therefore, becomes excessively burdensome unless all but a very limited number of terms of the series are neglected. This involves strong approximations. Graphical methods of treatment will be presented which avoid approximations and permit the ready plotting of the current characteristics of any branch in simple networks.

10. The Ionization Cross Section of the Silver L_{III} State. J. J. G. MCCUE,* *Cornell University.*—The cross section of silver atoms for excitation to the L_{III} state by cathode rays has been measured in arbitrary units as a function of cathode-ray energy, by using the thin target technique originated by Webster. The cathode-ray energies covered the range $1.5 \leqq U \leqq 9$, where U = (cathode-ray energy)/(excitation energy). The cross section was determined from the $L\alpha$ doublet intensity, measured as a function of tube voltage and corrected for the effects of diffusion, rediffusion, retardation and fluorescence. The values of cross section computed by Burhop[1] by using the Born approximation and hydrogenic wave functions, vary in approximate agreement with the experimental results; the agreement however is not within the estimated experimental uncertainty of 3 percent. Comparison of the present results with those of Webster and his colleagues for the K state establishes that for both the K and the L_{III} states of silver, the ionization cross section is a maximum when U is about 3.5, and that for $U > 3.5$ the decrease in ionization cross section with increasing cathode-ray energy is more rapid for the L_{III} state than for the K state.

* Introduced by L. G. Parratt.
[1] Burhop, Proc. Camb. Phil. Soc. **36**, 43 (1940).

11. Fine Structure in the X-Ray Absorption Edges of Potassium Chloride. J. W. TRISCHKA, *Cornell University.*—Variations in the absorption coefficient in the regions of the K edges of the potassium and chlorine in potassium chloride have been measured with a two-crystal vacuum x-ray spectrometer. The region studied extended from ten volts less than the energy of the first absorption line to forty volts greater. Absorbers were prepared by evaporation of the potassium chloride onto thin kodapak films. The lower limit of detectable variations in the absorption coefficients of the potassium and chlorine was three percent. Results were not corrected for the resolving power of the spectrometer. Using Sb $L\alpha_1$ and Pd $L\alpha_1$ as reference lines, the wave-lengths of the peaks of the first absorption lines were measured to be 3425.5 Siegbahn X.U. and 4378.8 Siegbahn X.U. for potassium and chlorine, respectively. The separation of the first two maxima in the chlorine edge was measured to be 3.9 volts as compared with the theoretical 4.2 volts calculated by Landshof[1] on the assumption that the maxima correspond to excitation states in the solid.

[1] R. Landshof, Phys. Rev. **55**, 631 (1939).

12. An Error Arising from the Use of Small Carbon-Lined Ionization Chambers in the Measurement of Low Voltage X-Rays in Roentgens. EDITH H. QUIMBY AND ELIZABETH F. FOCHT, *Memorial Hospital.*—With 44-kv x-rays, small ionization chambers of lucite lined with Aquadag give lower values for ionization per cc than open air chambers. In a parallel plate chamber of the lucite-Aquadag type, with electrodes perpendicular to the x-ray beam, ionization per cc increases steadily with electrode separation from 0.2 mm to 2.0 mm; after that, the *increment* of ionization per unit increase in volume is constant. The effect is attributable to the difference in the photoelectrons emitted by the carbon-coated electrodes, and by the air between the electrodes. When one electrode is made of aluminum the effect is reversed, the ionization per cc decreasing from 0.2 to 2.0 mm spacing. Theoretically, the ratio between the readings in carbon and aluminum chambers of this type, with very small spacing, can be calculated on the basis of Kramer's formula, the accepted formulae for ${}_{a}\tau$ and ${}_{a}\sigma_{a}$, and published absorption data. The ratio thus obtained is in satisfactory agreement with the experimental results. It is concluded that, for the measurement of x-rays in the voltage range in which photoelectric absorption is important, small carbon-lined ionization chambers do not satisfy the requirements imposed by the definition of the roentgen.

13. Electromagnetic Method for the Determination of Velocity Distribution in Fluid Flow. ALEXANDER KOLIN, *Columbia University.*—A method has been developed which

utilizes the principle of electromagnetic induction for determining the velocity distribution in a liquid. An homogeneous magnetic field is maintained at right angles to the direction of fluid flow. A potential gradient is established in the liquid by induction. Its magnitude at any given point is: $d\mathbf{E}/dz=\mu\mathbf{H}\times\mathbf{v}$. The local instantaneous velocity component in a direction perpendicular to the magnetic field and to the Z axis is determined by measuring dE at a given point. This is accomplished by introducing a probe consisting of two fine wires, insulated except at the tip (dz, the separation of the wire tips, is in the order of a few thousandths of an inch). The induced e.m.f. picked up by the probe is amplified and photographically recorded. The probe can be placed at any point where the instantaneous local velocity is to be measured. Since the method has no lag, it furnishes the velocity distribution in time as well as in space. To avoid difficulties due to polarization, an alternating magnetic field is utilized. This work was sponsored by the Department of Civil Engineering, and the author wishes to thank Professor B. A. Bakhmeteff for guidance and suggestions, and Professor J. K. Finch for his interest and generous support.

14. Molecular Absorption of Vibration. C. W. CHAMBERLAIN, *Michigan State College.*—The solution of vibration problems by means of springs is complicated by limitations introduced by resonance, load carrying capacity, stability, and dampening factor. Springs constructed of organic materials like rubber in shear, sponge rubber, cork, and highly compressed felt obey, to a greater or less degree, the same law as springs made of metal. A gas-filled cylinder with movable piston obeys the gas law and possesses high load carrying capacity. Its dampening factor, due to the fact that cooling of the gas on expansion is less than the heating on compression, is small. It has been found feasible to construct a series of gas-filled cylinders so short that the low heat conductivity of the confined gas introduces no limitation. Work done on the confined gas by the moving piston is directly transmitted to the cylinder base and rapidly disposed of by conduction. In operation although the initial temperature of the gas is high the temperature of the assembly of cylinders is comparatively low. Highly efficient absorption cushions composed of 100 cylinders in series and only $\frac{1}{4}$ inch thick have been successfully installed under machines varying in weight from a few pounds to 500 tons.

15. On the Excitation Functions of Proton-Induced Reactions in Lithium. E. D. COURANT, *University of Rochester.*—Evidence for the hypothesis that the ground state of $_3Li^7$ is odd has been obtained by comparing the experimental excitation functions of the reactions $_3Li^7(p,\gamma)_4Be^8$ [1] and $_3Li^7(p,2\alpha)$ [2] to the computed penetration probabilities for protons of angular momentum 0 and 1. If $_3Li^7$ is odd, the γ-reaction is produced by protons of even angular momentum and the α-reaction by protons of odd angular momentum, and vice versa. When the effect of the Coulomb potential barrier is eliminated by dividing the observed excitation functions by the penetration factor, the result corresponds to theoretical expectations only when the α-excitation function is associated with the penetrability for $l=1$, and the γ function with $l=0$, and not the other way around, leading to the conclusion that the ground state of $_3Li^7$ is odd. The penetrability has been taken to be proportional to $1/G^2\rho$ in the notation of Yost, Wheeler, and Breit.[3]

[1] Gentner, Zeits. f. Physik **107**, 354 (1937); Curran and Strothers, Proc. Roy. Soc. **A172**, 72 (1939).
[2] Haworth and King, Phys. Rev. **54**, 38 (1938); Rumbaugh, Roberts, and Hafstad, Phys. Rev. **54**, 657 (1938).
[3] Yost, Wheeler, and Breit, Terr. Mag. Atmos. Elec. **40**, 443 (1935).

16. The Isotopes of Cerium and Rhodium. ARNOLD A. COHEN,* *University of Minnesota.*—An analysis of the isotopes of cerium and rhodium has been made with a mass spectrometer in which ion currents are detected by an electron multiplier of the type described by Allen.[1] Dempster's[2] discovery of Ce^{136} and Ce^{138} was confirmed, and the abundance of these relative to Ce^{140} measured as 1/500 and 1/400, respectively. No isotopes other than the four known ones were found, but the following upper limits of abundance relative to Ce^{140} were set: Ce^{134}, Ce^{135}, 1/20,000; Ce^{137}, 1/10,000; Ce^{139}, 1/1000; Ce^{141}, 1/1500; Ce^{142}, Ce^{144}, Ce^{145}, Ce^{146}, 1/25,000. Rhodium was studied in an attempt to verify the existence of Rh^{101}, reported by Sampson and Bleakney[3] as being present to 1/1300 of Rh^{103}. Although 1/30,000 of Rh^{103} could have been detected, no Rh^{101} peak was found. Other upper limits relative to Rh^{103} were determined as follows: Rh^{105}, 1/60,000; Rh^{104}, 1/6000; Rh^{102}, 1/5000. Columbium was also investigated, but a zirconium impurity prevented a search for Cb^{91}. An upper limit for Cb^{95} was set at 1/4000 of Cb^{93}.

* Present address: RCA Manufacturing Co., Harrison, New Jersey.
[1] J. S. Allen, Phys. Rev. **55**, 966 (1939).
[2] A. J. Dempster, Phys. Rev. **49**, 947 (1936).
[3] M. B. Sampson and W. Bleakney, Phys. Rev. **50**, 732 (1936).

17. Disintegration Scheme of Co^{55}. L. G. ELLIOTT AND M. DEUTSCH, *Massachusetts Institute of Technology.*—Radioactive cobalt was separated from a nickel target which had been exposed to fast neutrons from the M.I.T. cyclotron. Examination of this source in the gamma-ray spectrometer[1] shows that it emits a gamma-ray of 0.810 $\pm$0.015 Mev. No other gamma-rays were observed. The beta-ray spectrometer shows that it emits positrons with a maximum energy of 0.470$\pm$0.015 Mev. A counter sensitive to iron x-rays shows that a number of the disintegrations are by K capture. The number of observed coincidences between beta- and gamma-rays and a knowledge of the efficiency curve for the gamma-ray counter used show that each positron is on the average accompanied by one 0.810 Mev gamma-ray. Observation of coincidences between the x-rays and gamma-rays show that at least 80 percent of the disintegrations by K capture are also to the excited state 0.810 Mev above the ground state in the Fe^{55} nucleus.

[1] M. Deutsch and A. Roberts, Phys. Rev. **60**, 362 (1941).

18. The Mg II λ4481 Line in the Spectrum of Algol. F. T. ROGERS, JR., *The University of Houston.*—A rather simple equation has been found for the profile of the λ4481 line in the uneclipsed spectrum of Algol. It is a representa-

tion of data taken by Struve and Elvey[1] from seven spectrograms (10A per mm dispersion at λ4500), and was developed for a further analysis[2] for rotation by the method of Carroll.[3] If λ represents wave-length in cm, λ_0 being the proper wave-length of the line, then the measured absorption in percent is

$$i(x) = 25.8e^{-1.21x^2}, \quad (1)$$

where

$$x = |\lambda - \lambda_0| \times 10^8. \quad (2)$$

This representation differs from the actual data by an average deviation of 0.3 unit of absorption, which is only about one-third the A. D.'s of previous representations.

[1] O. Struve and C. T. Elvey, M. N. R. A. S. 91, 663 (1931).
[2] J. A. Carroll and Miss L. J. Ingram, M. N. R. A. S., 93, 508 (1933); also reference 1.
[3] J. A. Carroll, M. N. R. A. S., 93, 478 (1933).

19. Thermal Diffusion Experiments with Ammonia and Argon. W. W. WATSON AND D. WOERNLEY, *Yale University*.—Calculations from viscosity data indicated that even at 450°K the thermal diffusion constant α of NH_3 might be negative. In view of the nature of the intermolecular forces for NH_3, its critical temperature, and the known trend in R_T values with varying temperature (R_T = ratio of α to the value for hard spheres), it was thought that with decreasing temperature R_T for NH_3 might change from + to − at some available T. With a "two-bulb" experiment, and NH_3 of about 15 percent N^{15} content to increase the accuracy of the mass spectrometer analyses, which were made after converting to N_2, we have detected this effect. The shift from + to − values for α occurs, however, at about room temperature. At mean temperatures of 377°K, 285°K, and 247°K, α is +0.011, −0.004, and −0.009, respectively, indicating a rapid decrease in the repulsive force index and marked "softening" of the NH_3 molecule with decreasing T. With tank argon at 100 cm³/hr, two 3-meter hot-wire columns in series have been set into operation, the procedure being based upon the results of R. Simon. With the wires at 1100°K the separation factor is observed to increase at the average rate of 2.56 per day. After four weeks no decrease in this steady rate of rise has been noted.

20. Determination of Chlorine Vibrations in Dichlorobenzenes from Intensities and Polarizations of their Raman Lines. GERTRUD NORDHEIM AND H. SPONER, *Duke University*.—To facilitate the assignment of observed Raman lines of the dichlorobenzenes to motions in which mainly chlorine atoms are partaking, the intensities and polarization properties of these vibrations are studied theoretically. It is assumed that the change of polarizability in these vibrations is connected primarily with displacements of the chlorine atoms and that contributions from the individual atoms are additive. The Raman tensors belonging to the chlorine vibrations are then obtained by either adding or subtracting the single C−Cl contributions with reference to a chosen system of axes rigidly connected with the molecule. The following results were obtained: (1) *Valence vibrations*. The intensity ratio between the symmetrical and unsymmetrical vibrations is 8 : 1 (meta and ortho, the unsymmetrical vibration is forbidden in the para-spectrum). Lines representing symmetrical vibrations are highly polarized, lines representing unsymmetrical vibrations have the depolarization factor 6/7. (2) *Deformation vibrations*. Our simplified theory gives complete depolarization for all allowed deformation vibrations, i.e., for symmetrical and unsymmetrical ones and also in and out of the plane. Lines from planar symmetrical vibrations are three times stronger than from unsymmetrical ones. Similar relations hold for nonplanar vibrations. These results are discussed in connection with existing experimental data.

21. Transition Probabilities of the Asymmetric Rotor. PAUL C. CROSS, *Brown University* AND G. W. KING, *Arthur D. Little, Inc.*—The successive convergents of the continued fraction used in calculating the energy levels of the asymmetric-rotor are closely related to the elements of the transformation matrix expressing the asymmetric-rotor wave-functions as linear combinations of symmetric-rotor functions.[1] This transformation was evaluated and applied to the direction-cosine matrices for the symmetric rotor in order to determine the Einstein transition probabilities for rotors having various degrees of asymmetry. The values determined enable interpolation to be carried out with sufficient accuracy for any molecule. The change in intensity of a given transition with increasing asymmetry is most marked for levels of high or low τ-values, i.e., where the difference in the two limiting K values is highest. Strictly speaking, the intensities given apply only to the pure rotational spectrum of a rigid molecule. In electronic and vibrational transitions the moments of inertia are markedly changed, but the tables can be used to give a satisfactory picture of the rotational structure to be expected in any given case.

[1] G. W. King, R. M. Hainer and P. C. Cross, J. Chem. Phys. 11, 27 (1943).

22. Raman Spectra of Symmetrical Top Acetylenes. FORREST F. CLEVELAND AND M. J. MURRAY, *Illinois Institute of Technology*.—Raman data have been obtained for (A) 1-iodo-1-propyne ($CH_3C{\equiv}CI$), (B) 1-bromo-1-propyne ($CH_3C{\equiv}CBr$), (C) 1-chloro-1-propyne ($CH_3C{\equiv}CCl$), and (D) 3,3-dimethyl-1-butyne ($C(CH_3)_3C{\equiv}CH$) in the liquid state. Relative intensities and depolarization factors were obtained by use of a Gaertner microdensitometer. C_2H_3Br was present as an impurity in the sample used in obtaining the spectrum of (C) and depolarization factors were not obtained for this compound. Calculation shows that the $CX_3C{\equiv}CY$ molecule should have five A_1 frequencies and five E frequencies, all of which are active in the Raman effect. The A_1 frequencies should be polarized, the E frequencies depolarized. The observations confirm these expectations, although there are some cases of doubling of lines due to resonance interaction. Since there is only a small increase in frequency for the gaseous state for such molecules, it is possible to make approximate thermodynamical calculations for molecules (A) and (B). In the triple bond region a line of medium intensity and smaller displacement than the strong triple bond line was observed for compounds (A), (B), and (C). This may be due to resonance interaction with the difference tone of the 2900

and 700 cm^{-1} fundamentals. For compound (D), two lines, rather than the usual one for monosubstituted acetylenes were observed at 2106 and 2137 cm^{-1}.

23. A Dynamical Approach to the Condensation Problem. M. DRESDEN AND WILFRED KAPLAN, *University of Michigan.*—A number of attempts have been made to explain the condensation of a gas on the basis of statistical mechanics, starting from the classical or quantum-mechanical partition function. From this one proved essentially the existence of a singularity in the p, V curve for sufficiently low temperatures. However this proof does not elucidate the physical mechanism of condensation. It might be possible to understand the condensation phenomena by linking it with the stability conditions for dynamical systems. Consider the gas as a classical N-body problem, then by generalizing the concept of dynamic stability we can show that the stability of the system is essentially determined by the local structure of the energy manifold in the $3N$ dimensional phase space. So in order to determine where transitions can occur we must find out where the topology of the energy manifold changes, as we vary the total energy. For simple cases it has been shown that such changes occur;[1] dynamically, they correspond to the transition from bounded to unbounded orbits. The extension to the general case and the possibility of computing transition temperatures will be discussed.

[1] Wilfred Kaplan, Am. Math. Monthly, No. 5 (May, 1942).

24. The "Génies" of Poincaré, and Carnot's Principle. PIERRE DEMERS, *Montreal.*—Poincaré has proposed that perhaps a being that he calls a "génie," would see the individual molecules in a fluid mass; he could manipulate a trap to allow the faster molecules to accumulate in one compartment, where temperature would rise, against Carnot's principle. Maxwell has proposed the same, with "demons." This scheme was supposed to involve no energy expense. The theoretical possibility of this experiment is examined with the following conclusions: (1) Manipulating the trap involves *a minimum energy* $\sim kT/2$, from kinetic considerations. (2) To locate the molecules we can detect *photons*, diffused or emitted in a thin layer of molecules. A microscopist, or an automatic device, could manipulate the trap. It is seen that anyway some energy must be spent from the outside. (3) We can enclose the molecules to avoid loss of radiation, keeping them in *thermal and radiative equilibrium;* then we have a blackbody, in which details and individual molecules are indistinguishable; the "génie" would be unable to locate the origin of any one quantum perceived. Not seeing the molecules, he would be unable to sort them.

25. On Strong-Coupling and Weak-Coupling Theories of the Meson Field. W. PAULI, *The Institute for Advanced Study.*—With the assumption that the meson has spin 0 and is described by a pseudo-scalar field, the model of an extended heavy particle (nucleon) leads to the strong coupling condition $f^2 \gg a^2$, where f is the coupling constant with the dimension of a length, and a is the size of the source. In connection with the prediction of excited states (isobars) of the nucleon, this theory leads to serious difficulties, since Dancoff and Serber[1] showed that the theory is in contradiction to the well-known saturation properties of the nuclear force, and Pauli and Dancoff[2] showed that it gives for the magnetic moments of the proton and the neutron values equal in magnitude but opposite in sign. On the other hand purely classical theories of the meson field which are based on the picture of a point source and which fulfil the condition of relativistic invariance were developed by Bhabha[3] and Fierz.[4] The singularities of the field due to the point character of the source are avoided by a suitable subtraction formalism. The author has shown that the classical point-source theories can be translated to quantum theory by the use of the so-called λ limiting process of Wentzel and Dirac. The application of this method to the theory of meson field produces automatically the value 0 for the spin inertia, K, and gives convergent results for all quantum theoretical problems where the nucleons can be considered to be at rest. Such a weak coupling theory with point sources avoids all difficulties of the strong coupling theory with an extended source. For the scattering cross section of mesons by nucleons (due to the non-electromagnetic interaction), the results of this theory agree completely with that given by Heitler and Peng,[5] which is in fairly good agreement with experiment. No stable isobars of the nucleon exist in such a theory as long as $(f\kappa)^2 \ll 1$, a condition which is certainly fulfilled. In the problem of the interaction between two (or several) nucleons at rest, the perturbation theory holds for distances, r, of the nucleons for which $r^2 \gg f^2$ which can be derived by the method given by Stückelberg and Patry.[6]

[1] S. M. Dancoff and R. Serber, Phys. Rev. **61**, 394A (1942).
[2] W. Pauli and S. M. Dancoff, Phys. Rev. **62**, 85 (1942).
[3] H. J. Bhabha, Proc. Roy. Soc. **A178**, 314 (1941).
[4] M. Fierz, Helv. Phys. Acta **14**, 257 (1941).
[5] W. Heitler and H. W. Peng, Proc. Camb. Phil. Soc. **38**, 296 (1942).
[6] E. C. G. Stückelberg and J. F. C. Patry, Helv. Phys. Acta **13**, 167 (1940). E. C. G. Stückelberg, Helv. Phys. Acta **13**, 347 (1940).

26. On the Theory of a Mixed Pseudo-Scalar and a Vector Meson Field. S. KUSAKA AND W. PAULI, *The Institute for Advanced Study.*—The authors have investigated in more detail Schwinger's[1] modification of Møller-Rosenfeld's theory of nuclear forces which is based on a mixture of a pseudo-scalar and a vector meson field. With the assumption of an extended source of the nucleon, the strong coupling condition is fulfilled, and if the coupling constants of the two fields are taken to be equal, the excitation energy of the isobars turns out to be $\frac{1}{3}$ of its value in the pseudo-scalar theory. The interaction between two nucleons is described with sufficient accuracy by a Hamiltonian which consists of three parts: (1) the isobar excitation energy of the nucleon; (2) the kinetic energy of the nucleon; and (3) the potential energy of the interaction between the nucleons. In the most interesting case of the symmetrical theory, the last expression is the same as the corresponding expression of the weak coupling theory with the spin and the isotopic spin matrices replaced by the more general e_k^α vectors of Pauli and Dancoff. A classification of the energy levels of the two-nucleon system has been made, and a preliminary estimate indicates that a suitable choice of the coupling constant and the masses of the mesons can

be made in such a way that the binding energy and the quadrupole moment of the deuteron agree with the observed values, and such that the size of the source is small compared to the Compton wave-lengths of both mesons and that the excitation energy of the isobar is large compared to the binding energy of the deuteron. However, this theory gives for the magnetic moment of the deuteron a value only a few percent of the observed value, and the difficulties for higher nuclei described in the preceding paper are also present here. Hence we propose to consider this theory in the weak coupling scheme with a point source of the kind described in the preceding paper. More accurate calculations for the wave functions of the ground state of the deuteron are in progress.

[1] J. Schwinger, Phys. Rev. 61, 387A (1942).

27. On the Meson Field Theory of the Magnetic Moment of Proton and Neutron. J. M. JAUCH, *Princeton University.*—It is shown that the application of the λ-limiting process together with Dirac's introduction[1] of a second type of field oscillators with negative energy leads in the case of the pseudo-scalar theory to a convergent result for the magnetic moment of the heavy particles in the approximation of the order of the square of the coupling constant.

[1] P. A. M. Dirac, Proc. Roy. Soc. **A180**, 1 (1942).

28. Ionization Yield of Radiation Energy. U. FANO, *Carnegie Institution of Washington.*—According to experiments with ionizing radiations acting on various substances, the average energy absorbed per ionization produced is approximately 30–35 ev and bears no apparent relation to the ionization potential of the particular substance. Bagge's theoretical calculation of this energy proved correct for atomic hydrogen, but for other substances incorrectly indicated a positive correlation with the ionization potential.[1] This discrepancy is accounted for qualitatively by giving proper consideration to the fact that most energy absorptions are due to electric dipole oscillations. Available theoretical information shows that the oscillator strength of ionization in certain characteristic atoms is directly and critically related to their ionization potential: the greater the energy actually required to ionize individual atoms, the smaller is the average energy "wasted" in producing excitations. A crude theory complementary to Bagge's has been applied to H and He. It indicates that the factor considered here is essentially sufficient to balance the great difference between the ionization potentials of these two atoms. This accounts for one particularly puzzling feature of the known experimental data, but does not positively establish a yield of one ionization per every 30–35 ev as a theoretical result valid for all substances.

[1] E. Bagge, Ann. der Physik **30**, 72 (1937).

29. A High Pressure Cloud Chamber of New Design. T. H. JOHNSON, R. P. SHUTT, AND S. DE BENEDETTI, *Bartol Research Foundation.*—A cloud chamber is described which operates at a pressure of 200 atmospheres without the difficulty of having to subject its transparent walls to high pressure differentials. The chamber consists of a glass ring of ¼-inch wall thickness, 12 inches in diameter, and 3 inches deep covered on the front with a ¾-inch thick glass plate of the same diameter and on the back with a synthetic rubber diaphragm. The chamber is mounted in the center of a large steel tank. The tank is filled with transparent white oil which subjects the outside of the cloud chamber to a hydrostatic pressure equal to the internal gas pressure. The chamber is compressed by pumping additional oil into the tank, and it is expanded by releasing a valve connecting the tank with an evacuated vessel of adjusted volume. Ample space is provided inside the tank for magnetic field coils and the heavy walls of the tank will serve as the magnetic conductors. The apparatus has already been operated at a pressure of 110 atmospheres giving excellent cosmic-ray tracks. At this pressure its efficiency for observation of rare events such as mesotron decay is about 1000 times that of a chamber of the same size operating at atmospheric pressure.

30. Some Results Obtained with a New High Pressure Cloud Chamber. S. DE BENEDETTI, T. H. JOHNSON, AND R. P. SHUTT, *Bartol Research Foundation.*—460 pictures have been taken in a newly designed high pressure cloud chamber, most of them in an atmosphere of *n*-propyl alcohol, water vapors, and argon at a pressure of 110 atmospheres. The volume expansion ratio decreases almost linearly with pressure, and at 110 atmospheres it becomes as low as 1.05. Owing to small diffusion at such pressures, the sensitive time of the chamber is increased by almost 10 times that at normal pressure, making counter control unnecessary. At 110 atmospheres each random picture contains the equivalent of 3 full length tracks, corresponding to more than 10^4 cm of air at normal pressure. A total length of 5×10^6 cm of air equivalent has been observed, which equals the track length obtained in 500,000 random pictures, or 150,000 pictures controlled by counters, in a cloud chamber of the same dimensions but at normal pressure. Among the results obtained are several cases of heavily ionized tracks attributable to the proton component, one case of a mesotron disintegration, and several pictures of "knock on" electrons of energies above 20 Mev produced in the gas. Typical pictures will be shown.

31. Experiments Concerning the Origin of the Second Hump in the Rossi Curve. W. F. G. SWANN, *Bartol Research Foundation of the Franklin Institute.*—Former experiments at the Bartol Foundation have confirmed the existence of the second hump. These experiments have now been varied in a manner calculated to give further information on the significance of the hump. The minimum between the two humps occurs at a thickness of about 10 cm of lead. After carrying observations out to this thickness, the thickness was further increased by the addition of tin. This caused an immediate rise in the curve of an amount comparable with that for the first hump in tin itself. On the other hand, when a similar experiment was performed starting with a thickness of tin corresponding to the minimum and increasing the thickness by the addition of lead, a diminution in the intensity of shower production with increase of thickness was observed. These experiments were suggested

by an attempt to account for the second hump on the hypothesis of the creation of electrons by the primary radiation after a certain degree of penetration, and their significance is discussed in relation to this view.

32. Production of Mesotrons by Ionizing and Non-Ionizing Radiation. MARCEL SCHEIN AND JULIUS TABIN, *University of Chicago.*—A cosmic-ray balloon experiment was carried out in the stratosphere using Geiger-Mueller counters in 6 different 4- and 5-fold coincidence arrangements. The equipment reached an altitude corresponding to 2.5 cm of Hg pressure. The following phenomena were investigated: (a) single mesotrons produced in 2 cm of Pb by non-ionizing rays, (b) multiple production of mesotrons by ionizing and non-ionizing rays, (c) cascade showers below 2 cm of Pb produced by electrons and photons, (d) high energy electron showers. Each individual event was registered separately on the same film and it was possible to obtain all the correlations between the different events. The results obtained can be summarized as follows. At a pressure of 3 cm Hg (first radiation unit from the top of the atmosphere) 47 percent of the penetrating particles is accompanied by multiples (mesotron showers) produced by ionizing rays in 7 cm of lead. The producing radiation probably consists of primary protons. At altitudes higher than 14 km the number of mesotrons produced by non-ionizing rays in a lead thickness of 2 cm is as high as 28 percent of the intensity of the penetrating component. The mesotrons produced in this process are of relatively low energies (1 to 2×10^8 ev) and most of them (87 percent) occur in singles. The other 13 percent probably consists of mesotron pairs or mesotron-proton pairs. The non-ionizing rays producing these mesotrons appear to be low energy photons. Practically none of these processes was accompanied by cascade showers registered below 2 cm of Pb.

33. X-Ray Diffraction Investigation of Sodium Stearate from Room Temperature to the Melting Point. ALEXANDER DE BRETTEVILLE, JR. AND JAMES W. MCBAIN, *Stanford University.*—X-ray photographs were obtained of the γ-form[1] of sodium stearate by means of a heating camera[2] starting at room temperature and continuing through the melting point at 288°C to 301°C. The photographs show a gradual coming together of the two most intense side spacings to form a single broad line, somewhere between a temperature greater than 145°C and less than 170°C. Since a phase change[3] exists at 167°C it is assumed that this is the temperature at which the radical change in structure takes place. Orientation of the long spacings is exhibited at 301°C. Complete interpretation of the photographs is not possible because of a lack of crystal structure data. However, assumptions can be made about the structure from other sources that enable one to show that sodium stearate exhibits phenomena analogous to phenomena exhibited by the paraffins.[4]

[1] A. de Bretteville, Jr. and J. W. McBain, Science, **96**, 470 (Nov. 20, 1942).
[2] A. de Bretteville, Jr., Rev. Sci. Inst., **13**, 481 (1942).
[3] M. J. Vold, J. Am. Chem. Soc. **63**, 163 (1941).
[4] A. Müller, Proc. Roy. Soc. **138**, 514–530 (1932).

34. The Shape of the Debye-Scherrer Lines. C. C. MURDOCK, *Cornell University.*—The equation for the shape of the Debye-Scherrer line has been derived for crystals of uniform size for the following cases: the $(h\,k\,l)$ line for tetrahedral and cubic crystals, the $(h\,k\,o)$ and $(h\,k\,k)$ lines for octahedral crystals and the (100), (110), and (111) lines for rhombic-dodekahedral crystals. When the crystal has a center of symmetry, the lines associated with Bragg planes which are approximately parallel to crystal faces have secondary maxima. Because of these the estimation of line breadth from experimental data in terms of "integral breadth" is less reliable than in terms of "half intensity breadth," $B_{\frac{1}{2}}$. Let $K=(B_{\frac{1}{2}}v^{\frac{1}{3}}\cos\theta)/\lambda$ in which v is crystal volume. For the dodekahedron, (100) and (110), $K=0.87$; (111), $K=0.91$. For the octahedron, K ranges from 0.82, (100), to 0.94, (111). For the cube, from 0.83, (110), to 0.91, (311), (411), and (511). For the tetrahedron, from 0.73, (110), to 1.03, (100). The equations give the same values for "integral breadth" as those computed by Stokes and Wilson.[1] For measurement of particle size, a line should be used for which K is insensitive to crystal shape. The results so far obtained suggest the (210) reflection, $K=0.89\pm0.02$, for this purpose.

[1] Proc. Camb. Phil. Soc. **38**, 313 (1942).

35. An X-Ray Diffraction Study of the Age-Hardening of a Cu-Al Alloy. CHARLES H. TOWNES AND WHEELER P. DAVEY, *The Pennsylvania State College.*—The age-hardening of Cu–Al alloys has been studied by many investigators using density, elastic limit, elongation, hardness, electrical conductivity, and lattice parameters. Results are summarized elsewhere.[1] The present work (using balanced filters and Geiger-Mueller counters) shows the time rate of change of the diffracting powers of the atomic planes of the Cu–Al solid solution and of its decomposition products (θ' and θ). Pre-strained 25S alloy was heated for 24 hours at 540°C (to dissolve all the Cu in the Al) and then water-quenched at 20°C. The Cu was then allowed to migrate at 309°C. It was found that: (1) In the Al "solid solution" phase the diffracting power of the (111) planes decreased to a constant value in 120 hours; the (100), (110), and (311) planes showed a decreased diffracting power followed by a considerable increase. (2) The (112) (2) plane of θ' decreased to a constant diffracting power in 120 hours. (3) The (001) (3), (101) (2), (112), (110) (2), and (211) planes of θ increased in diffracting power to a constant value in approximately 120 hours. Definite interpretations of the above are offered.

[1] "Age Hardening of Metals," Am. Soc. for Metals (1940).

36. X-Ray Measurement of Short Range Order and Long Range Order in Cu_3Au. Z. W. WILCHINSKY, *Massachusetts Institute of Technology.*—From a powder pattern, the value of long range order, S, can be obtained from intensity measurements of the superstructure lines. When S is zero it is possible to obtain the value of short range order by applying Fourier integral analysis to intensity measurements of the diffuse background. From diffraction theory the background intensity for the alloy A_3B is proportional to $(f_A-f_B)^2\,(3-\Sigma_i\,\sigma_i c_i\,\sin kr_i/kr_i)$ where f_A

and f_B are the atomic scattering factors, $k=4\pi \sin\theta/\lambda$, the r_i's are the interatomic distances, c_i is the number of atoms at distance r_i from a given atom, and σ_i is the generalized form of the short range order parameter as defined by Bethe. The dominant parameter, σ_1, was found to be 0.19 for sample quenched from 750°C; 0.55 for 540°C; and 0.67 for 400°C. The intensity of a superstructure line is proportional to $S^2(f_A-f_B)^2$. Values of S obtained are 0.842 for sample held at 250°C; 0.814 for 370°C and 0.804 for 380°C.

37. A Simplified Electron Microscope. C. H. BACHMAN AND SIMON RAMO, *General Electric Company.*—An electron microscope has been constructed to test a number of new attacks. The aim has been to obtain a resolving power in the range of the greatest present usefulness of electron microscopy (say ten times better than light microscopy), operating at a voltage range sufficient to obtain this resolution for the usual thin specimens, in as simple a manner as possible. The instrument is a combined electron and light microscope and utilizes unipotential electrostatic electron lenses. It has the following desirable characteristics: (1) The electrons are accelerated and focused by a single crudely regulated voltage. (2) The unipotential lenses can readily be used in a multiple-stage magnifying system of compact construction so that the chamber to be evacuated becomes very small. (3) A short electron path results from the use of a multiple lens electron-optical system in combination with a stage of light-optical magnification. This small cathode to fluorescent screen distance and the medium resolving power aim make it possible to align the entire electron-optical system permanently. (4) The chamber can be re-evacuated to operating conditions within a few minutes after insertion of a new specimen. (5) The overall weight and dimensions, if proper advantage is taken of the above conditions, are such that it is feasible to design a portable instrument.

38. Compact Electron Microscope with Magnetic Lenses. V. K. ZWORYKIN AND J. HILLIER, *RCA Manufacturing Company.*—To meet the demand of a small, simply operated and inexpensive electron microscope, a desk-type instrument has been developed, with a total length from electron source to observation screen or photographic plate of only 16 inches. The objective and projector lenses are of a new design, and the magnetomotive force is provided either by a coil or by permanent magnets. Focusing is accomplished by varying the stabilized operating voltage, normally maintained in the neighborhood of 30 kilovolts. The illumination is controlled by a bias voltage applied to a grid cylinder surrounding the cathode. The total volume of the instrument being only about 1 liter, airlocks are superfluous; the pumping-out time required for complete evacuation is only about 2 minutes. The microscope is mounted so that the observer views the final image directly on the rear of a transparent fluorescent screen.

39. Distance to Which the Attractive Field of a Solid Extends into a Liquid. WILLIAM D. HARKINS AND GEORGE JURA, *University of Chicago and the Universal Oil Products Company, Chicago.*—Various estimates of the distance to which the attractive field of a crystal extends into an adjacent liquid vary from the thickness of one to several thousand monolayers. A method has been developed for the determination of the variation of the energy with the distance. A definite amount of the vapor of the liquid is adsorbed on the surface of the solid, which must give a zero contact angle with the liquid. The powder is then immersed in the liquid in a sensitive calorimeter. The determination of area is described in the following paper. From the integral curve the energy of desorption per molecular layer, is calculated. With titanium dioxide (anatase) and water the excess of the energy of desorption over that for vaporization (10,480 cal. mole^{-1}) for the successive molecular layers is; 5360, 480, 110, 60, and 20 cal. mole^{-1}. Quartz would give slightly higher values. Although the energies of attachment of the higher layers are very small, films of slightly over nine layers of water or of nitrogen have been obtained before saturation is attained. The accuracy of the values can be improved by more extensive experimental work.

40. A Method for Determining the Area of a Crystalline Powder without the Assumption of a Molecular Area. GEORGE JURA AND WILLIAM D. HARKINS, *University of Chicago and Universal Oil Products Company.*—Emmett, Brunauer, and Teller have developed a gas adsorption method which gives the volume of gas adsorbed to fill the first monolayer on the surface of a solid. If the molecular area were known for each case the area could be calculated. In the application of this method they used porous solids of extremely large area, while we employed nonporous crystalline powders. We have developed a new method, independent of any assumption of a molecular area, based on a proof that a solid surface which gives a zero contact angle with a liquid is covered by a duplex film of that liquid when in equilibrium with saturated vapor. A duplex film is one just thick enough to exhibit the same surface energy as the liquid itself. At 250°C fine crystals of titanium dioxide, in equilibrium with saturated water vapor, and therefore covered by a duplex water film, were immersed in liquid water. Since the surface energy was that of water (118.5 erg cm^{-2}), the total energy of immersion, divided by this value, gave the area (14.0 meter g^{-1}), while nitrogen adsorption gave *exactly the same area when* Emmett's molecular area of 16.2A^2 was assumed.

41. Raman Spectra of Methylheptenes. FORREST F. CLEVELAND, *Illinois Institute of Technology.**—Continuing work on olefinic hydrocarbons containing eight carbon atoms, the Raman frequencies, relative intensities and depolarization factors of 2-methyl-1-heptene and 6-methyl-1-heptene have been obtained. The relative intensities and depolarization factors were obtained by use of a Gaertner microdensitometer. The strong lines characteristic of the $RHC=CH_2$ group, previously observed at 1293(94)0.88, 1415(42)0.77, 1641(134)0.15 and 3078(23)0.93 for 1-octene, appear at 1295(212)0.45, 1417(112)0.56, 1644(342)0.19 and 3079(70)*D* for 6-methyl-1-heptene. For 2-methyl-1-heptene, in which the group is $R(CH_3)C=CH_2$, the corresponding lines were observed at 1303(52)0.64, 1414(108)0.81,

1653(203)0.20 and 3077(47)*D*. It may be noted that the 1653 frequency is higher for the $R(CH_3)C=CH_2$ group than the corresponding value of 1642 in the $RHC=CH_2$ group. Furthermore, the frequency which was constant at 3000 cm^{-1} for the four octenes previously studied and for the 6-methyl-1-heptene drops to 2978 cm^{-1} for the 2-methyl-1-heptene. The line 1334(48)0.55 in the spectrum of 6-methyl-1-heptene was not observed for the 2-methyl-1-heptene or for the four octenes previously studied while the line observed at 1383(69)0.64 for the latter compound was observed in the previous investigation only for *cis*+*trans* 2-octene and *trans*-3-octene.

* To be called for after Paper No. 22 if time permits.

42. A Method for the Accurate Determination of the Adsorption of a Vapor on the Surface of a Solid. WILLIAM D. HARKINS AND GEORGE JURA, *University of Chicago.**—While it is easy to obtain a moderately accurate isotherm for the adsorption of a vapor on a porous solid by the ordinary volumetric method, or by a McBain-Bakr quartz spiral, these methods are not accurate if non-porous sheets of powders are under investigation. Our method is extremely accurate, not affected by time, and as many temperatures as are desired may be used. (1) As large a sample of sheets or powder as possible is put in a glass bulb in which it can be outgassed. During the adsorption process this bulb is kept in a thermostat. (2) The samples of liquid are placed in sealed glass bulbs filled with proper amounts of the liquid. The empty and full bulbs are weighed on an analytical or a microbalance, and are held in a horizontal tube which is attached by a vertical tube to the adsorption bulb, and also to a small sensitive manometer. The horizontal tube is supplied with a mechanism to break any single bulb as desired. (3) In the application of this method it is often possible to adsorb on the solid 99 percent of the mass of liquid in the bulbs. The manometer is used to obtain the vapor pressure in order that the mass of vapor unadsorbed may be determined.

* To be called for after Paper No. 40 if time permits.

43. The Lift Function for an Oscillating Airfoil.* W. C. RANDELS AND S. SILVER, *University of Oklahoma.*—A method used by Biot[1] is applied to an airfoil undergoing torsional oscillations. The usual approximations of the linearized theory for thin airfoils have been made. The boundary conditions are shown to be satisfied by a function consisting of the sum of three functions corresponding to elementary singularities. The total lift and moment are given.

* To be read by title.
[1] M. Biot, J. Aer. Sci. 9, 185 (1942).

AUTHOR INDEX TO ABSTRACTS OF PAPERS PRESENTED AT THE NEW YORK MEETING

Bachman, C. H. and Simon Ramo—No. 37
de Bretteville, Alexander, Jr. and James W. McBain—No. 33
Brentano, J. C. M. and E. R. Schleiger—No. 8

Chamberlain, C. W.—No. 14
Cleveland, Forrest F.—No. 41
—— **and M. J. Murray**—No. 22
Cohen, Arnold A.—No. 16
Courant, E. D.—No. 15
Cox, R. T.—see Goertzel, Gerald
Cross, Paul C. and G. W. King—No. 21

Davey, Wheeler P.—see Townes, Charles H.
De Benedetti, S.—see Johnson, T. H.
——, **S., T. H. Johnson, and R. P. Shutt**—No. 30
Dees, Bowen C. and Bernard Hamermesh—No. 3
Demers, Pierre—No. 24
Deutsch, M.—see Elliott, L. G.
Dresden, M. and Wilfred Kaplan—No. 23

Ehrenhaft, Felix—No. 1
Elliott, L. G. and M. Deutsch—No. 17

Fano, U.—No. 28
Focht, Elizabeth F.—see Quimby, Edith H.
Friederich, L. M., S. J.—see Weber, A. H.

Gallagher, Charles J.—No. 5
Goertzel, Gerald and R. T. Cox—No. 2

Hamermesh, Bernard—see Dees, Bowen C.
Harkins, William D.—see Jura, George
—— **and George Jura**—Nos. 39 and 42
Henry, D. E.—see Rentschler, H. C.
Hillier, J.—see Zworykin, V. K.

Jauch, J. M.—No. 27
Johnson, T. H.—see De Benedetti, S.
——, **R. P. Shutt, and S. De Benedetti**—No. 29
Jura, George—see Harkins, William D.
—— **and William D. Harkins**—No. 40

Kaplan, Wilfred—see Dresden, M.
King, G. W.—see Cross, Paul C.
Kolin, Alexander—No. 13
Kusaka, S. and W. Pauli—No. 26

McBain, James W.—see de Bretteville, Alexander, Jr.
McCue, J. J. G.—No. 10
Murdock, C. C.—No. 34
Murray, M. J.—see Cleveland, Forrest F.

Nordheim, Gertrud and H. Sponer—No. 20

Pauli, W.—No. 25
—— see Kusaka, S.

Quimby, Edith H. and Elizabeth F. Focht—No. 12

Ramo, Simon—see Bachman, C. H.

Randels, W. C. and S. Silver—No. 43
Rentschler, H. C. and D. E. Henry—No. 6
Rogers, F. T., Jr.—No. 18

Schein, Marcel and Julius Tabin—No. 32
Schleiger, E. R.—see Brentano, J. C. M.
Shutt, R. P.—see De Benedetti, S.
—— see Johnson, T. H.
Silver, S.—see Randels, W. C.
Smith, Charles G.—No. 4
Sponer, H.—see Nordheim, Gertrud
Swann, W. F. G.—No. 31

Tabin, Julius—see Schein, Marcel
Townes, Charles H. and Wheeler P. Davey—No. 35
Trischka, J. W.—No. 11

Watson, W. W. and D. Woernley—No. 19
Weber, A. H. and L. M. Frederick, S. J.—No. 7
Wilchinsky, Z. W.—No. 36
Woernley, D.—see Watson, W. W.
Wold, P. L.—No. 9

Zworykin, V. K. and J. Hillier—No. 38